Estimating Dynamic Properties of RC Frame Structures with Various Infill Materials for Quick Assessment

Abdulrahman Julailati

Submitted to the
Institute of Graduate Studies and Research
in partial fulfillment of the requirements for the degree of

Master of Science
of
Civil Engineering

Eastern Mediterranean University
September 2022
Gazimağusa, North Cyprus

Approval of the Institute of Graduate Studies and Research

Prof. Dr. Ali Hakan Ulusoy
Director

I certify that this thesis satisfies all the requirements as a thesis for the degree of Master of Science of Civil Engineering.

Prof. Dr. Umut Türker
Chair, Department of Civil Engineering

We certify that we have read this thesis and that in our opinion it is fully adequate in scope and quality as a thesis for the degree of Master of Science of Civil Engineering.

Assoc. Prof. Dr. Giray Özay
Supervisor

Examining Committee

1. Prof. Dr. Serhan Şensoy

2. Assoc. Prof. Dr. Giray Özay

3. Assoc. Prof. Dr. Rifat Reşatoğlu

ABSTRACT

The effect of infill walls on frame rigidity is usually not considered in the performance assessment of structures nor the fundamental period, where infill walls would affect both the performance level and the structure's period negatively or positively depending on their plan and elevation distribution. Moreover, the need for a quick assessment tool to predict the performance level of structures is essential, especially considering infill wall effects. Therefore, buildings were designed according to the Turkish Seismic Code for Buildings 2018 (TSCB-2018) and the Requirements for Design and Construction of Reinforced Concrete Structures Code (TS-500). The number of analyzed models was 336, each with different combinations of peak ground acceleration, soil type, infill material, and infill walls layouts. The data in the Artificial Neural Network (ANN) models used analysis outcomes collected, such as the fundamental period, target displacement, and performance level, as a target, training, and validation data. Furthermore, for performance assessment, the commercial program Seismostruct 2022 was used for nonlinear static analysis (pushover analysis), while Matlab 2018 was used for the creation of neural network models.

Bayesian regularization backpropagation was used for all ANN models. ANN models showed excellent accuracy in all three models: period, performance, and target displacement. The models' accuracy obtained was as follows: in the performance level model at 96.15%, while for the fundamental period of the structure, it was 99.99% and lastly, the target displacement was 99.66%.

Keywords: ANN, Fundamental Period, Infill Wall, Performance, Target Displacement.

ÖZ

Dolgu duvarların çerçeve rijitliği üzerindeki etkisi, dolgu duvarların plan ve kot dağılımına bağlı olarak hem performans seviyesini, hem de yapının periyodunu olumsuz veya olumlu yönde etkileyeceği genellikle dikkate alınmaz. Ayrıca, özellikle dolgu duvar etkileri göz önüne alındığında, yapıların performans düzeyini tahmin etmek için hızlı bir değerlendirme aracına duyulan ihtiyaç esastır. Bu nedenle binalar Türk Deprem Yönetmeliği 2018 (TSCB-2018) ve Betonarme Yapıların Tasarım ve Yapım Kuralları Yönetmeliğine (TS-500) göre tasarlanmıştır. Analiz edilen 336 modelin, her biri farklı maksimum yer ivmesi, zemin tipi, dolgu malzemesi ve dolgu duvar yerleşimi kombinasyonlarına sahiptir. Bu analiz sonuçlarına göre yapının periyodunu, hedef yer değiştirmesini ve performans seviyesini verecek Yapay Sinir Ağı (YSA) modelleri oluşturulmuştur. Ayrıca, statik itme analizi (pushover) yöntemiyle performans değerlendirilmesi için, Seismostruct 2022 programı, Yapay Sinir Ağı modellerinin oluşturulması için de Matlab 2018 kullanıldı.

Tüm YSA modelleri için Bayes düzenlileştirme geri yayılımı kullanılmıştır. YSA modelleri, üç modelde de mükemmel doğruluk gösterdi: periyot, performans ve hedef yer değiştirme. Elde edilen modellerin doğruluğu şu şekildedir: performans düzeyi modelinde %96,15 iken, yapının temel periyodu için %99,99 ve son olarak hedef yer değiştirme %99,66 olmuştur.

Anahtar kelimeler: YSA, periyot, dolgu duvar, performans, hedef yer değiştirme.

Dedicated to My Family

Father's Soul Yasser & Mother Roshan

Brother Bakri & Sister Alia

And

WAMY Organization

ACKNOWLEDGEMENTS

I want to express my gratitude to Assoc. Prof. Dr. Giray Özay for his patience and guidance throughout the analysis and theoretical work required to complete this thesis. He taught me how to conduct myself professionally and constantly convinced me to do the right thing. I have been privileged to be among his students. Without his excellent contributions and advice, the objectives of this thesis would not have been attained.

Words cannot express my gratitude for my family's exceptional love and support. Firstly, my father, Yasser (may his soul rest in peace), has well equipped me with the fundamentals of learning and experience that have enabled me to reach this point. I would also like to express my deepest gratitude to my mother, Roshan, for her unending love and encouragement to continue my academic studies. My brother and sister, Bakri and Alia, who have always been there for me, and never forget my best friends especially, Mohammad Herbawi; I'm incredibly grateful for their support and love, so I would like to express my love and most profound appreciation to all of them. Lastly, I am deeply indebted to WAMY organization where this endeavor would not have been possible without their bursary and support.

TABLE OF CONTENTS

ABSTRACT iii

ÖZ v

DEDICATION vi

ACKNOWLEDGEMENTS vii

LIST OF TABLES xii

LIST OF FIGURES xiii

LIST OF SYMBOLS AND ABBREVIATIONS xvii

1 INTRODUCTION 1

1.1 General 1

1.2 Previous Work Done 1

1.2.1 Effect of Infill on Structure Performance 4

1.2.2 Effect of Infill Walls on Fundamental Period 6

1.2.3 Effect of Infill Walls on Target Displacement 7

1.2.4 Artificial Neural Networks 7

1.3 Aim and Scope 8

1.4 Organization of the Thesis 9

2 ANALYSIS METHODS AND MODELING OF INFILL WALLS 11

2.1 Introduction 11

2.2 Seismic Analysis Procedures 11

2.2.1 Linear Static Procedure 12

2.2.2 Linear Dynamic Procedure 13

2.2.3 Nonlinear Static Procedure 13

2.2.4 Nonlinear Dynamic Procedure 15

2.3 Turkish Seismic Code for Buildings 2018 (TSCB-2018) 16
2.3.1 Differences to Previous Earthquake Code 17
2.3.2 Nonlinear Static Pushover Analysis 18
2.4 Building Performance Assessment in Accordance with TSCB-2018 20
2.5 Modeling of Infill Walls 23
2.5.1 Micro Models 23
2.5.2 Macro Model 23
3 ARTIFICIAL NEURAL NETWORKS 29
3.1 Introduction 29
3.2 Artificial Neural Networks Overview 29
3.3 Architecture of the Network 31
3.3.1 Feedforward Net 32
3.3.2 Competitive Net 33
3.3.3 Recurrent Net 34
3.4 Setting the Weights 34
3.4.1 Supervised Training 35
3.4.2 Unsupervised Training 35
3.4.3 Reinforcement Training 35
3.5 Activation Functions 35
3.5.1 Binary Step Function 37
3.5.2 Linear Function 38
3.5.3 Sigmoidal Functions 39
3.6 Training Methods 40
3.6.1 Back Propagation Learning Methods 40
3.6.2 Resilient Backpropagation 40

3.6.3 BFGS Quasi-Newton Backpropagation 41
3.6.4 Levenberg-Marquardt Backpropagation 41
4 RESEARCH METHODOLOGY 43
4.1 Introduction 43
4.2 Research Approach 43
4.3 Input Parameters 44
4.3.1 Plan Symmetry and Stories Number 44
4.3.2 Width of Building in X Direction 47
4.3.3 Width of Building in Y Direction 48
4.3.4 Number of Stories 48
4.3.5 Infill Walls Materials and Thickness 48
4.3.6 Infill Wall Layout 49
4.3.7 Columns Ratio 50
4.3.8 Shear Wall Ratio 51
4.3.9 Soil Type 51
4.3.10 Peak Ground Acceleration 51
4.4 Buildings Design 52
4.4.1 Building Materials and Loads 52
4.4.2 Reinforcement of Buildings with Plan Symmetry-1 55
4.4.3 Reinforcement of Buildings with Plan Symmetry-2 55
4.4.4 Reinforcement of Buildings with Plan Symmetry-3 56
4.5 Adaptive Pushover Analysis 56
4.5.1 Scaling Method 58
4.5.2 Modal Participation Factors and Degrees-of-Freedom 58
4.5.3 Spectral Amplification 58

4.6 Artificial Neural Network 59
5 RESULTS AND DISCUSSIONS 61
5.1 Introduction 61
5.2 Capacity Curves (Pushover Analysis Curve) 61
5.2.1 Mid-rise Buildings Capacity Curves by Infill Layouts Difference 61
5.2.2 High-rise Buildings by Infill Layouts Difference 66
5.3 Performance Levels 72
5.4 Fundamental Structure Period Plots 79
5.5 Target Displacement Reduction Percentage by Infill Walls Layouts 82
5.6 ANN Models Results 84
5.6.1 Performance Level Model 86
5.6.2 Fundamental Period Model 88
5.6.3 Target Displacement Model 91
6 CONCLUSION 94
6.1 Introduction 94
6.2 Buildings Capacity and Performance Level 94
6.3 Fundamental Period 95
6.4 ANN Models 95
6.5 Recommendations for Future Studies 96
REFERENCES 97
APPENDICES 106
Appendix A: Input Parameters 107
Appendix B: Neural Network Training 121

LIST OF TABLES

Table 1: Evaluation of structure performance..... 22

Table 2: Building plan symmetry summary..... 44

Table 3: Buildings width in x direction. 48

Table 4: Buildings width in y direction. 48

Table 5: Infill wall materials compressive strength Šipoš K.T. (2019). 49

Table 6: Infill walls layout considered..... 49

Table 7: Building plans columns ratios. 50

Table 8: Building plans shear wall ratios..... 51

Table 9: Buildings materials and loads definitions..... 52

Table 10: Structural members sizes and reinforcement of the mid-rise building. 55

Table 11: Structural members sizes and reinforcement of the high-rise building. 55

Table 12: Structural members sizes and reinforcement of the mid-rise building. 55

Table 13: Structural members sizes and reinforcement of the high-rise building. 56

Table 14: Structural members sizes and reinforcement of the mid-rise building. 56

Table 15: Structural members sizes and reinforcement of the high-rise building. 56

Table 16: Transfer functions and number of used neurons in all ANN models. 60

LIST OF FIGURES

Figure 1: Linear static procedure. (Antoniou, S, 2022) 13

Figure 2: Linear dynamic procedure. (Antoniou, S, 2022) 13

Figure 3: Nonlinear static procedure. (Antoniou, S, 2022) 14

Figure 4: Nonlinear dynamic procedure. (Antoniou, S, 2022) 16

Figure 5: Capacity demand curve (TSCB-2018). 20

Figure 6: Capacity curve and performance levels (TSCB-2018). 22

Figure 7: Equivalent diagonal strut and shear strut models for infilled frames (Crisafulli & Carr, 2007) 24

Figure 8: Area versus axial strain of the infill wall (Smyrou et al., 2006). 27

Figure 9: Architecture of a typical neural network (MathWorks. 2018). 30

Figure 10: Connection structures of some ANN (Sivanandam et al., 2006). 32

Figure 11: Single layer neural network (Chrislb, 2005). 33

Figure 12: Multilayer neural network (Chrislb, 2005). 33

Figure 13: Structure of a recurrent neural network (Chrislb, 2005). 34

Figure 14: Artificial neuron diagram (Chrislb, 2005). 36

Figure 15: Binary step function (Sivanandam et al., 2006). 38

Figure 16: Example of a linear activation function (Sharma et al., 2020). 39

Figure 17: Sigmoidal function (Sivanandam et al., 2006). 40

Figure 18: Mid-rise symmetry-1 building plan view. 45

Figure 19: High-rise symmetry-1 building plan view. 45

Figure 20: Mid-rise symmetry-2 building plan view. 46

Figure 21: High-rise symmetry-2 building plan view. 46

Figure 22: Mid-rise symmetry-3 building plan view. 47

Figure 23: High-rise symmetry-3 building plan view. 47
Figure 24: 3D view of the infill walls layouts. 50
Figure 25: Selected spectrum curves. 52
Figure 26: Concrete stress strain diagram. 53
Figure 27: Steel stress strain diagram. 54
Figure 28: Capacity curves for plan symmetry-1 and IM1. 62
Figure 29: Capacity curves for plan symmetry-1 and IM-2. 62
Figure 30: Capacity curves for plan symmetry-1 and IM-3. 63
Figure 31: Capacity curves for plan symmetry-2 and IM-1. 63
Figure 32: Capacity curves for plan symmetry-2 and IM-2. 64
Figure 33: Capacity curves for plan symmetry-2 and IM-3. 64
Figure 34: Capacity curves for plan symmetry-3 and IM-1. 65
Figure 35: Capacity curves for plan symmetry-3 and IM-2. 65
Figure 36: Capacity curves for plan symmetry-3 and IM-3. 66
Figure 37: Capacity curves for plan symmetry-1 and IM-1. 67
Figure 38: Capacity curves for plan symmetry-1 and IM-2. 67
Figure 39: Capacity curves for plan symmetry-1 and IM-3. 68
Figure 40: Capacity curves for plan symmetry-2 and IM-1. 68
Figure 41: Capacity curves for plan symmetry-2 and IM-2. 69
Figure 42: Capacity curves for plan symmetry-2 and IM-3. 69
Figure 43: Capacity curves for plan symmetry-3 and IM-1. 70
Figure 44: Capacity curves for plan symmetry-3 and IM-2. 70
Figure 45: Capacity curves for plan symmetry-3 and IM-3. 71
Figure 46: Performance levels of plan symmetry-1 mid-rise buildings according to infill walls layouts. 72

Figure 47: Performance levels of plan symmetry-2 mid-rise buildings according to infill walls layouts. 73
Figure 48: Performance levels of plan symmetry-3 mid-rise buildings according to infill walls layouts. 74
Figure 49: Performance levels of plan symmetry-1 high-rise buildings according to infill walls layouts. 75
Figure 50: Performance levels of plan symmetry-2 high-rise buildings according to infill walls layouts. 76
Figure 51: Performance levels of plan symmetry-3 high-rise buildings according to infill walls layouts. 77
Figure 52: Mid-rise models performance percentages. 78
Figure 53: High-rise models performance percentages. 78
Figure 54: Models fundamental period versus infill walls layouts. 79
Figure 55 Fundamental period reduction percentage for the mid-rise models based on infill wall material and different layouts. 80
Figure 56: Fundamental period reduction percentage for the high-rise models based on infill wall material and different layouts. 81
Figure 57: Models fundamental period versus structure height. 81
Figure 58: Mid-rise models target displacement versus infill walls layouts 82
Figure 59: High-rise models target displacement versus infill walls layouts. 82
Figure 60: Target displacement reduction percentage for the mid-rise models based on infill wall material and different layouts. 83
Figure 61: Target displacement reduction percentage for the high-rise models based on infill wall material and different layouts. 84
Figure 62: Performance of performance level ANN model. 86

Figure 63: Training progress of the ANN model. 87
Figure 64: Performance of period ANN model. 88
Figure 65: Training progress of the ANN model. 89
Figure 66: Results plot of the ANN model and target data versus model number. ... 89
Figure 67: Error plot of the ANN model. 90
Figure 68: Performance of target displacement ANN model. 91
Figure 69: Training progress of the ANN model. 92
Figure 70: Results plot of the ANN model and target data versus model number. ... 92
Figure 71: Error plot of the ANN model. 93

LIST OF SYMBOLS AND ABBREVIATIONS

A_1	Area of Strut
ANN	Artificial Neural Network
AAC	Autoclaved Aerated Concrete Blocks
β_a	Auxiliary Point After Unloading
τ_o	Bond Shear Strength
ε_{cl}	Closing Strain
μ	Coefficient of Friction
CC	Collapse Case
CP	Collapse Prevention
CD	Controlled Damage
e_{x1}	Degradation Stiffness Controlling Parameter
E_m	Elastic Modulus
x_{oi}	Horizontal Offset
$f_{m\theta}$	Infill Compressive Strength
IM	Infill Material
IWL	Infill Walls Layout
LD	Limited Damage
LDP	Linear Dynamic Procedures
LSP	Linear Static Procedures
τ_{max}	Maximum Shear Stress
γ_{plr}	Modulus of Reloading After Unloading
γ_{plu}	Modulus of the Hysteretic Curve at Zero Stress

NDP	Nonlinear Dynamic Procedures
NSP	Nonlinear Static Procedures
PGA	Peak Ground Acceleration
PBE	Performance Based Engineering
RC	Reinforced Concrete
A_2	Residual Area of The Strut
RSA	Response Spectrum Analysis
α_s	Shear Reduction Factor
α_{re}	Strain After Unloading at Envelope
α_{ch}	Strain at Inflection Point
ε_m	Strain at Max Stress
e_{x2}	Strain Raising Parameter at Envelope
β_{ch}	Stress at the Inflection Point
f_t	Tensile Strength
t_w	Thickness
3D	Three Dimensional
TS-500	Turkish Requirements for Design and Construction of Reinforced Concrete Structures
TSC-2007	Turkish Seismic Code 2007
TSCB-2018	Turkish Seismic Code for Buildings 2018
2D	Two Dimensional
ε_u	Ultimate Strain
γ_{un}	Unloading Parameter
y_{oi}	Vertical Offset
h_z	Vertical Separation Between Struts

γ_s	Wall Stiffness Ratio

Chapter 1

INTRODUCTION

1.1 General

Engineers design reinforced concrete (RC) structures to withstand during earthquakes without structural failures and dissipate vast amounts of energy, so that these structures are ensure the safety of occupants. Failure to provide sufficient capacity results in severe damage and, in most cases, catastrophes. Turkey is susceptible to several earthquakes due to its presence on the Alp-Himalayas Fault, one of the world's most active seismic zones. (Soyluk & Harmankaya, 2012). Many parts of Turkey are in active seismic zones, resulting in the tragic loss of human life and the destruction of buildings and other infrastructure. Because of this, the way buildings are built to be safe and resistant to earthquakes has changed in the past few years, and research will continue for the foreseeable future.

Moreover, an earthquake is a continuous tumult created by forces under the earth's surface layer (the lithosphere) that spreads through the crust. It may also be defined as the intense shaking of the earth's surface caused by the release of energy into the earth's crust. This release of energy can be brought on by abrupt imbalances or volcanic activity in the crust.

1.2 Previous Work Done

The term infill wall refers to the masonry wall used to fill the bare structural frame to serve as a cladding element or interior partitions. The impact of infill walls is not

addressed during structural design. Although the effect of infill walls on the performance of structures was observed in the past, nowadays, practice classifies infill walls as nonstructural elements (Perrone et al., 2017).

Studies on infill wall frames were conducted in an attempt to estimate the lateral strength and stiffness of infill wall frame systems. At the conclusion of these tests, it was shown that infill walls react similarly to comparable compression struts, which are still utilized in modelling today (Buonopane & White, 1999).

Mehrabi et al. (1996) conducted studies on frames with brick infill and frames with open brick infill. They found that by increasing the vertical load on infill walls, the overall horizontal load-bearing capability of the composite frame can increase by up to 25%.

According to Altin et al., (1992), the rigidity of the reinforced concrete frame with infill walls will increase significantly in case of an accurate defined relationship between the frame and the infill wall.

The findings show that the contact surface of the infill and the surrounding frame significantly impacts the horizontal rigidity and strength of infill wall frames (Stafford, 1962, 1966).

According to the plastic theory established by Liauw and Kwan (1984), nonlinear finite elements were utilized to estimate the failure modes and additionally equivalent strengths for single and multi-story frames. Consequently, it was discovered that the

frame's bending strength is the most significant characteristic, and empirical and analytical investigations were taken into consideration.

Infill walls enhance structural strength and rigidity, according to Dowrick (1987), while infill walls shorten structural periods and improve system rigidity.

According to Ahmad et al., (2019) study, the frame's joint shear hinging was prevented by using masonry infill. The infill also helped the building dissipate energy by allowing the masonry to slide through many cracks. This allowed the structure to minimize structural damage while controlling seismic displacement demand and resisting substantially greater ground motions.

More lateral load-resisting systems should be employed to strengthen the stiffness of the multi-story structure since the impact of the infill wall's stiffness will be decreased as building height increases. Additionally, the results demonstrate that the infill walls' stiffness is effective for low- and medium-rise buildings (Parsaeimaram et al., 2013).

Infill walls may improve the system's horizontal rigidity. If these infill walls are not positioned appropriately, they might negatively affect the structure's dynamic properties. Different infill materials were adopted which are Autoclaved Aerated Concrete blocks (AAC) infill and normal brick. Brick infill walls performed better than AAC infilled walls under lateral loads (Coşan, 2014).

Pushover analysis shows more significant base shear for RC frames with infill walls than bare frames, despite the infill walls' brittle failure mechanism. 3,4,6,8, and 12-story buildings had similar findings. In seismic zones, infilled frames should be chosen

over open first-story frames (soft-storey) since first-story displacement is much larger than upper-story displacement, which may cause structural collapse. Infill walls impact the seismic response of frame structures and improve their strength and stiffness (Karim, 2016).

Infill walls have a significant role in the seismic behavior of RC structures and interact strongly with RC elements. When infills are placed uniformly in plan and elevation, infill walls may contribute favorably to the global response of the building. However, when certain irregularities are found, the infill walls may acquire critical failure mechanisms, including torsion and soft storey failures (Furtado et al., 2021).

1.2.1 Effect of Infill on Structure Performance

Despite the fact that severe damage experienced during seismic events demonstrates the effect of masonry infill walls on the seismic performance of structures, the conventional design approach treats infill walls as non-structural elements. Various empirical and analytical investigations have been conducted on the influence of infill walls on structural systems. There have been significant advancements in reinforced concrete frames. While infills are constructed using various materials and techniques, and while numerous studies have been conducted in recent years to examine the interaction between infill walls and structural elements, few studies have examined the effect of masonry infills on structural performance.

To study the impacts of infill walls, Jadhao and Pajgade (2013) analyzed the seismic behavior of multi-story structures under seismic loads. They compared the performance of frames with complete infill and bare frames at the conclusion of the study. They discovered that frames with traditional clay bricks and AAC infill wall models outperformed bare frames by a substantial margin.

Infills have a substantial influence on the global response of reinforced concrete structures, including both in terms of horizontal strength and stiffness. This impact is proportional to the infill walls' relative contribution to horizontal strength in comparison to the RC frame. The base shear force of completely infilled frames rises between 227% and 365% over the bare frame structure. In the context of inter-story drift ratios, infills resulted in a more uniform distribution throughout the height compared to the equivalent bare frame. With smaller seismic intensities, lateral deformations are distributed uniformly throughout the height. The findings from D'aragona et al. (2021) research highlight the importance of the infill constitutive model used in the seismic performance assessment of reinforced concrete structures.

Khan et al. (2021) study showed that detailed analysis results, combined with in-situ investigations of earthquake-struck buildings, confirm the well-established observation that infill walls have a significant effect on the structural performance of the building and that the frames were stiffened by the infill walls, thereby reducing damage to the reinforced concrete elements. Their analysis was conducted on SAP2000 using three dimensional (3D) and two dimensional (2D) models of bare frames and infilled frames.

Koçak (2020) studied the effect of infill walls on the performance of a six-story existing damaged reinforced concrete structure with a partially enclosed basement. Where the structure sustained significant damage during the 1999 Kocaeli earthquake, his investigation revealed that the number of beams and columns within the minimum damage level was more significant in the building model that included the infill wall effect. In contrast, in the building model that did not include the infill wall effect, some of these columns achieved substantial or advanced damage.

Infill wall mechanical properties affect the performance assessment of the structures. Perrone et al. (2017) performed a parametric study to determine the effect of the masonry infill's mechanical and geometrical characteristics on the response of a structure. The seismic behavior's capacity, ductility, and collapse mechanisms have been investigated. The results indicated that prior to proceeding with the seismic vulnerability evaluation of existing buildings, the mechanical characteristic of masonry infills should be thoroughly investigated since they have a substantial effect on the global performance of reinforced concrete frames.

In Kareem & Güneyisi's (2019) study, the data revealed that the placement of the infill walls across the elevation of the frame significantly affected the structural performance. In the instance of infills that were terminated at the ground level, capacity degradation was found to be particularly severe.

1.2.2 Effect of Infill Walls on Fundamental Period

Even though the fundamental period appears to be one of the most crucial factors for the seismic design of buildings using the modal superposition technique, the ideas for its calculation currently available in the literature are often contradictory, making their use unclear. Furthermore, most of these suggestions ignore the existence of infill walls in the structure, regardless of the fact that infill walls enhance the structure's rigidity and weight, causing considerable changes in the fundamental period range of values. The fundamental period of vibration is governed by mass distribution and structural stiffness. As a result, the existence of non-structural components that may cause these characteristics to vary should be carefully examined.

As it directly influences structural stiffness, the masonry infill walls generate a considerable change in the structure's fundamental period of around 15% to 50%. In

addition, the influence of material classes on the fundamental period was studied and found to range between 5 and 10 percent for all material categories (Dilmac et al., 2018).

1.2.3 Effect of Infill Walls on Target Displacement

In Kameli et al., (2011) study a multilayer perseptron (MLP) employing Levenberg-Marquardt (LM) backpropagation algorithms and a Radial Basis function (RBF) were trained to predict roof displacement and base shear. Eight hundred fifty-five model data sets were used for modeling neural networks using the finite element approach (FEM) with six parameters, including the number of bays, stories, masonry infill thickness, infilled wall ratio, presence of soft stories, and spectral design acceleration. Findings show that MLP and RBF ANNs for target displacement prediction have low error and fast speed. Compared to MLP networks, RBF trains data faster.

As a result of the existence of the infill walls, the displacement at the top storey reduces from 25.87%, 24.62%, and 17.1% to 16.01% for five, seven, nine, and eleven stories respectively, compared to the bare frame. And findings indicate that the stiffness of infill walls is effective for medium and low-height structures (Parsaeimaram et al., 2013).

In Dilmac et al., (2018) investigation revealed that the infill walls contributed positively to the building's stiffness, roof displacements, and seismic performance.

1.2.4 Artificial Neural Networks

In Charalampakis et al., (2020) study, the prediction of the fundamental period of vibration of masonry-filled RC frame structures was addressed using Machine Learning approaches, the ANN used back propagation algorithm which yielded superior findings compared to the existing literature.

The estimated displacement and base shear values at the performance point for sample buildings using an ANN and considering the effect of infill walls differ from the actual values by a maximum of 4.89% and 2.04%, respectively. Where results demonstrated that ANN predictions were accurate (Parsaeimaram et al., 2013).

In Alshaer, (2016) study it was discovered that shear wall ratio is the most influential structural component. It was discovered that the projections in plan and slab discontinuities were the least important characteristics. According to the research, the prediction accuracy of ANN as 90% accurate for nonlinear (pushover analysis technique) and about 89% accurate for linear performance analytical approach.

As in Asteris et al., (2016) study, ANNs were utilized to predict the fundamental period of infilled RC structures. A large data set was utilized for training and validating the ANN based on a careful examination of the factors that impact RC structures' fundamental period. A new heuristic algorithm was suggested. The fundamental period values predicted using multilayer feed-forward neural networks were near to the precise findings, as proven by mean square error.

1.3 Aim and Scope

This work aims to establish a technique for quickly estimating the structural performance, fundamental period of vibration, and target displacement of reinforced concrete framed buildings using various infill materials. The research will also examine the positive and negative effects of infill walls in buildings.

The following methodology will be used: Previous work conducted on artificial neural networks, the effects of infill walls. The performance of structures will be assessed using pushover analysis. The artificial neural network that will be established will use

a set of input parameters and outputs for training, testing, and validation. Input parameters include plan symmetry, the width of the building in x and y directions, columns ratio, shear walls ratio, layout of the infill walls, infill wall material type, peak ground acceleration, and soil type. The outputs are the performance level of the structure, the fundamental structure period, and target displacement. Therefore, the ANN models will estimate the three outputs mentioned using various infill wall materials for quick assessment.

1.4 Organization of the Thesis

This research is divided into six main chapters, which are:

The current chapter provides background information, a broad review of the topic, and a look at recent research findings in the field. Similarly, state the study's objectives and scope.

The second chapter illustrates the Turkish Earthquake Design Code improvements, seismic analysis procedures, building performance assessment with the Turkish Seismic Code for Buildings 2018 (TSCB-2018), and infill walls modeling techniques.

The third chapter provides definitions of artificial neural networks, explaining their architecture, functions, and training methods.

The fourth chapter is about research methodology, addressing the research approach, input parameters, buildings design, adaptive pushover analysis adopted, and ANN definitions.

The fifth chapter presents performance analysis results and discussions by presenting the building's capacity curves, performance levels, fundamental period, target displacement, and the ANN models outcomes.

The sixth chapter provides a concise review of the study and focuses on the findings it obtained. In addition to the limitations of this research, some insights for future studies are presented.

Chapter 2

ANALYSIS METHODS AND MODELING OF INFILL WALLS

2.1 Introduction

Because of its nonlinear behavior, the infilled wall is mainly ignored throughout the assessment. The most fundamental reason for the nonlinear action of infilled frames is material nonlinearity, which necessitates a very complex computational approach for structural design. In contrast, infill walls in reinforced concrete buildings can significantly increase the structure's frame's strength, hardness, and energy dissipation. (Kumar et al., 2018). This chapter includes selected modeling techniques for the infill walls, the codes used, and the nonlinear analysis method adopted for assessing the structures.

2.2 Seismic Analysis Procedures

Engineers use linear analysis, which is a quicker approach and needs less computational time, to design structures such that stress concentration within the structural components does not surpass the yielding stress of the structural materials. However, with unexpectedly large loads (such as seismicity of high magnitude), the stresses within the structural components may be greater than the yield stress of the building material, leading the structural elements to behave nonlinearly. Thus, scientists have created analytic techniques capable of simulating the varied behaviors of structural components within a particular structure, both linearly and nonlinearly.

All contemporary codes have offered four alternative analysis approaches within the Performance-Based Engineering (PBE) framework, with only little variances between them. Firstly, a static analysis method is called the Linear Static Procedure (LSP), which does not include the variable load. Secondly, The LDP (Linear Dynamic Procedure) is basically the Response Spectrum Method (RSA). The Nonlinear Static Procedure (NSP) is the third method, also known as the well-known Pushover Analysis, which may be used in either conventional or adaptive mode. The Nonlinear Dynamic Procedure (NDP) is the fourth, also known as the Nonlinear Dynamic Time-history Analysis.

2.2.1 Linear Static Procedure

With the Linear Static Procedure, a structure that is linear and elastic all across the evaluation receives a triangular force distribution that resembles the seismic loading. The foundational principles of elasticity are applicable, the building's stiffness is maintained, and an irrational, linear force vs. displacement curve is produced as the load increases. In order to account for the drop in stiffness caused by this inelasticity, a lower stiffness is used for the analysis (in a fundamental, almost simplistic approach) since it is implicitly expected that the structure would sustain damage during a significant seismic event. After comparing the action consequences from the analysis to the members' capabilities, always within terms of forces, the structure is deemed safe if the capacities exceed the demands.

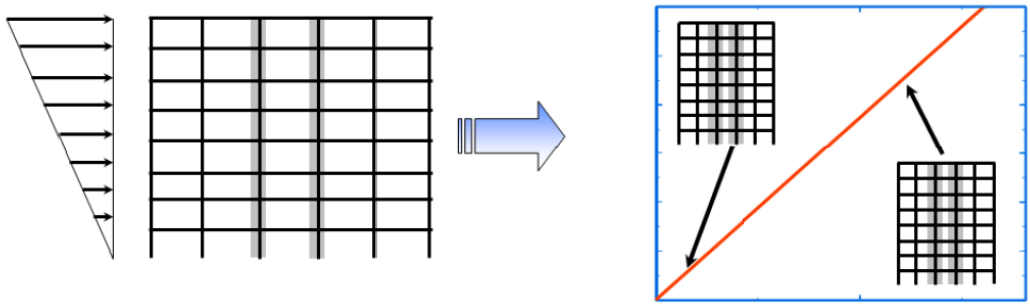

Figure 1: Linear static procedure. (Antoniou, S, 2022)

2.2.2 Linear Dynamic Procedure

The LDP and LSP are comparable in model behavior. Elasticity laws apply, and stiffness doesn't degrade throughout analysis. The approach is more complicated since the pattern of the lateral loading is no longer arbitrary but determined as a combination of the structure's modes. If the structural members' action effects are less than their force capacities, the structure is safe. The Linear Dynamic Procedure is commonly used to design new structures, thus engineers are more acquainted with it.

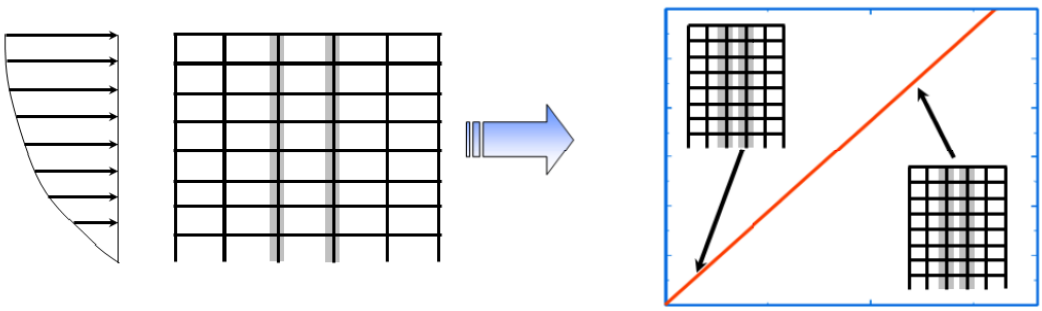

Figure 2: Linear dynamic procedure. (Antoniou, S, 2022)

2.2.3 Nonlinear Static Procedure

The structural behavior is no longer linear in the Nonlinear Static Procedure, and the elasticity laws no longer be held valid. The relationship between stresses and strains, forces, and displacement, and bending moments and curvatures is not linear. There are

various alternative force distribution types that may be used to apply a lateral force profile that roughly matches the seismic loading, including triangular, uniform, modal, and even adaptive patterns that vary from step to step. As plastic hinges form at the regions of structural damage, the structural and component stiffness is therefore no longer constant but is instead updated at every step, causing the structure to progressively soften. Due to the structural deformations increasing disproportionally with the degree of lateral loading, the force vs. deformation curve, or so-called capacity curve, is no longer linear and now has a parabolic shape. In other respects, when going farther into the inelastic region, the rise in the deformations becomes bigger for a given degree of load increase.

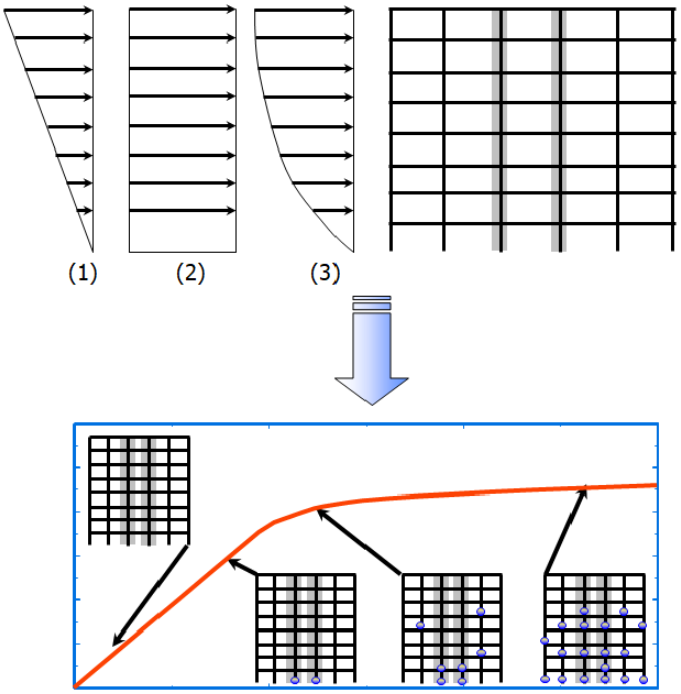

Figure 3: Nonlinear static procedure. (Antoniou, S, 2022)

By evaluating and taking into account the actual deformation and strength capacities of the structural parts and comparing those capacities with the demands at the relevant performance levels, pushover analysis aims to evaluate the structural performance.

Important response characteristic information is given which is not possible to obtain using more traditional elastic approaches (either static or dynamic). Pushover analysis may be used to derive the following response characteristics:

- Realistic forces on potentially brittle components, such as axial forces on columns, moment on beam-to-column connections, or shear forces on short, shear-dominated elements.
- Estimates of the inelastic deformation needs of energy-dissipating components.
- Effects of damaged elements on structural stability.
- Identifying crucial locations with substantial inelastic deformations.
- Identifying plan or elevation strength irregularities that modify inelastic dynamic properties.
- Interstorey drift estimates considering strength and stiffness discontinuities. This controls damage to non-structural parts.
- Sequence of member yielding and failure and structural capacity curve.
- Verification of the load path, including structural and nonstructural factors.

2.2.4 Nonlinear Dynamic Procedure

In the Nonlinear Dynamic Procedure, structural response is nonlinear and inelastic, hence forces are not proportionate to deformations. With the NSP, monotonic force displacement curves are no longer adequate for structural modeling, and complete hysteretic principles must be incorporated for all structural elements (or at for those one expect they behave inelastically). Instead of lateral loads patterns, a seismic record is applied to the building's foundation, and then assess structural behavior, member strengths, and plastic hinge formation over time.

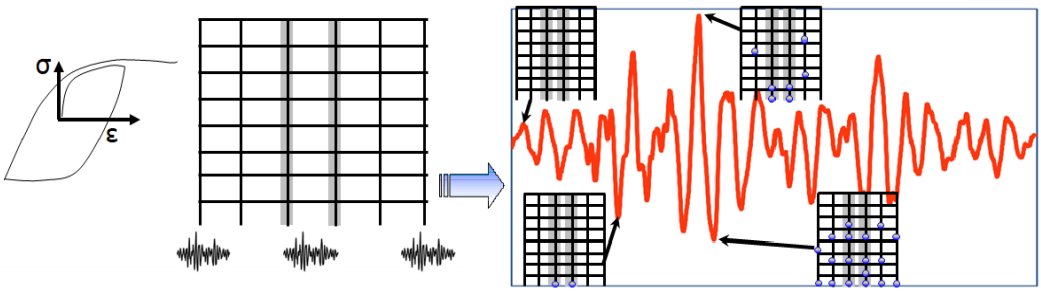

Figure 4: Nonlinear dynamic procedure. (Antoniou, S, 2022)

All Codes prohibit the usage of simpler techniques due to their varying complexity. That is because simple approaches can only approximate the structural behavior of simple structures. Only the Nonlinear Dynamic Procedure may be utilized for any construction and any loading, as demonstrated below. Nonlinear Static Procedure cannot handle complicated seismic loading and higher mode effects since pushover analysis is dependent on the structure oscillating in just the fundamental mode. The Linear Dynamic Procedure cannot handle scenarios with substantial inelasticities, while the Linear Static Procedure can only be used for normal, low-rise structures.

Table 1: Various analytical techniques usage limitations (Antoniou, S, 2022).

Analysis Procedure	Structural irregularity	High Inelastic Demand	Higher mode effects	Near source earthquakes
LSP	✗	✗	✗	✗
LDP	✓	✗	✓	✗
NSP	✓	✓	✗	✗
NDP	✓	✓	✓	✓

2.3 Turkish Seismic Code for Buildings 2018 (TSCB-2018)

There are many active earthquake zones in Turkey, which cause fatalities and significant structural damage. As a result, earthquake-resistant building design has

improved recently, necessitating the development of a new Turkish standard to incorporate information from recent seismic activities and new research findings.

2.3.1 Differences to Previous Earthquake Code

The key differences between the previous code Turkish Seismic Code 2007 (TSC-2007), and the new code TSCB-2018 are summarized below:

- Adding two additional site categories based on how the ground's shear velocity disperses (Z_a, Z_b, Z_c, Z_d, Z_a, Z_e, and Z_f).
- Sorting buildings into distinct categories based on their height above ground level.
- Performance-based design is no longer restricted to elastic spectral design, as was the case under the previous standard.
- The short period and one-second period are used to calculate the spectral acceleration, not the peak ground acceleration.
- Emphasizing the element of seismic forces that decreases ductility.
- Establishing a minimum column and beam dimension of 30 cm.
- Increasing the minimum required concrete C25 compressive strength.
- Specifying in depth the required elastic seismic performance for the structure.
- Instructions for conducting nonlinear pushover and time history analyses are provided in a step-by-step layout.
- Restrictions on the number of chosen recordings and the selection of earthquake records (11 minimum).
- Increasing the confinement of the structural component by tightening restrictions on reinforcing features.

2.3.2 Nonlinear Static Pushover Analysis

The modal displacement during an earthquake is calculated using the maximum displacement of the single modal degree of freedom system, which is shown by the modal capacity diagram. According to the equation below, the nonlinear spectral displacement is the greatest displacement of the modal system with a single degree of freedom.

$$d_{1,max}^{(X)} = S_{di}(T_1) \tag{2.1}$$

Where:

$d_{1,max}^{(X)}$: The maximum displacement of the modal single degree of freedom system.

S_{di}: Nonlinear spectral displacement.

T_1: The first natural vibration period for the lateral force resisting system.

Moreover, the nonlinear spectral displacement for the first natural vibration period for the lateral force-resisting system is represented by the equation below:

$$S_{di}(T_1) = C_R S_{de}(T_1) \tag{2.2}$$

Where:

S_{de}: Elastic design spectral displacement.

C_R: Spectral displacement ratio.

Furthermore, spectral displacement ratio is defined in equation 2.3

$$C_R = \frac{\mu(R_y, T_1)}{R_y} \tag{2.3}$$

Where:

$\mu(R_y, T_1)$: Ductility demand with respect to the yield strength and natural vibration period.

R_y: The yield strength reduction coefficient.

The yield strength reduction coefficient is the yield strength derived directly from the pushover analysis for the strength-based design method, as shown in Equation 2.4:

$$R_y = \frac{f_e}{f_y} = \frac{S_{ae}(T_1)}{\alpha_{y1}} \tag{2.4}$$

Where:

f_e: Demand of elastic strength.

$S_{ae}(T_1)$: Elastic spectral acceleration at the fundamental natural period of vibration.

f_y: Yield strength.

α_{y1}: Yield acceleration.

As shown by Equation 2.5, Considering the equal displacement criteria, the ductility demands of an earthquake is identical to yield strength reduction factor for laterally force-resisting systems that have low stiffness.

$$\mu(R_y, T_1) = R_y \qquad T_1 > T_B \tag{2.5}$$

Moreover, for high rgidity systems lateral force resisting systems the equation given below.

$$\mu(R_y, T_1) = 1 + (R_y - 1)\frac{T_B}{T_1} \qquad T_1 \leq T_B \tag{2.6}$$

Hence, the Equation 2.7 can be derived as follows:

$$C_R = 1 \qquad T_1 > T_B$$
$$C_R = \frac{1 + (R_y - 1)\frac{T_B}{T_1}}{R_y} \geq 1 \qquad T_1 \leq T_B \tag{2.7}$$

Modal displacement versus modal acceleration in terms of coordinates, the modal capacity diagram, and the fundamental vibration mode are all provided. Additionally,

in the figure below with coordinates of spectral displacement versus spectral acceleration a linear seismic spectrum is illustrated on the same chart.

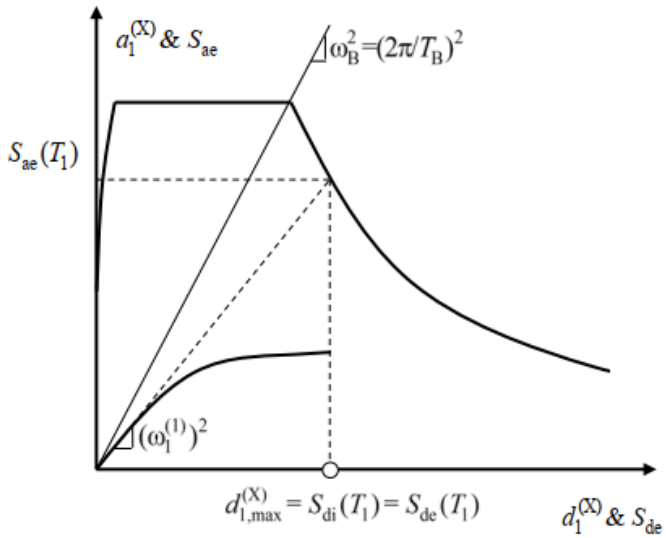

Figure 5: Capacity demand curve (TSCB-2018).

2.4 Building Performance Assessment in Accordance with TSCB-2018

Performance refers to a building's state after a natural disaster, i.e., a degree of damage predicted or a load that could be sustained. Building performance measures how effectively a building meets user demands. Acceptable performance means damage or condition levels that enable continuous facility operation. Design experts utilize performance-based design to develop buildings that safeguard functionality and service availability. The performance of existing structures is correlated to the anticipated internal damage that resulted from applied seismic forces and is classified into four primary damage categories:

1- Limited Damage Performance: Damage to the structural components of buildings that achieve this building performance level is anticipated to be limited, and minimal damage is anticipated for the nonstructural components. In the period following of a

significant earthquake, it is safe to reoccupy a building intended for this performance level. The design of all new hospitals, shelters, and schools should have this as a goal.

2- Controlled Damage Performance: Buildings that satisfy the life safety building performance level may sustain significant damage to both nonstructural and structural components. Before re-occupancy, repairs could be necessary, although in certain circumstances, comprehensive restoration or rebuilding would not be financially feasible. At this desired performance level, there is very little chance of fatalities. This building performance category permits somewhat more severe damage than would be expected for newly built structures intended to withstand earthquakes.

3- Collapse Prevention Building Performance: Although structures that reach this building performance level may represent a considerable risk to life safety due to failure of nonstructural components, it is possible to prevent major loss of life by avoiding the collapse of the complete building. However, many structures created to reach this performance level could end up being a total financial loss. Because it reduces the most serious risks to life safety at the lowest possible cost, this performance level is sometimes used as the foundation for laws requiring seismic restoration. The Collapse Prevention Building Performance Level does not permit continuous occupancy, functioning, or efficient damage repair of structural and nonstructural elements and is primarily meant to avoid the most severe structural failures.

4- Collapse Case: The building is a collapse case if it does not meet the performance level requirements for collapse prevention. In terms of life safety, the building's use in its current state is risked.

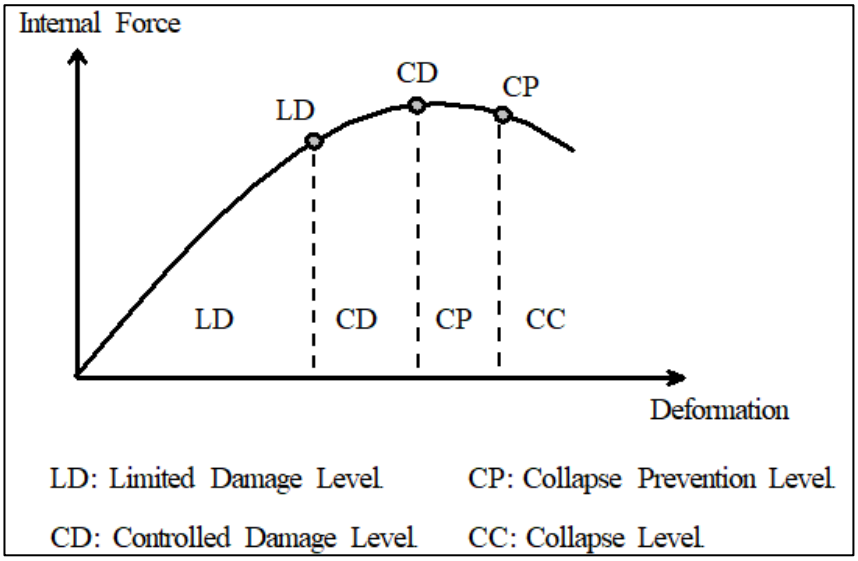

Figure 6: Capacity curve and performance levels (TSCB-2018).

Table 1: Evaluation of structure performance.

Performance Assessment for Limited Damage Level
At most 20% of beams can enter **LD-CD** Region at each story
All other elements shall be in **B-LD** Region
Performance Assessment for Controlled Damage Level
At most 30% of beams can enter **CD-CP** Region at each story
Shear force sustained by vertical elements in **CD-CP** Region shall be below 20%
Shear force sustained by vertical elements in **CD-CP** Region shall be below 40% at top story
Shear force sustained by vertical elements which exceed **LD-CD** Region shall be below 30%
All other elements shall be in **B-LD** or **LD-CD** Region
Performance Assessment for Collapse Prevention Level
At most 20% of beams can enter **CP-C** Region at each story
All other elements shall be in **B-LD**, **LD-CD** or **CD-CP** Region
Shear force sustained by vertical elements which exceed **LD-CD** Region shall be below 30%

2.5 Modeling of Infill Walls

Infilled frames exhibit extremely nonlinear inelastic behavior due to interaction between the infill wall and the adjacent frame, making its analytical modeling a challenging problem. Methods for analyzing infilled frames may be broadly classified into two categories, simplified or macro-models, and local or micro-models, in terms of the number of components they take into account. In the first, a small number of components are used to model an infill wall with the objective of understanding overall physical behavior, whereas in the second, a significant number of elements are examined to simulate local effects exactly by dividing the structure into several segments. Examples of the aforementioned models are equivalent compression struts and the planar finite element modeling.

2.5.1 Micro Models

Mallick and Severn utilized the finite element technique to simulate buildings with infills for the first time in 1967. Due to the composite nature of infilled frames, this model must includes beam or surrounding frame continuum elements, interface, and infill wall continuum components for frame-wall interaction. The finite element model displays local impacts of cracking, crushing, and contacting interaction as well as infilled frame behavior. Input data preparation and analysis take more time than with simpler macro models. Nonlinear infill behavior must be handled by describing constitutive qualities of different components (infill and frame-wall interface elements) for trustworthy results and to minimize wasted computing effort.

2.5.2 Macro Model

The first analytical research to look at the impacts of infill walls were done by Polyakov (1960). He loaded masonry-filled frames laterally for this purpose and looked for the diagonal compression failure mechanism. Then he proposed that a

single diagonal strut working in compression may replace the infill components of frames. A four-node masonry wall element for modeling the nonlinear response of infill walls in framed buildings that was created and first programmed by Crisafulli (1997) and integrated in Seismostruct by Blandon (2005). Six strut members are used to represent each wall; two parallel struts are used in each diagonal direction to transfer axial loads across two opposing diagonal corners, and a third strut is used to transmit shear from the top to the bottom of the wall. This later strut only affects the diagonal that is under compression, hence the wall's deformation controls how it is "activated." The shear strut utilizes a specific bilinear hysteresis rule, while the axial load struts use the masonry strut hysteresis model.

As illustrated in the figure below, to accurately model the contacting points between the infill and frame, definition of four internal nodes is considered. Moreover, to account for the contacting length between the infill wall and frame definition of dummy nodes is carried out. Therefore, the four outside nodes receive the transferred forces from the infill wall and be applied to the adjacent frame.

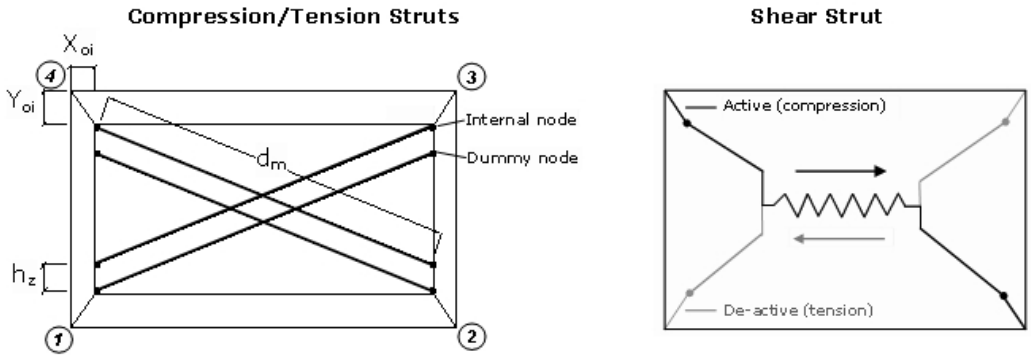

Figure 7: Equivalent diagonal strut and shear strut models for infilled frames (Crisafulli & Carr, 2007).

There are two distinct groups of input parameters model this type of infill element and fully characterize it. The first one concentrates on the mechanical and geometrical parameters, while the second one concentrates on the empirical parameters (Crisafulli, 1997). Seismostruct is a finite element software suite built on a fiber-based meshing and analysis framework. It can predict how space frames would behave when subjected to large displacements under dynamic or static loading. The masonry's material inelasticity and geometric nonlinearities should be taken into consideration.

Geometrical and mechanical parameters:

In order to adequately characterize the behavior of the masonry struts, it is required to take into account a number of mechanical and geometrical parameters. Such as:

- **Compressive strength $f_{m\theta}$:** This is the parameter which, in the basic meaning, controls the compressive resistance of the strut (Zhang, 2006).

- **Elastic modulus E_m:** There is a significant amount of variation in the values of this parameter, which is used to represent the initial slope of strain-stress curve.

- **Tensile strength f_t:** It shows the masonry's tensile strength or the strength of the connection at the contact between the frame and the infill wall. Its presence suggests a broad scope for the concept. However, given that it is substantially lower than the compressive strength and has no effect on the total reaction, it may even be accepted as zero (Varum, 2003).

- **Strain at max stress ε_m:** It indicates the strength level under maximum strain and is affected by changes in the secant stiffness of the stress-strain curve's ascending branch. It has been discovered that the value 0.0012 may provide adequate results (Smyrou et al., 2006).

- **Ultimate strain ε_u:** It may be used to modify the stress-strain curve's decreasing branch. A parabola is used to represent it in order to provide more control over the strut response. For larger values, like 20 ε_m, the compressive strength decline is considerably more gradual. Smyrou et al. (2006) recommend 0.024 as the quantity.

- **Closing strain ε_{cl}:** It helps in the formation of compression stresses. For larger values, the model does not account for such effects. Different numbers between 0 and 0.003 are advised. The models use the value 0.003 (Zhang, 2006).

- **Bond shear strength τ_o and Coefficient of friction μ**: The values for the parameters may be derived using direct shear strength or design standards. Paulay and Priestley reported a value of 0.3 for μ for design reasons and a range of τ_o values between 0.1 and 1.5 MPa (1992). The values 0.3 and 0.7 Mpa have been used to fit τ_o and μ in the models (Smyrou et al., 2006).

- **Maximum shear stress τ_{max}:** It represents the maximum allowable shear stress in the infills and may be anticipated by the typical mechanism of failure using the assumptions brought forward by the modified Mann and Muller's theory (Crisafulli, 1997). One MPa is used as a value (Smyrou et al., 2006).

- **Horizontal and Vertical offset, x_{oi} and y_{oi}:** They are intended to demonstrate how the depth of the structural frame causes the infill wall's size to reduce.

- **Vertical separation between struts h_z:** Crisafulli (1997) suggests contact length values of 1/3 and 1/2.

- **Thickness t_w:** This indicates the wall's thickness. In all models, exterior walls were deemed to be 20 cm thick.

- **Area of strut A_1:** It is the result of the wall thickness and the strut's corresponding width. Typically, this makes about 10% to 25% of the diagonal infill wall. There are several experimental statements for evaluating the equivalent width (Zhang, 2006).

- **Residual Area of the strut A_2:** Once the lateral displacement and subsequently the axial displacement rise as a consequence of infill wall cracking, the length of contact between both the frame and the infill also decreases. The area of an equivalent strut is affected by the increased axial displacement as a result. The residual area value is introduced to the model as a percentage of the starting area with the aim of obtaining variety and taking control of the stiffness differences and axial strength of the strut. The ratio A_2/A_1, which was suggested by Decanini and Fantin in 1986, was used to calculate the residual cracking-related area.

- **Opening:** The effect of the openings was investigated by reducing the originally computed equivalent strut area and stiffness of the infill walls as well (Zhang, 2006).

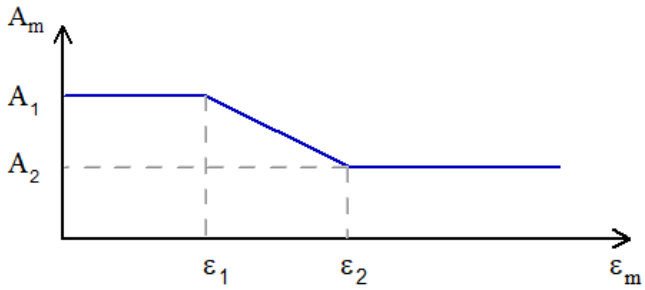

Figure 8: Area versus axial strain of the infill wall (Smyrou et al., 2006).

Empirical Parameters:

In the model where numerous experimental parameters were involved, a definition is required. The definitions are briefly described here.

- γ_{un}**:** This alters the internal cycles but not the envelope and explains the unloading modulus in proportion to E_{mo}.

- α_{re}**:** This calculates the strain at which, after unloading, the loop hits the envelope.

- α_{ch}**:** This calculates the strain at which the reloading curve inflection point, which regulates loop fatness.

- $\boldsymbol{\beta_a}$**:** This discusses the auxiliary point that is utilized to describe the plastic deformation after beyond the whole unloading.

- $\boldsymbol{\beta_{ch}}$**:** This provides an explanation for the stress that's been generated on the inflection point being shown by the reloading curve.

- $\boldsymbol{\gamma_{plu}}$**:** After complete unloading, it describes the modulus of the hysteretic curve at zero stress in proportion to E_{mo}.

- $\boldsymbol{\gamma_{plr}}$**:** This explains the modulus of reloading after the full unloading.

- $\boldsymbol{e_{x1}}$**:** This takes the control of the effect of ε_{un} in the degradation stiffness.

- $\boldsymbol{e_{x2}}$**:** When the unloading is complete, this parameter raises the strain when the envelope curve is achieved and displays the accumulated damage from numerous cycles. It becomes important when the same inner loops have repeated successive cycles.

- $\boldsymbol{\gamma_s}$**:** This shows the wall stiffness ratio on shear spring.

- $\boldsymbol{\alpha_s}$**:** The reduction shear factor displays the ratio of the maximum shear stress to the wall's average stress.

Chapter 3

ARTIFICIAL NEURAL NETWORKS

3.1 Introduction

This chapter introduces the neural networks, provides an overview of the ANNs, explains the network's architecture and designs, and explains the weights of an ANN. Moreover, commonly used activation functions are described in addition to the training methods.

3.2 Artificial Neural Networks Overview

Inspired by the biological nerve system, a neural network connects essential parts functioning simultaneously across several processing layers. The input layer, one or even more hidden layers, as well as an output layer, comprise the network. There are multiple nodes, or neurons, in each layer. The nodes in every layer utilize the outcomes among all nodes in the preceding layer as inputs, whereby all neurons are interconnected via the layers. Typically, each neuron is allocated a weight that is altered throughout the learning process and drops or increases in weight affect the signal strength of that neuron. Changing the weights (connection values) may train a neural network to carry out a particular task (Sivanandam et al., 2006).

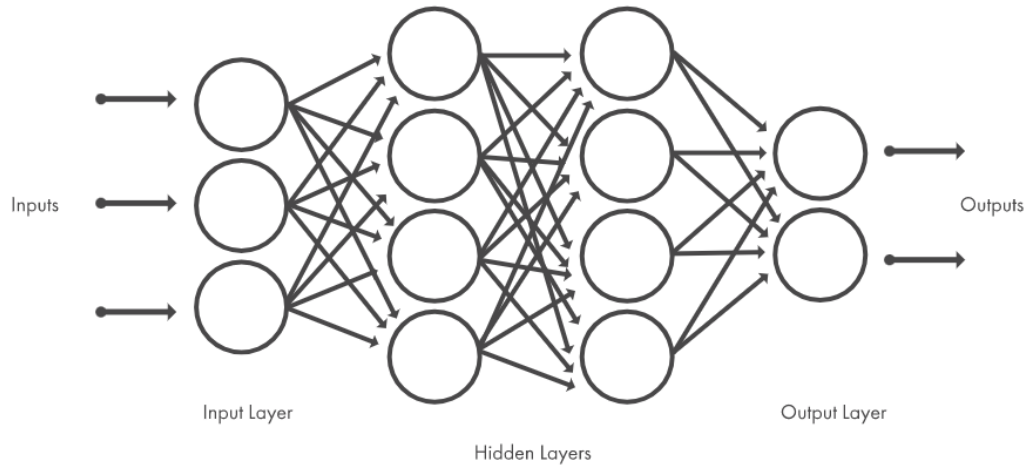

Figure 9: Architecture of a typical neural network (MathWorks. 2018).

The primary objective of network training is to lower output errors by controlling the weights of the neural network model. Due to the nonlinearity of the model parameters and the need for a nonlinear algorithm, backpropagation the most prominent learning technique. A minor downside is that the strategy is slower owing to its learning rate (Setyawati, et al., 2002). In contrast, they conducted two trials that involves with variables and matching datasets training in order to compare regression analysis and the ANN. Therefore, it was determined that the best ANN model outperformed the best linear regression model.

Recognition system, identification, classifying, communication, vision, and control mechanisms are just a few of the complicated tasks that neural networks have already been trained to carry out. It is also possible to train neural networks to tackle issues that are challenging for either humans or traditional computers to understand. Fundamental components of an artificial neural network are architecture of the network, setting the weights and activation function.

Vafaei et al. (2018) have examined the capabilities of neural networks in dealing with extreme nonlinear relations such as the values of strain measured and the applied load.

Information-processing models known as ANNs are trained to work with a particular application. Therefore, to increase the computational effectiveness, a trained ANN may be used as a metamodel of a numerical data analysis process by quickly mapping a given input into the required output values (like curve fitting processes). Keeping in mind that the validation and training date conditions must include the complete range of input parameter values, a trained ANN has a significant computational effectiveness advantage over traditional numerical analytic techniques like regression analysis (Asteris et al., 2016).

3.3 Architecture of the Network

The architecture of the network is the layout of neurons into layers and the pattern of connection within and between layers. Neurons within a layer are either completely linked or not interconnected. The number of layers in the network may be described as the number of layers of weighted linked linkages between each neuron slab. If two layers of linked weights are present, it is determined that there are hidden layers. There are several types of network designs, including feedforward, feedback, completely linked network, and competitive network, among others (Sivanandam et al., 2006).

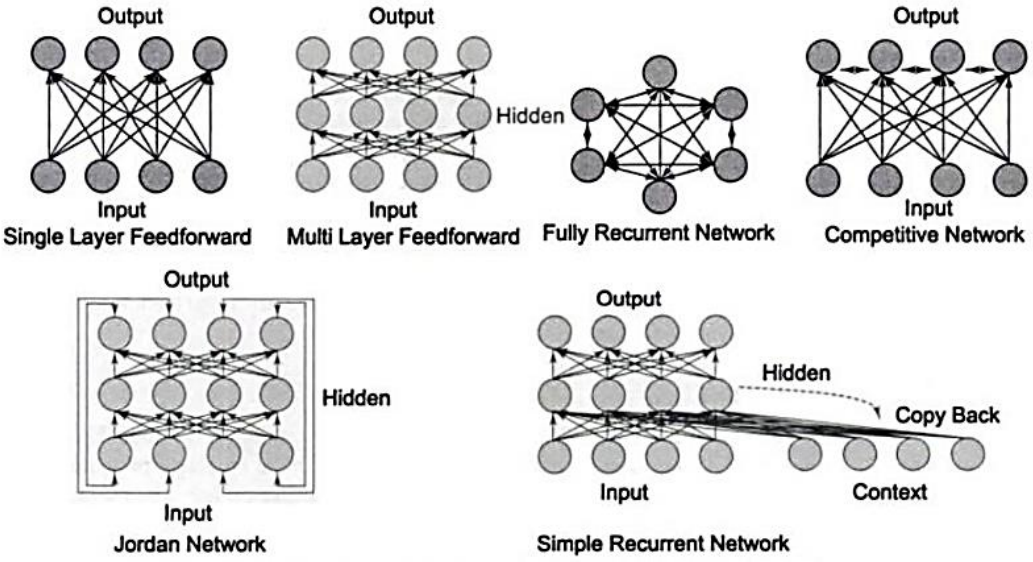

Figure 10: Connection structures of some ANN (Sivanandam et al., 2006).

3.3.1 Feedforward Net

Feedforward networks might just have a single weight layer in which the inputs are directly coupled to the outputs, or many layers with hidden unit sets in between. Neural networks build internal representations of input patterns using hidden units. Given enough hidden units, it has been shown that arbitrary functions may be approximated by a simple feedforward network. This discovery has inspired individuals to use neural networks to tackle a variety of problems (Samarasinghe, 2016).

1. **Single layer net:** That is a feedforward network with just a single layer of weighted linkages. Inputs may be completely coupled to output units. However, there is a possibility that none of the input or output units are coupled to other input or output units.

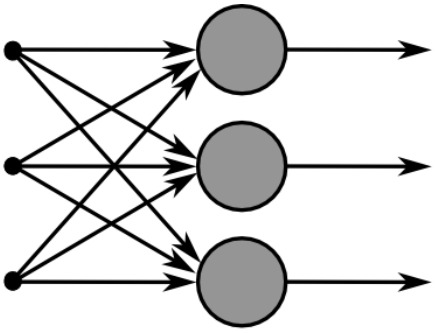

output layer

Figure 11: Single layer neural network (Chrislb, 2005).

2. **Multilayer net:** it is also a feedforward network, i.e., the network in which signals flow forward from the input units towards the output units. There are one or even more layers of nodes here between input and output units in the multilayer network. This is preferable to a single-layer network because it may be utilized to handle more complex problems.

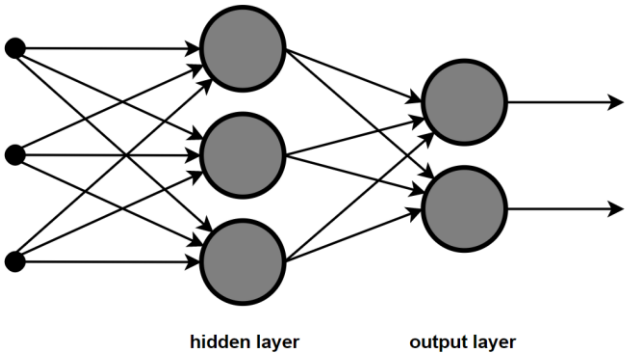

Figure 12: Multilayer neural network (Chrislb, 2005).

3.3.2 Competitive Net

The competitive net is comparable to a feedforward network with a single layer, except that there are often negative connections between the output nodes. As a result of these linkages, output nodes tend to compete with one another to reflect the current input pattern.

3.3.3 Recurrent Net

The fully recurrent network is possibly the simplest architecture of neural network. Every unit is linked to every other unit, and every unit serves as both input and output. Recurrent networks are also advantageous since they can handle sequential information.

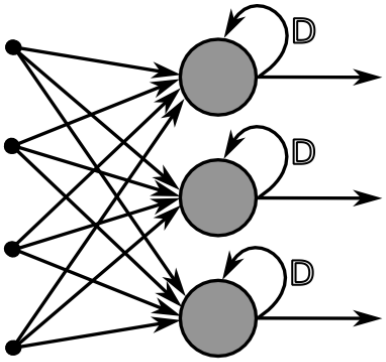

Figure 13: Structure of a recurrent neural network (Chrislb, 2005).

3.4 Setting the Weights

The way of establishing the weights' values facilitates the learning or training process. Training a network is the act of altering the weights of the connections among network layers in order to get the desired output. Learning is the internal process that occurs when a network is taught. Typically, there are three forms of training which are supervised training, unsupervised training and reinforcement training (Sivanandam et al., 2006).

Its efficiency is highly dependent on the quality of the dataset utilized for its initial training. Owing to the unavailability of a specific criterion in the training procedure, training is conducted in an iterative way. The ANN output is compared to the output

supplied. If the divergence seen between ANN output and the given output is acceptable, iteration terminates (Kose, 2009).

3.4.1 Supervised Training

Supervised training is the process of delivering a series of sample inputs to the network and comparing the output to the predicted answers. Training will continue until the network can provide the desired answer. In a neural network, target output vectors may exist for a series of training input vectors. The weights may then be modified using an algorithm for learning. This is known as supervised training.

3.4.2 Unsupervised Training

If the intended output is unknown for such training input vectors in a neural network, the training process is referred to as unsupervised training. The net may adjust the weight such that the input vector with the greatest similarity is allocated to same output unit. Unsupervised networks are significantly more complicated and challenging to implement.

3.4.3 Reinforcement Training

In this approach, it is presumed that a teacher is present, but the correct response is not given to the network. However, the network is just informed about whether the output response is correct or incorrect. The network should then make use of this data to enhance its performance.

3.5 Activation Functions

In the absence of an activation function in a neural network, the output signal would seem to be a simple linear function with a degree of one quadratic. Although linear equations are simple and straightforward to solve, their complexity is restricted, and they cannot adapt or detect complicated mappings from data. Almost all of the time, a Neural Network without such an activation function performs as a Linear Regression

Model of low performance and capability. It is preferable for a neural network to not only train and estimate a linear function, but also handle more complex tasks, such as modeling complex sorts of input, such as photos, videos, audio, voice, and text. That's why users employ activation functions and artificial neural network methodologies such as Deep Learning, which make sense of complex, high-dimensional, and nonlinear datasets in which the model has multiple hidden layers and a complicated architecture for retrieving information, which is indeed our ultimate objective (Sharma et al., 2020).

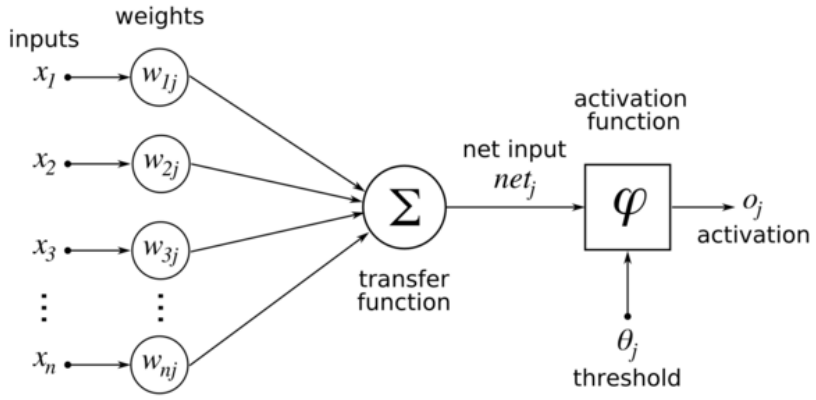

Figure 14: Artificial neuron diagram (Chrislb, 2005).

Therefore, in order to make the network dynamic, one must apply an activation function to it. This gives the network the capacity to extract difficult information from data and to express nonlinear complex randomized functional mappings among input and output. Therefore, one is able to do nonlinear mappings between inputs to outputs by introducing nonlinearity to the network with the assistance of nonlinear activation functions. Differentiability is an important characteristic of an activation function. An activation function must be differentiable in order to be able to implement a backpropagation optimization strategy. This allows to compute the errors or losses

with respect to the weights, and eventually optimize the weights utilizing gradient descend or other optimization technique to reduce errors.

Types of activation functions, where first three are the most commonly used:

1. Binary Step Function.
2. Linear.
3. Sigmoid.
4. Hyperbolic tangent function Tanh.
5. Rectifier ReLU.
6. Leaky ReLU.
7. Parametrized ReLU.
8. Exponential Linear Unit.
9. Swish.
10. SoftMax.

3.5.1 Binary Step Function

The binary step function is now the most used kind of activation function, and it may be built in Python via the use of standard if-then clauses. When building a binary classifier, binary activation functions are often used as one of the methods. However, the binary step function cannot be applied in this situation since the carryable in question is multiclass. Additionally, the gradient of the binary step function is zero, which implies that the derivative of f(x) with respect to x is equal to zero. This might provide an issue for the backpropagation step since it indicates that the derivative is equal to zero.

$$f(x) = \begin{cases} 1, & if\ f(x) \geq \theta \\ 0, & if\ f(x) < \theta \end{cases} \tag{3.1}$$

where,

θ: is called threshold which is a factor that is used in the activation calculations for a given net. Where, outputs depend on the value of this factor.

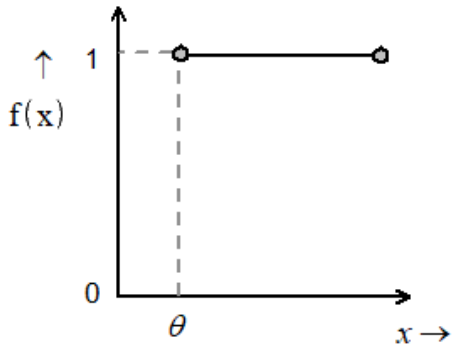

Figure 15: Binary step function (Sivanandam et al., 2006).

3.5.2 Linear Function

The linear activation function has a response which is proportionate, or directly proportional, to the input. The fact that there was no x component in the binary step function meant that its gradient was always zero. This was the binary step function's most significant shortcoming. Utilizing a linear function is one option for getting rid of that problem. The function is defined as follows:

$$f(x) = ax \tag{3.2}$$

Where the variable “a” value might be any constant that the user defined. In this case, the derivative of the function f(x) is not zero; rather, it corresponds exactly to the value of the constant that was used. Because the gradient is not zero but a constant value that is independent of the input value x, it appears to follow that the weights and biases would be adjusted during the backpropagation step even though the updating factor will remain the same. Since the gradient is not zero but a constant value, it follows that the gradient is independent of the input value x. Using a linear function would not provide a significant advantage since the neural network will not reduce the error because the value of the gradient would remain the same during each iteration. In

addition, the network will be unable to recognize intricate patterns within the data that is provided. Hence, linear functions are perfect for straightforward endeavors and situations where interpretability is essential.

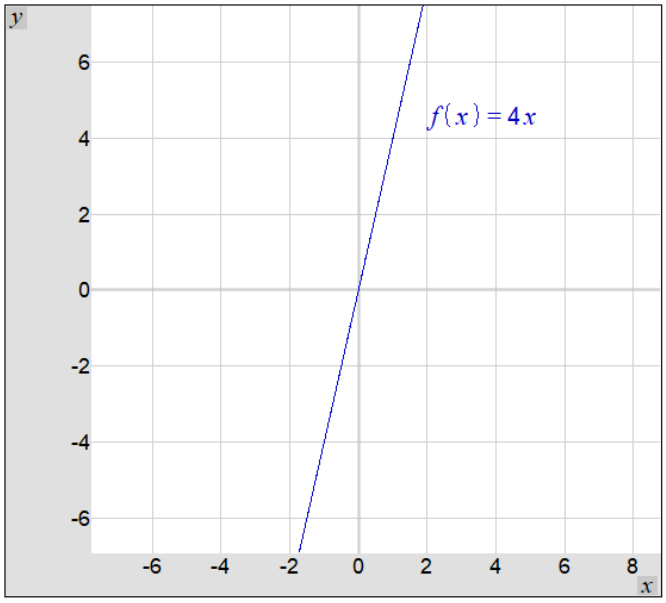

Figure 16: Example of a linear activation function (Sharma et al., 2020).

3.5.3 Sigmoidal Functions

Typically, these functions take the form of an S-shaped curve. The hyperbolic and logistic functions are often used. These functions are used by multilayer networks such as backpropagation networks, radial basis function networks, and others. Due to the fact that it is a nonlinear function, the activation function is often used. The Sigmoid function is used to modify values ranging from 0 to 1. And the function can be defined as follows:

$$f(x) = \frac{1}{1 + e^{-\sigma x}} \tag{3.3}$$

where,

σ: is called steepness parameter.

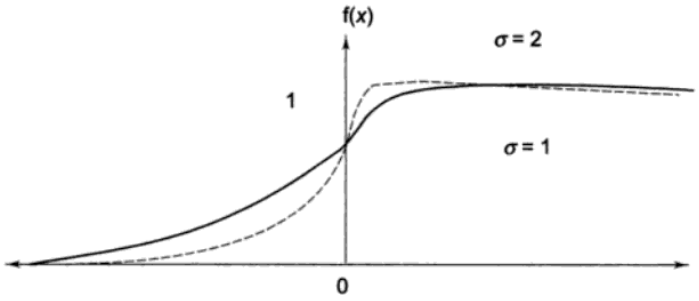

Figure 17: Sigmoidal function (Sivanandam et al., 2006).

3.6 Training Methods

An approach for training creates a decision function that modifies the network's weights. The training algorithms come in a wide variety. The algorithms modify the weights and biases of the network in order to convert arbitrary inputs to outputs in an accurate manner. There are plenty of training methods such as Gradient Descent, Conjugate Gradient, Quasi-Newton, Resilient Backpropagation, and Levenberg-Marquardt algorithms (Cömert & Kocamaz, 2017).

3.6.1 Back Propagation Learning Methods

During the process of training the network, a backpropagation algorithm makes continual adjustments to the weights and biases of every node. This procedure goes until the network achieves a stable state in which there are no more significant variations in the network weights (Charalampakis et al., 2020).

3.6.2 Resilient Backpropagation

In the process of building multilayer networks, the transfer functions often are transformed into a kind of function known as the squashing function. owing to the fact that the function attempts to condense the infinite data collection into a limited data

set. Because of this, the gradient of the set of data becomes closer and closer to being zero as the input value gets higher. Which will result in very little to no changes in the weights and biases if the iteration process is repeated. Therefore, in order to get out of these issues, resilient backpropagation algorithms have been developed. This technique, on the other hand, eliminates away the value of the derivative but the sign of the gradient is important, as seen in the equation below (Naoum. 2012).

$$dx_{k+1} = (x_{k+1} - x_k)\, sign(\nabla f(x_k)) \quad (3.4)$$

where;

dx_{k+1}: Input data partial derivative.

$sign(\nabla f(x_k))$: Gradient sign (magnitude is not deemed).

3.6.3 BFGS Quasi-Newton Backpropagation

The usage of this training method is to find solutions to nonlinear optimization issues that are not bound by iterative solutions. The Quasi-Newton method is used in this approach. This method seeks for a point on the curve which may be designated by two distinct kinds of functions. Once the gradient approaches zero or in accordance with the user's preferences, then solution has been reached (Dennis Jr and Schnabel, 1996).

$$x_{k+1} = x_k - H_k^{-1} g_k \quad (3.5)$$

where;

H_k: is the Hessian matrix, often known as the second derivatives of the performance index with the weights and biases set to their present values.

x_k: Data point at point k.

g_k: The function gradient.

3.6.4 Levenberg-Marquardt Backpropagation

This approach focuses primarily on minimizing the error caused by the sum of square roots since this quantity acts as a performance function for the model. In contrast to

the Quasi-Newton method, this methodology does not involve the creation of a hessian matrix of the second order. As shown in the equation below, the gradient of this method may be calculated by multiplying the transpose of the Jacobean matrix by the unit vector of the network's error. This strategy has been shown to be effective in reducing error. Calculating the sum of square root error derivative with relation to the network's biases and weight and is the first step in the process of constructing the Jacobean matrix (Sapna. 2012).

$$\nabla = J^{T}e \tag{3.6}$$

∇: The gradient descent coefficient.

J^{T}: Jacobean matrix that is developed due to the derivative of sum of square root error.

e: Network error unit vector.

Chapter 4

RESEARCH METHODOLOGY

4.1 Introduction

This chapter includes the selected building's geometry, plans, materials, and design outcomes. Furthermore, considered infill wall materials and cases are presented. In addition, performance assessment parameters and the ANN model adopted to estimate the structures' fundamental period, target displacement, and performance.

4.2 Research Approach

This study aims to develop an artificial neural network model to predict and estimate three outputs, which are the fundamental period of vibration of the building, target displacement, and seismic performance of the structure. Reinforced concrete residential buildings considered in this study are in Istanbul province, four-story buildings as mid-rise and ten-story high-rise structures. The building plans were selected as regular and irregular, and under different soil types and spectral ground acceleration, the buildings were designed using the Turkish Seismic Code for Buildings (TSCB-2018) and the Turkish Requirements for Design and Construction of Reinforced Concrete Structures (TS-500). Furthermore, a performance assessment of the 336 models is carried out. Data collected from the analysis will be used as inputs to train, validate, and test the ANN model to obtain the outputs with minimal error.

4.3 Input Parameters

In this section, an explanation of the input parameters that were used in the neural network and models are presented. The input parameters are selected from a range of parameters, which are provided as follows:

1- Plan symmetry case (1, 2, 3)

2- Width of building in X direction (21.5m, 25.9m, 16.5m).

3- Width of building in Y direction (14.3m, 13.7m, 9.3m)

4- Number of stories (4, 10).

5- Infill material (1, 2, 3).

6- Infill walls layout (0, 1, 2, 3, 4, 5).

7- Columns ratio.

8- Shear wall ratio.

9- Soil type (ZB, ZC).

10- Peak ground acceleration (0.45g, 0.75g).

4.3.1 Plan Symmetry and Stories Number

Three different plans were selected based on the plan symmetry; where the first one represents a building plan that is symmetric about both the x and y-axis, the second plan represents a building that is symmetric about one axis; and the third plan, where the building has no symmetry about either the x-axis or the y axis.

Table 2: Building plan symmetry summary.

Building Plan Symmetry	**Explanation**
1	Symmetric building plan about x and y axis
2	Symmetric building plan about one axis only
3	Unsymmetric building plan

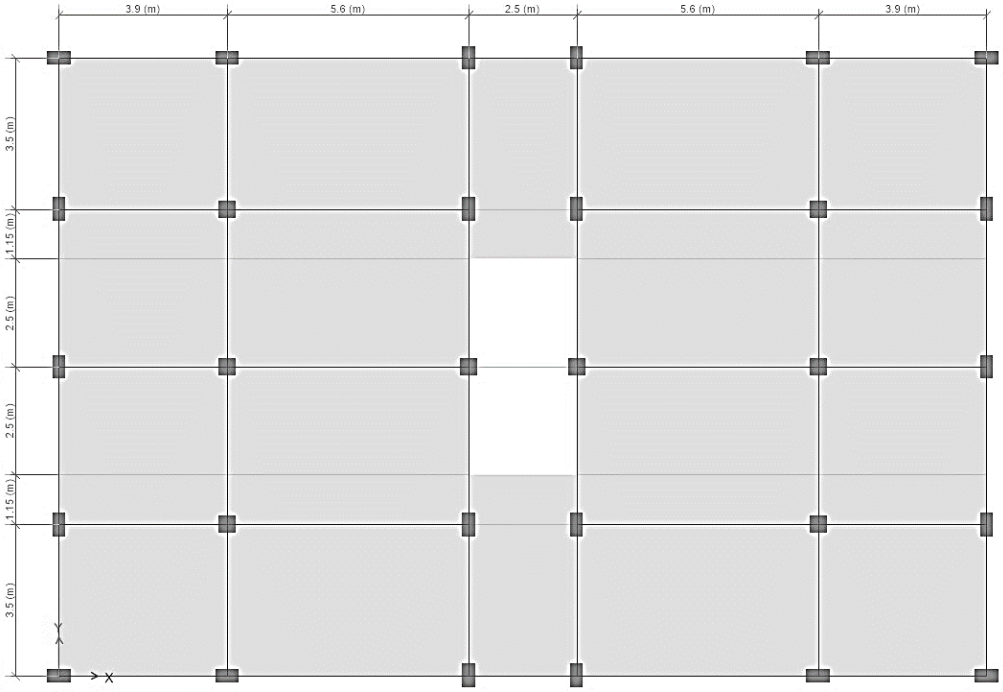

Figure 18: Mid-rise symmetry-1 building plan view.

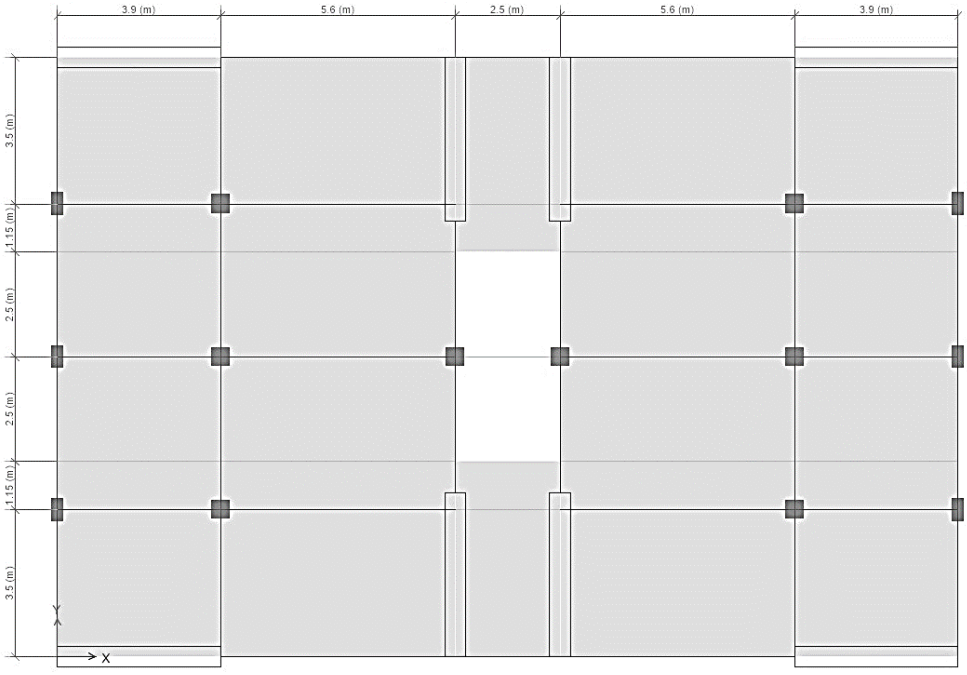

Figure 19: High-rise symmetry-1 building plan view.

Figures 18 and 19 show four-story and ten-story building plans, respectively, with symmetry-1, where the plan is symmetric about both the x and y-axis.

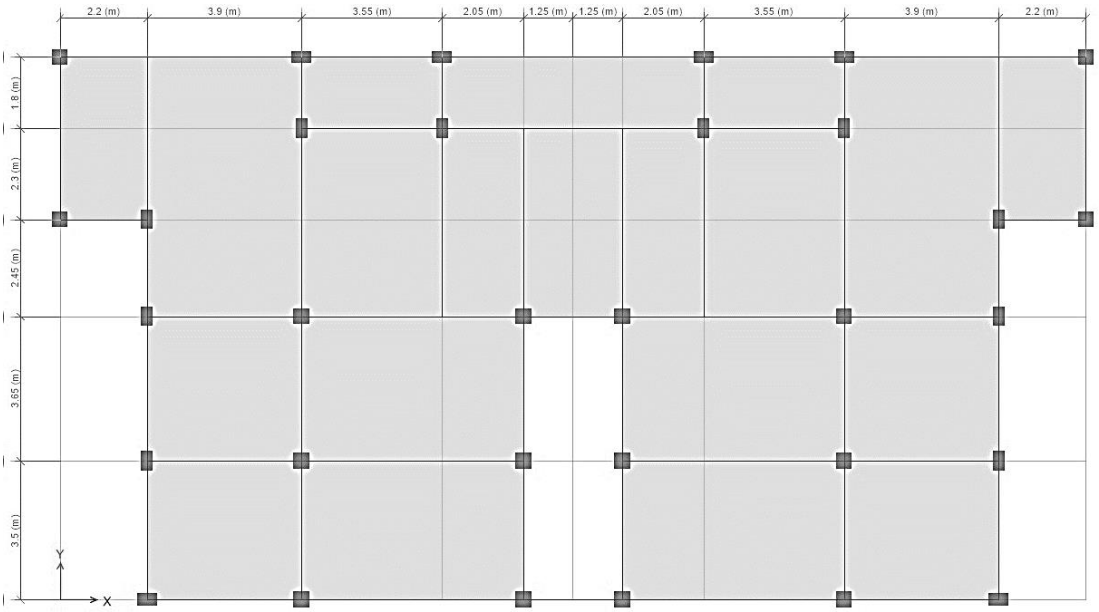

Figure 20: Mid-rise symmetry-2 building plan view.

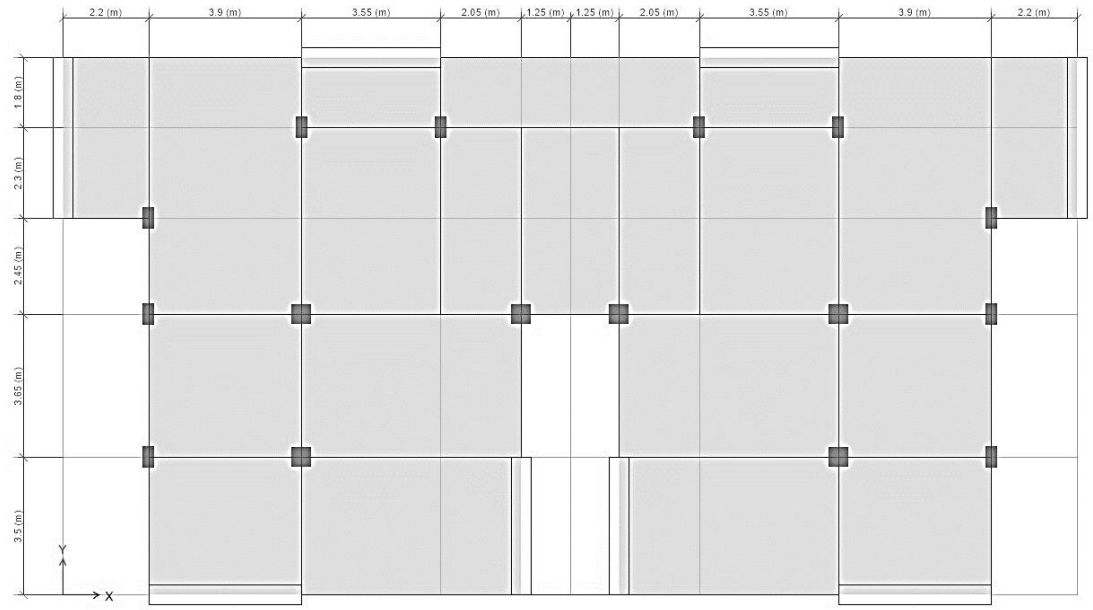

Figure 21: High-rise symmetry-2 building plan view.

The previous two figures (20 and 21) show the four-story and ten-story building plans with symmetry-2, where the plan is symmetric about the y-axis only.

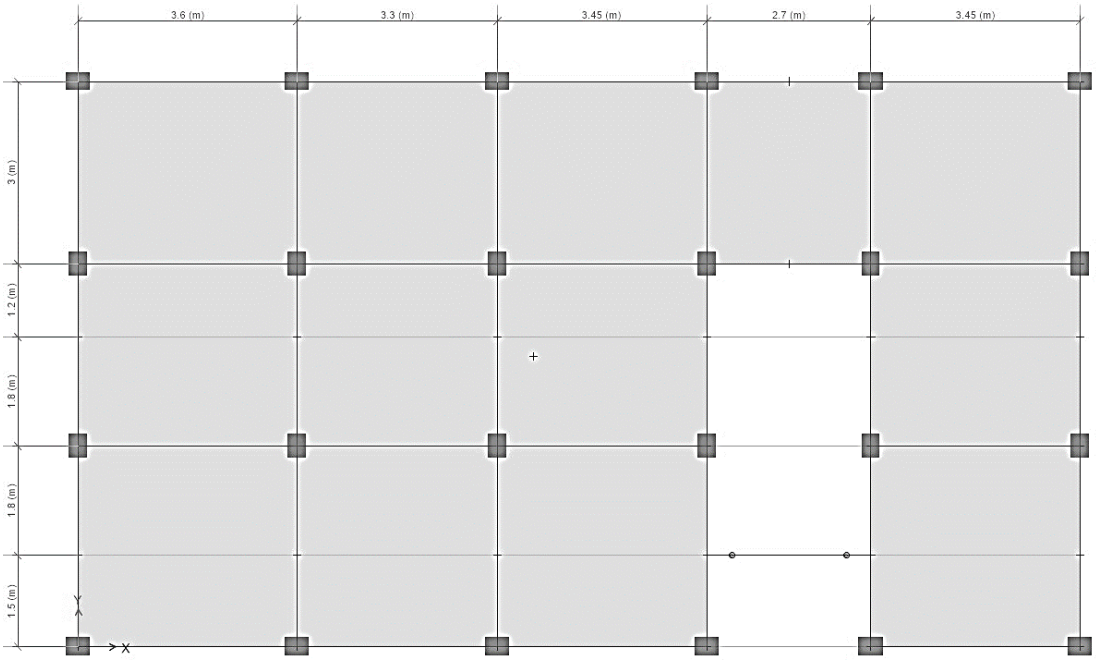

Figure 22: Mid-rise symmetry-3 building plan view.

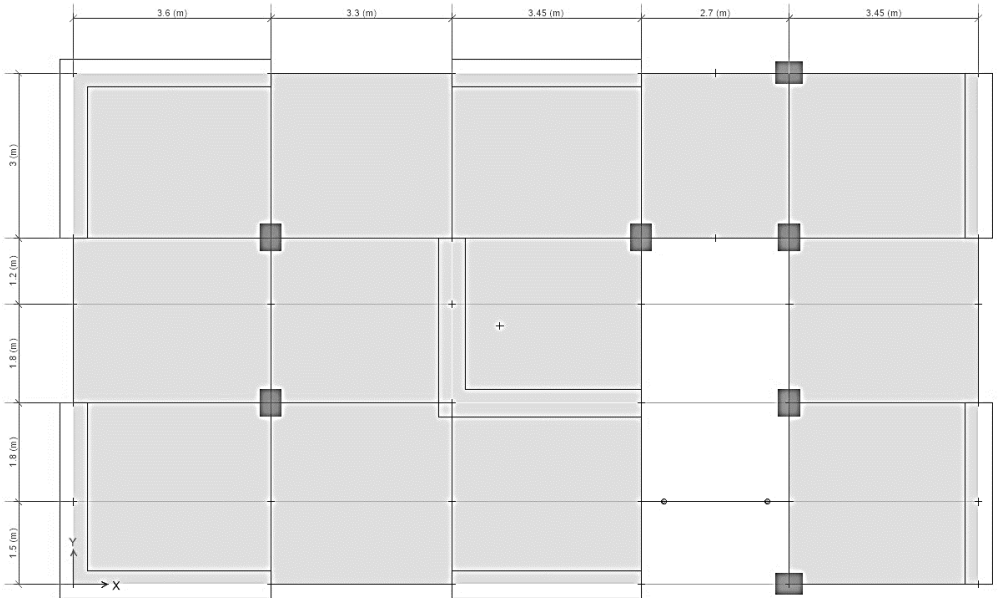

Figure 23: High-rise symmetry-3 building plan view.

Building plans with symmetry-3 are shown in figures 22 and 23, where the plan is not symmetric about either the x or y-axis.

4.3.2 Width of Building in X Direction

The width of the buildings in X direction was used as an input parameter as well, the table below shows this input values for the three buildings cases.

Table 3: Buildings width in x direction.

Building Plan	Building Width (m)
	X direction
1	21.5
2	25.9
3	16.5

4.3.3 Width of Building in Y Direction

Additionally, the width of the buildings in Y direction is being considered as well, the table below shows this input values for the three buildings cases.

Table 4: Buildings width in y direction.

Building Plan	Building Width (m)
	Y direction
1	14.3
2	13.7
3	9.3

4.3.4 Number of Stories

Mid-rise (four stories) and high-rise (ten stories) reinforced concrete residential buildings were considered with a 5 meters base story height, which represents real cases where the ground story is used as shops in practice, and the typical storey height as 3.5 meters.

4.3.5 Infill Walls Materials and Thickness

In terms of infill materials, different materials were adopted as different infill walls materials are used in construction, therefore implementing various materials was necessary, and the compressive strength of each type is tabulated below. Additionally, thickness of the exterior infill walls was selected as 20cm.

Table 5: Infill wall materials compressive strength Šipoš K.T. (2019).

Infill Wall Material	Infill Block Type	Strength Notes	Compressive Strength (MPa)	Brick Illustration
IM-1	Solid	Strong	20	
IM-2	Hollow Clay	Medium	10	
IM-3	AAC	Weak	3	

4.3.6 Infill Wall Layout

In order to study the effects of infill walls on performance, fundamental period, and target displacement, five different layouts of the infills were considered. These layouts consider the regular and irregular distribution of the infill walls in-plan and in-elevation. Each layout is explained in table 6 and sample 3D view of each layout can be seen in figure 24.

Table 6: Infill walls layout considered.

Layout Id	Explanation
IWL-0	Infill walls effect not considered (bare frame)
IWL-1	Infills are in plan and in elevation symmetrically placed in all the floors.
IWL-2	No infill walls in the ground storey while infills are considered in all other stories.
IWL-3	No infill walls in the south and west elevations of the building while infills are considered in all other elevations and stories.
IWL-4	No infill walls in the north, south and west elevations of the building while infills are considered in east elevation only.
IWL-5	No infill walls in the west, south and east elevations of the building while infills are considered in north elevation only.

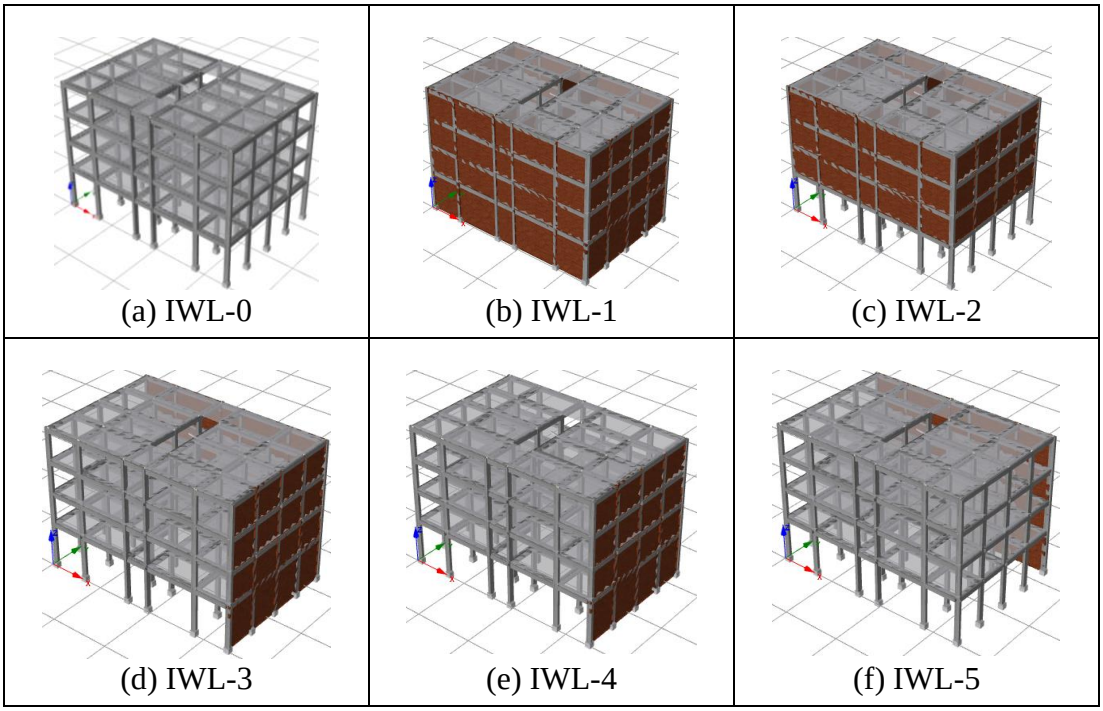

Figure 24: 3D view of the infill walls layouts.

4.3.7 Columns Ratio

The ratio of columns area to floor area (also known as the column ratio) is derived by dividing the total column area in one principal direction by the plan area of the floor.

Table 7: Building plans columns ratios.

Building Plan	**Number of Stories**	**Columns Ratio (%)**
1	4	1.66
	10	0.88
2	4	1.58
	10	1.01
3	4	3.52
	10	1.03

4.3.8 Shear Wall Ratio

Moreover, the shear wall area to floor area ratio (also known as the shear wall ratio) is calculated by dividing the overall shear wall area in one primary direction by the ground floor's plan area.

Table 8: Building plans shear wall ratios.

Building Plan	Number of Stories	Shear Walls Ratio (%)
1	4	-
	10	2.64
2	4	-
	10	2.45
3	4	-
	10	5.72

4.3.9 Soil Type

Selected building location were Istanbul, and two different soil types were considered which are ZB and ZC.

4.3.10 Peak Ground Acceleration

The location selection of Istanbul is considered since it is seismically risky in terms of earthquake hazard. Therefore, to cover a broad range of peak ground acceleration (PGA) selection of 0.45g and 0.75g (2% and 10% of exceedance within 50 years) was made.

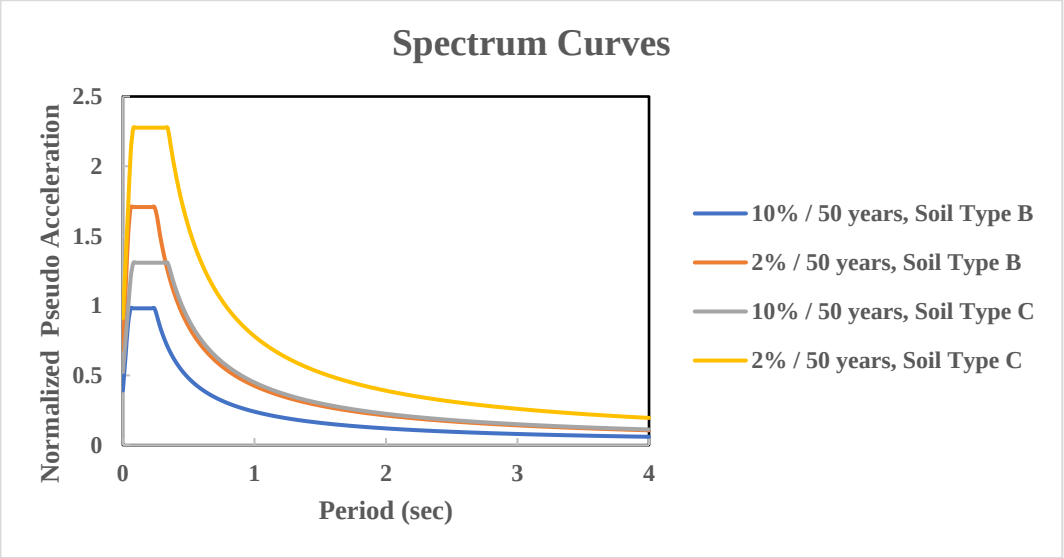

Figure 25: Selected spectrum curves.

4.4 Buildings Design

Other definitions for building design are addressed in this section, such as building materials properties and loads. Moreover, structural members' reinforcement is presented.

4.4.1 Building Materials and Loads

The defined stress strain relationship of concrete and steel are presented in the figures 26 and 27 below. In addition to that, discussion on the improvements of these two models is addressed. Lastly, summary to the building materials (concrete and steel grades), slabs thickness, and vertical loads applied are provided in table 9.

Table 9: Buildings materials and loads definitions.

Parameters	**Value**	**Unit**
Concrete strength	25	MPa
Modulus of elasticity of concrete, E	23500	MPa
Steel tensile yield strength	420	MPa
Slab thickness	20	cm
Additional dead load	1.8	kPa
Live load + interior partition wall load	3	kPa

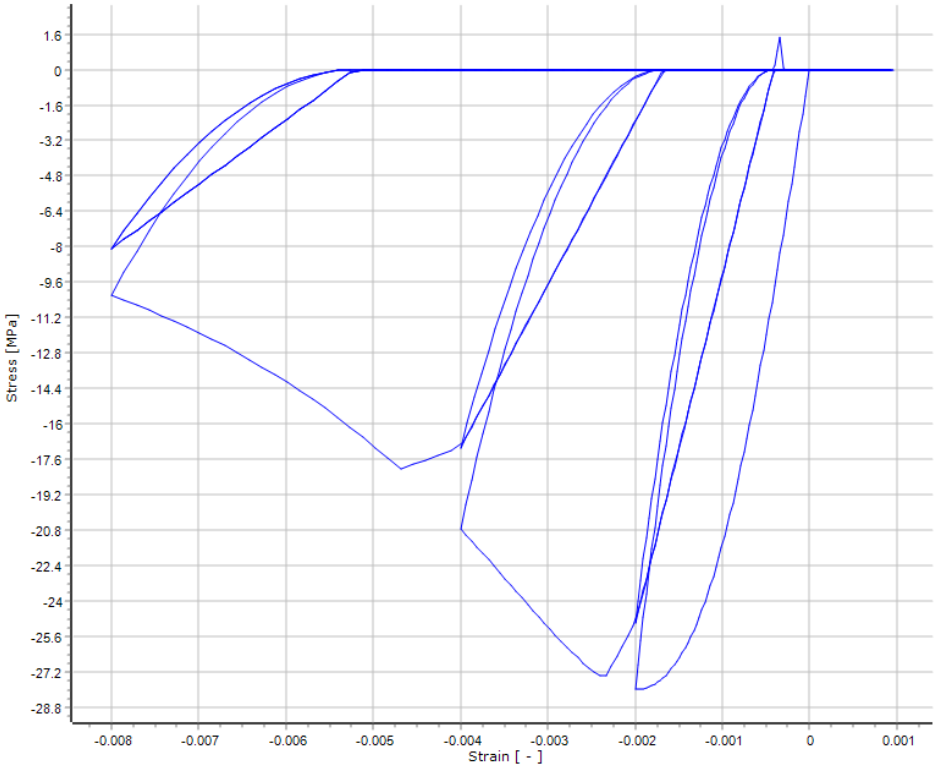

Figure 26: Concrete stress strain diagram.

This uniaxial nonlinear steady confinement model was first developed by Madas (1993) and adheres to the cyclic principles established as Martinez-Rueda and Elnashai (1997) in addition to the constitutive connection presented by Mander et al. (1988). The Mander et al. (1988) principles, which assume continuous confining pressure across the whole stress-strain range, integrate the confinement effects supplied by a lateral transverse reinforcement.

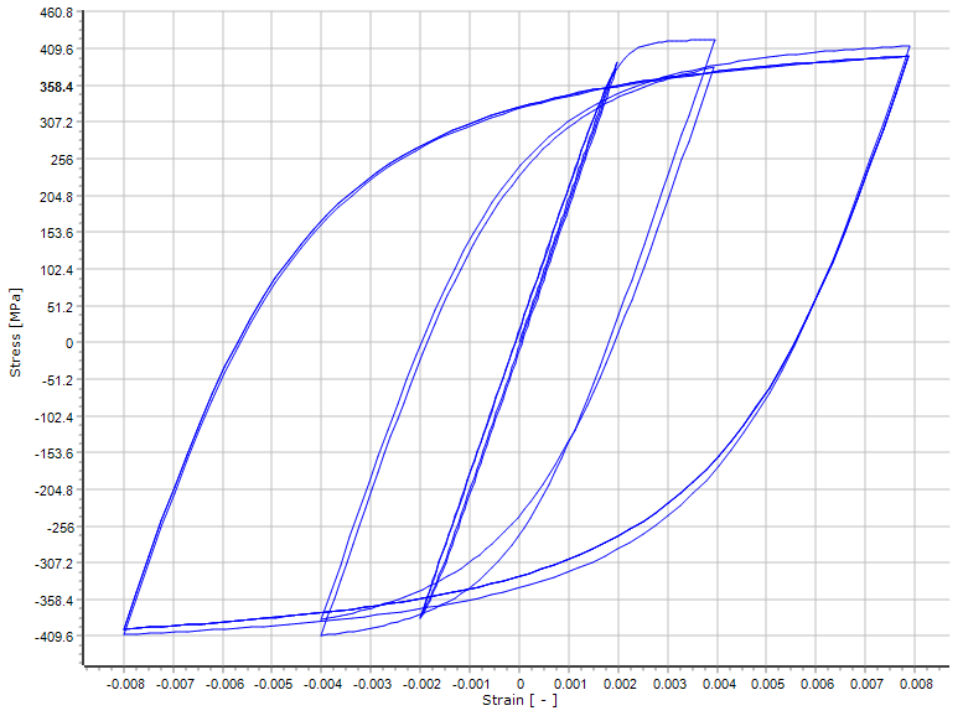

Figure 27: Steel stress strain diagram.

As Menegotto and Pinto (1973) presented efficient and basic stress-strain relationship, Yassin (1994) programmed the first steel model (uniaxial). And established based on proposed principles of isotropic hardening by Filippou et al. (1983). The present system was implemented by Monti et al. (1996). For greater numerical reliability under transient seismic stress, Fragiadakis et al. (2008) proposed a memory rule. It should be used to represent reinforced concrete buildings with complicated loading histories and considerable load reversals. According to Prota et al. (2009), this model, first created for ribbed rebars, may also be used to simulate smooth rebars, typically encountered in existing constructions.

4.4.2 Reinforcement of Buildings with Plan Symmetry-1

Table 10: Structural members sizes and reinforcement of the mid-rise building.

Structural Element	Size (cm)	Reinforcement
Beam	50×30	Start/End: 0.56% Middle: 0.32%
Columns	55×30	Longitudinal: 2.62% Transverse: Ø10/20/10
	40×40	Longitudinal: 1.74% Transverse: Ø10/20/10

Table 11: Structural members sizes and reinforcement of the high-rise building.

Structural Element	Size (cm)	Reinforcement
Beam	50×30	Start/End: 0.54% Middle: 0.28%
Columns	55×30	Longitudinal: 1.35% Transverse: Ø10/20/10
	50×50	Longitudinal: 2.96% Transverse: Ø10/20/10
	45×45	Longitudinal: 2.99% Transverse: Ø10/20/10

4.4.3 Reinforcement of Buildings with Plan Symmetry-2

Table 12: Structural members sizes and reinforcement of the mid-rise building.

Structural Element	Size (cm)	Reinforcement
Beam	50×30	Start/End: 0.56% Middle: 0.32%
Columns	50×30	Longitudinal: 3.11% Transverse: Ø10/20/10
	40×40	Longitudinal: 1.71% Transverse: Ø10/20/10

Table 13: Structural members sizes and reinforcement of the high-rise building.

Structural Element	Size (cm)	Reinforcement
Beam	50×30	Start/End: 0.89% Middle: 0.32%
Columns	55×30	Longitudinal: 3.95% Transverse: Ø10/20/10
	50×50	Longitudinal: 1.22 % Transverse: Ø10/20/10

4.4.4 Reinforcement of Buildings with Plan Symmetry-3

Table 14: Structural members sizes and reinforcement of the mid-rise building.

Structural Element	Size (cm)	Reinforcement
Beam	50×30	Start/End: 0.42% Middle: 0.32%
Columns	50×30	Longitudinal: 3.23% Transverse: Ø10/20/10

Table 15: Structural members sizes and reinforcement of the high-rise building.

Structural Element	Size (cm)	Reinforcement
Beam	50×30	Start/End: 1.06% Middle: 0.30%
Columns	50×40	Longitudinal: 2.83% Transverse: Ø10/20/10

4.5 Adaptive Pushover Analysis

Adaptive pushover analysis is used to estimate a structure's horizontal capacity, taking deformation and input motion frequency into consideration. Adaptive pushover may effectively use deformation profiles in addition to force distributions (Antoniou & Pinho, 2004b; Pinho & Antoniou, 2005). As an analysis tool, it offers more precise results for performance based structural assessment. That is because the lateral load patterns are adjusted considering the modal dynamic characteristics inherenting the drawbacks displacement pushover with fixed pattern. Moreover, in terms of response

estimation this tool offers better results compared to the conventional methods, particularly when the structure has irregularities in its stiffness or strength or when higher mode effects may be present.

Loads are imposed on the structure in an adaptive pushover in a way that is comparable to that of a conventional pushover, with the following differences:

- In adaptive pushover, the inertia mass of the structures must be modeled in order to perform eigenvalue analysis, which is used to update the loading vector. Additionally, and especially in the case of force-based adaptive pushover, the mass must be evenly distributed across the nodes where the incremental loads are to be applied in order to compute the incremental forces, which are determined by multiplying the mass by the acceleration.
- One can use different load values at different nodes, similarly in a conventional pushover analysis, an equal incremental loads values are more preferable and advised to be used as a constant load profile. Therefore, to determine the nodes applied load the spectral shape and modal characteristics of the structure are used.
- SeismoStruct's adaptive algorithm is incredibly adaptable and can take a variety of different parameters to fit the unique needs of each project. Examples include (e.g., Clough and Penzien, 1994; Chopra, 1995) that support both SRSS and CQC modal combination techniques and explicitly state the number of modes to be taken into account.

Because adaptive pushover is an advanced static analysis approach, it necessitates the creation of several new parameters. The following are the parameters:

4.5.1 Scaling Method

Three methods can be used to obtain the normalized modal scaling vector, which is used to determine the shape of the load vector (or load increment vector) at each step: force-based scaling, displacement-based scaling, and inter-story drift-based scaling. The scaling vector reflects the modal force distribution at that step (the scaling vector reflects the modal inter-story drift distribution at that step). Notably, the latter demands that the nominal lateral displacements be supplied in order and cannot be used in 3D adaptive pushover assessments (the 1st-floor load being defined first, followed by the displacement nominal load at level 2, and so on).

4.5.2 Modal Participation Factors and Degrees-of-Freedom

For the calculation of the modes' participation factors, which are needed in the modal scaling vector calculation, definition of degrees of freedom is needed. It is advisable to define multiple translation degree of freedom for a three-dimensional adaptive pushover analysis, for example in x and y directions. Moreover, it is possible to define rotation degrees of freedom as well. Typically, in two-dimensional analysis one translation degree of freedom is defined (Meireles et al., 2006).

4.5.3 Spectral Amplification

For the potential effect of Spectral amplification on the various solutions of modal load vector analyzer shall define this in the program. Moreover, a computation of acceleration response spectrum might be initiated in the program when type of scaling is force based. On the other hand, computation of displacement response spectrum might be initiated in case of scaling in terms of drift. In both cases, one need proper definition for degree of viscous damping where it is constant throughout the analysis and an accelerogram time history.

4.6 Artificial Neural Network

The neural network module from MATLAB 2018 is utilized in this study to build and train the network. A three-layer feedforward artificial neural network architecture is used. A series of layers makes feedforward networks. The first layer has network input. After that, each layer connects to the one below. The last layer generates network output. Feedforward networks can map any inputs to outputs. Furthermore, any finite input-output mapping problem may be solved by a feedforward network with one hidden layer and enough neurons.

The network's main structure is made up of many input cells, many hidden layers set by the user, as well as an output layer, which are all interconnected. The input parameters include plan symmetry, the width of the building in x and y directions, columns ratio, shear walls ratio, infill wall material, infill walls layout, soil type, and peak ground acceleration.

Bayesian regularization backpropagation is adopted for the network training where it uses Levenberg-Marquardt optimization, the weight and bias parameters are updated by the network training function. In order to create a network that generalizes effectively, it optimizes a combination of squared errors and weights while figuring out the ideal combination. In terms of limitations for the Bayesian regularization backpropagation for computations, this function utilizes the Jacobian, which assumes that performance is a mean or sum of squared errors. The mean squared error (MSE) or sum of squared estimate of errors (SSE) performance function must be used by networks trained with this function.

Table 16: Transfer functions and number of used neurons in all ANN models.

Layer	**Number of Neurons**	**Transfer function**
1	10	TRANSIG
2	-	PURELIN

Chapter 5

RESULTS AND DISCUSSIONS

5.1 Introduction

This chapter presents the performance analysis results of the selected models, showing the pushover curves, building performance charts, period plots versus building height, infill layouts, and target displacement.

5.2 Capacity Curves (Pushover Analysis Curve)

The pushover analysis results indicate that an infill wall increases an RC frame structure's stiffness, strength, and energy dissipation compared to a bare RC frame. That is true if infills were evenly or symmetrically distributed in the plans and elevations of the structure. As mentioned in the previous chapter, several infill layouts were adopted to determine the seismic behavior of infill walls in RC frame structures, both positively and negatively.

5.2.1 Mid-rise Buildings Capacity Curves by Infill Layouts Difference

Capacity curves for the mid-rise structures with different infill wall layouts are presented below. One infill material is shown in one chart that includes the capacity curves of one building plan symmetry case with different infill wall layouts.

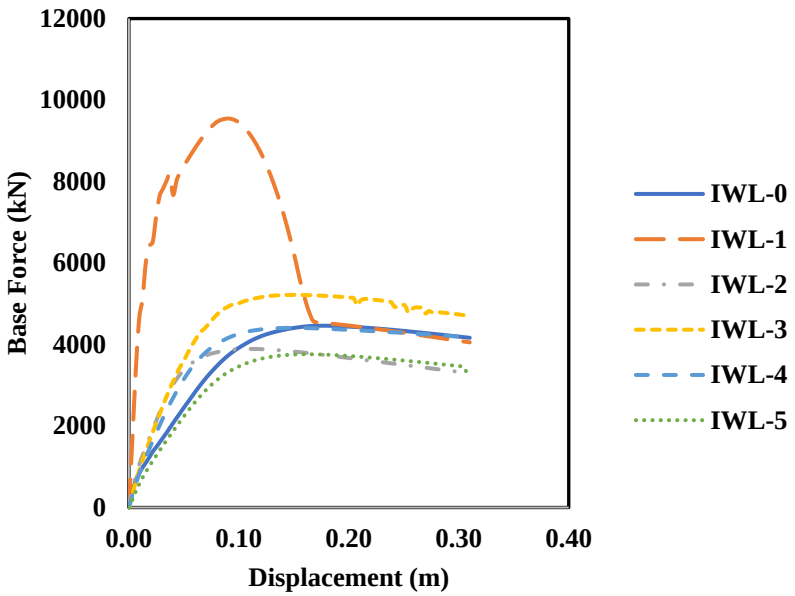

Figure 28: Capacity curves for plan symmetry-1 and IM1.

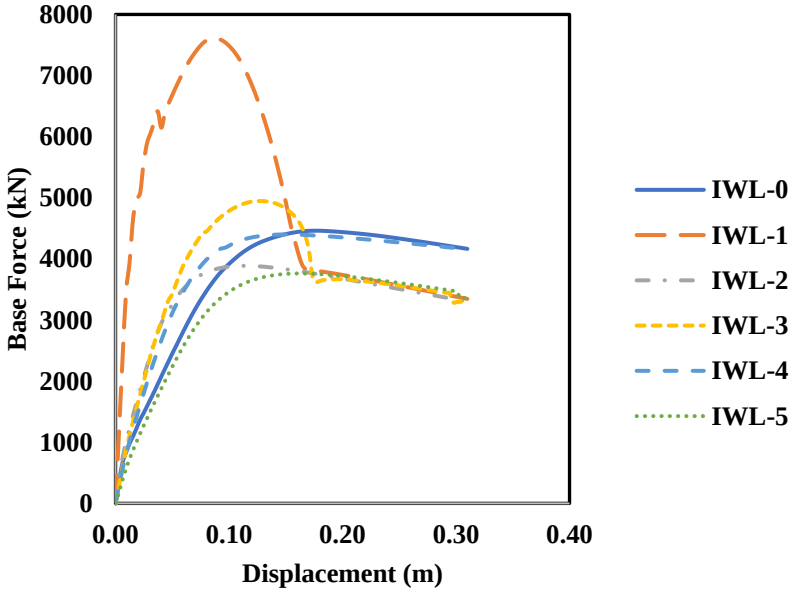

Figure 29: Capacity curves for plan symmetry-1 and IM-2.

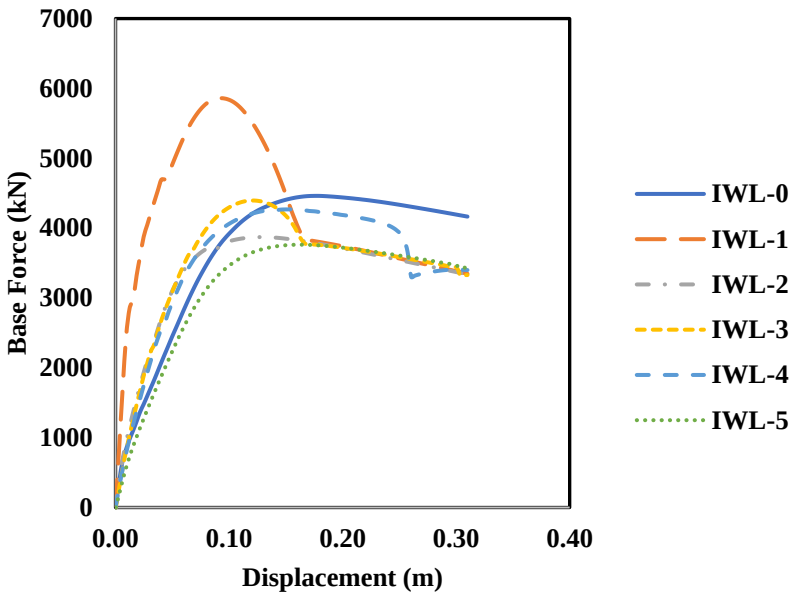

Figure 30: Capacity curves for plan symmetry-1 and IM-3.

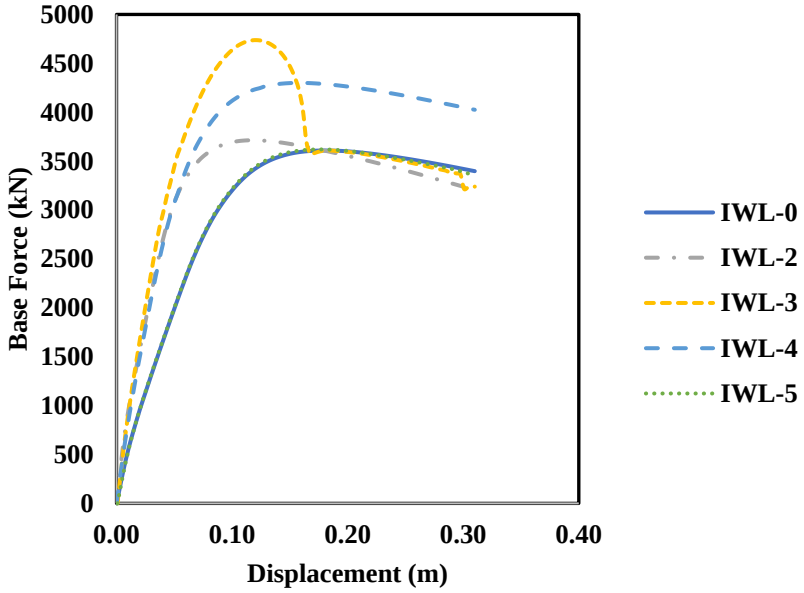

Figure 31: Capacity curves for plan symmetry-2 and IM-1.

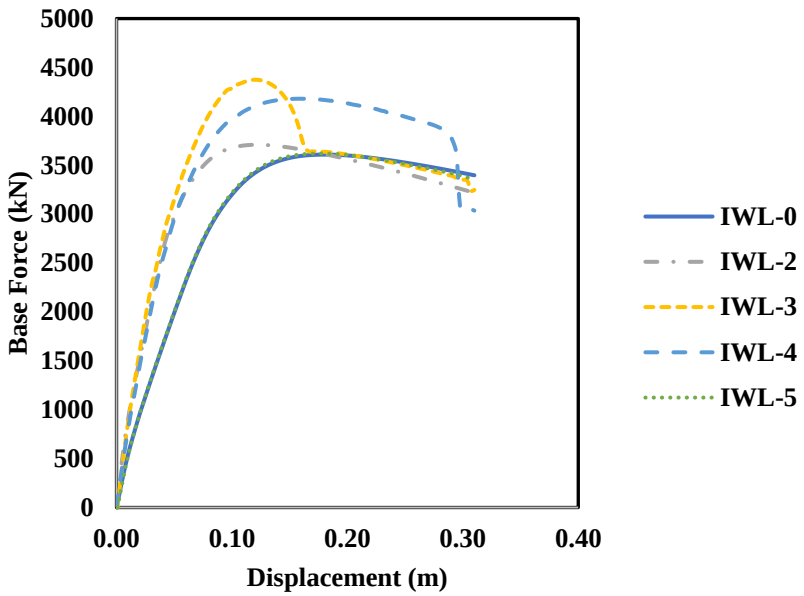

Figure 32: Capacity curves for plan symmetry-2 and IM-2.

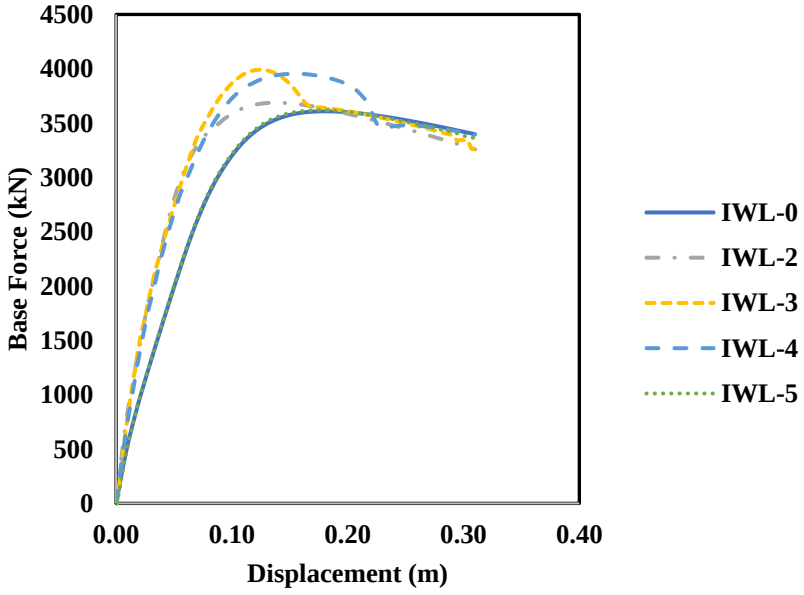

Figure 33: Capacity curves for plan symmetry-2 and IM-3.

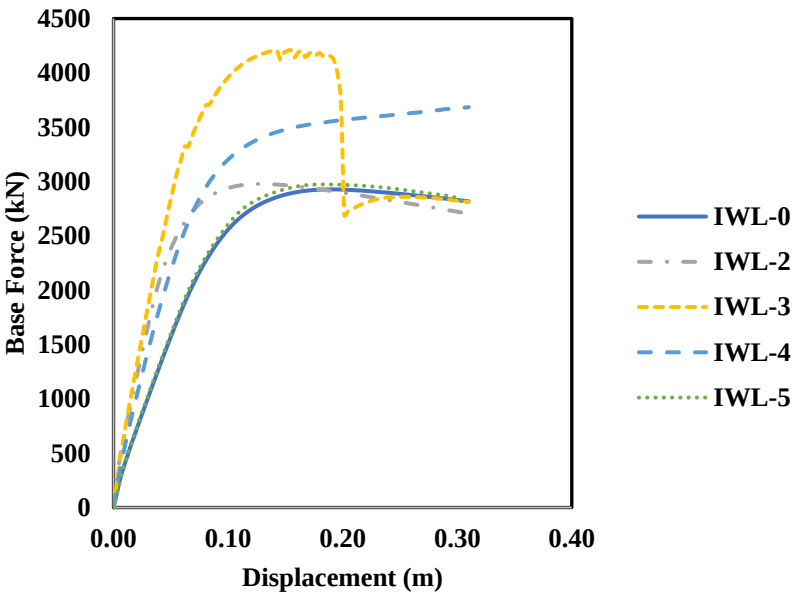

Figure 34: Capacity curves for plan symmetry-3 and IM-1.

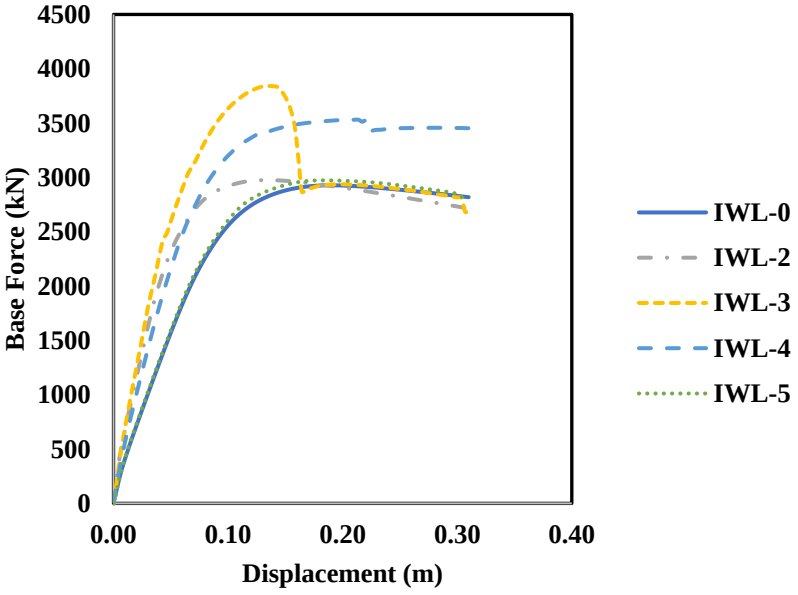

Figure 35: Capacity curves for plan symmetry-3 and IM-2.

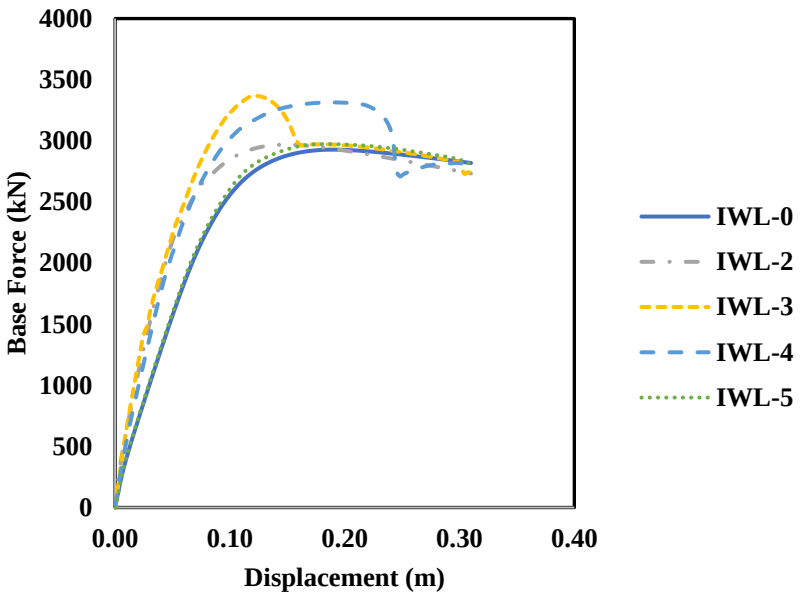

Figure 36: Capacity curves for plan symmetry-3 and IM-3.

From mid-rise building capacity curves, the following can be observed. For the effect of infill material on building capacity, lower capacities were observed with weaker infills, while the strong infill had higher capacities in all infill layouts. Regarding infill layouts, positive and favorable effects were observed in IWL-1 where it showed a significant increase in capacity and structure performance. A reduction in capacity was observed in IWL-5. Therefore, infill has dramatically affected the capacity of mid-rise buildings, both positively and negatively.

5.2.2 High-rise Buildings by Infill Layouts Difference

Capacity curves for the high-rise structures with different infill wall layouts are presented below. As mentioned, one infill material is shown in one chart that includes the capacity curves of one building plan symmetry case with different infill wall layouts.

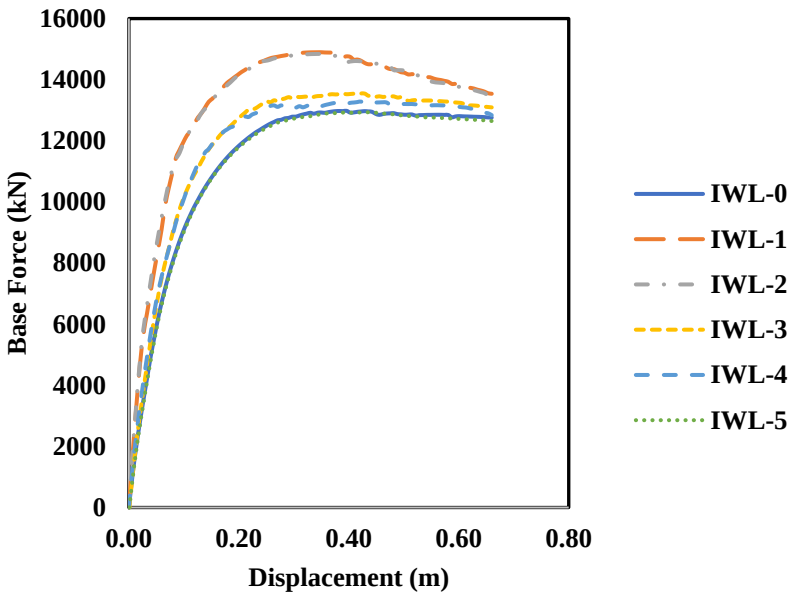

Figure 37: Capacity curves for plan symmetry-1 and IM-1.

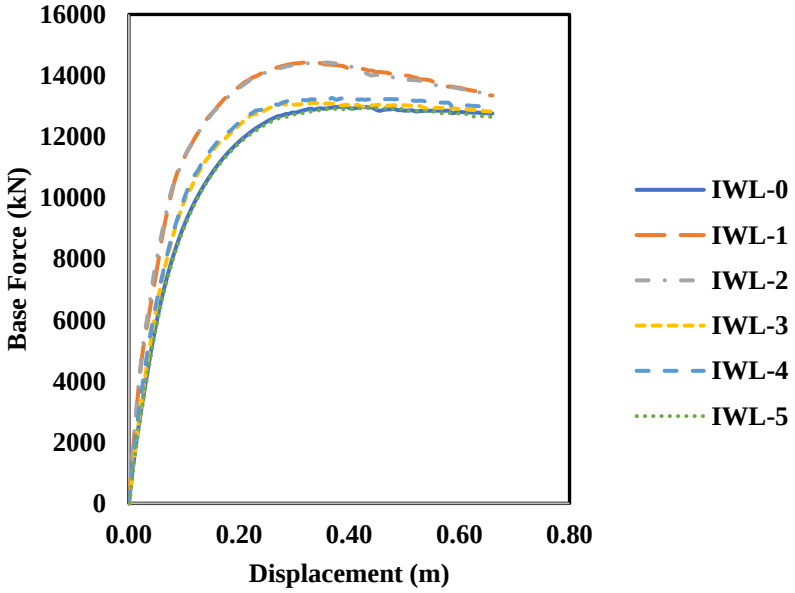

Figure 38: Capacity curves for plan symmetry-1 and IM-2.

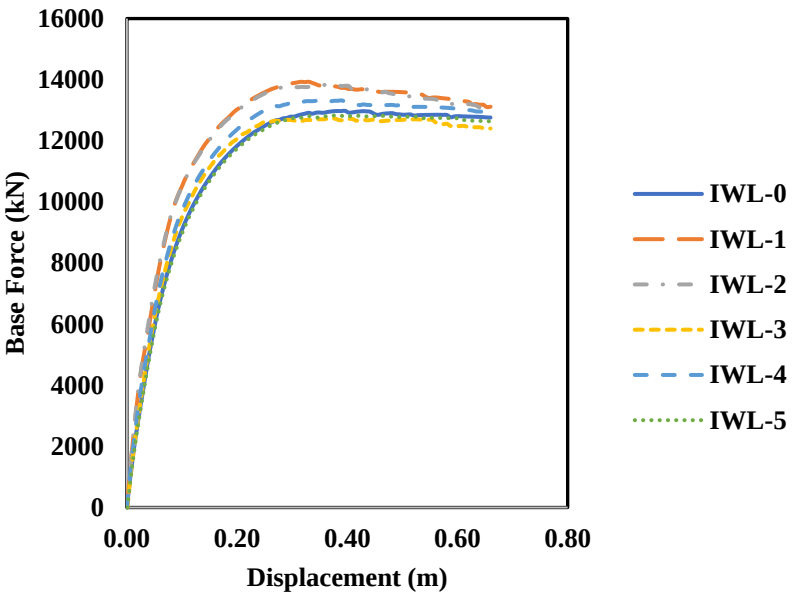

Figure 39: Capacity curves for plan symmetry-1 and IM-3.

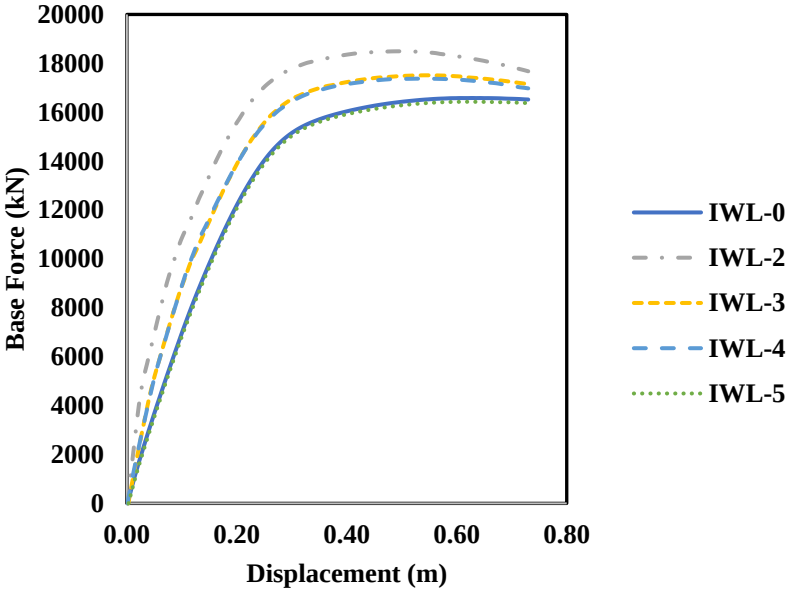

Figure 40: Capacity curves for plan symmetry-2 and IM-1.

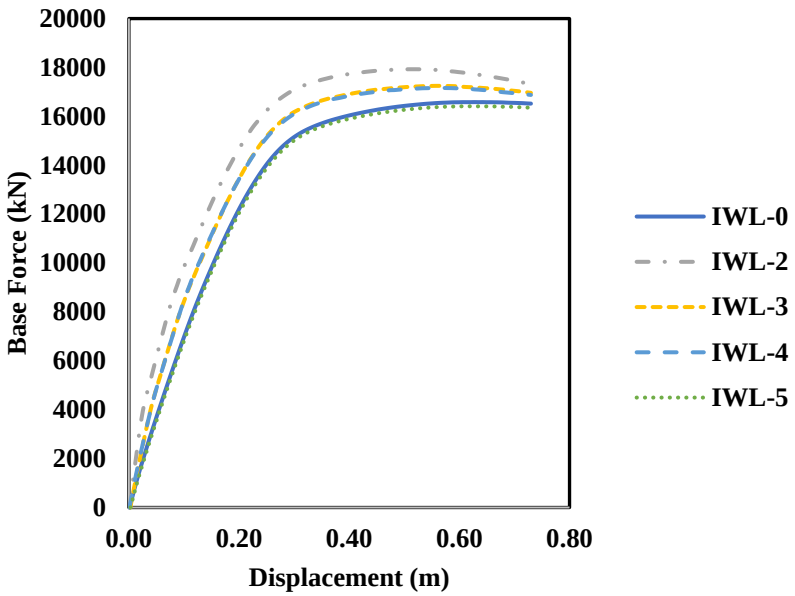

Figure 41: Capacity curves for plan symmetry-2 and IM-2.

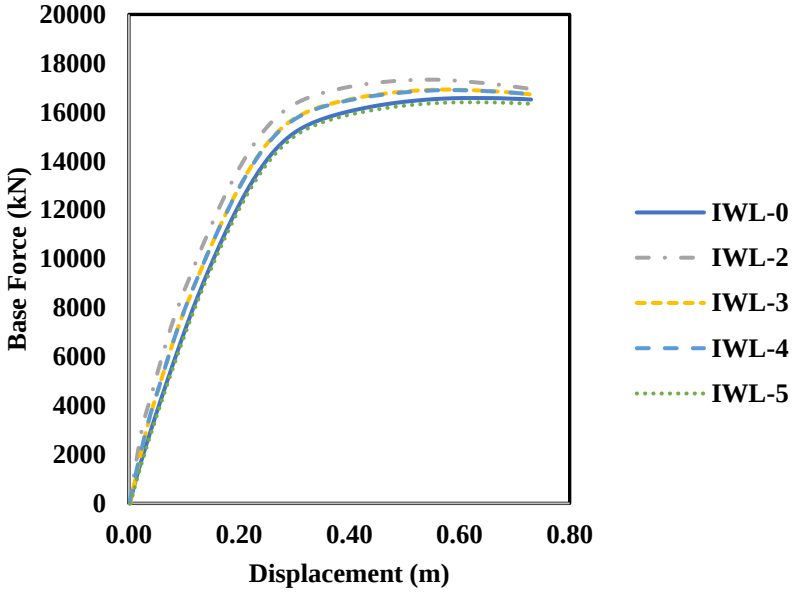

Figure 42: Capacity curves for plan symmetry-2 and IM-3.

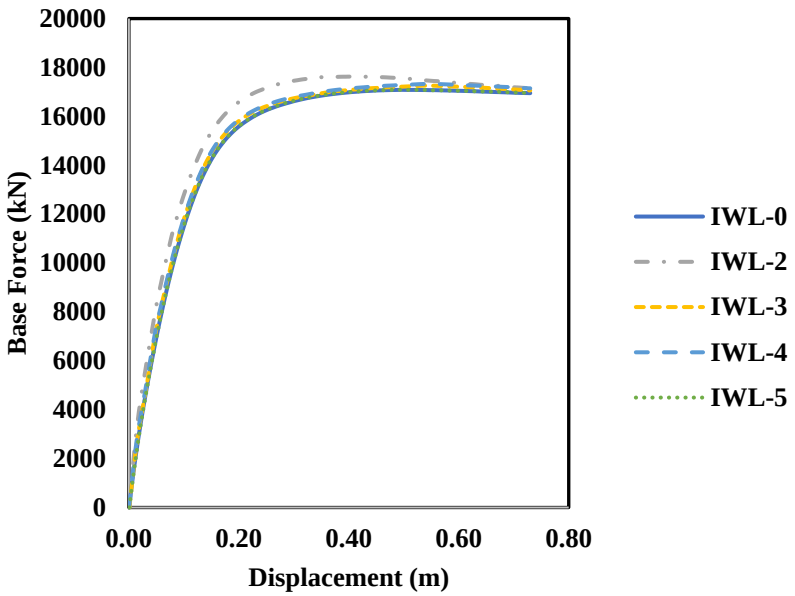

Figure 43: Capacity curves for plan symmetry-3 and IM-1.

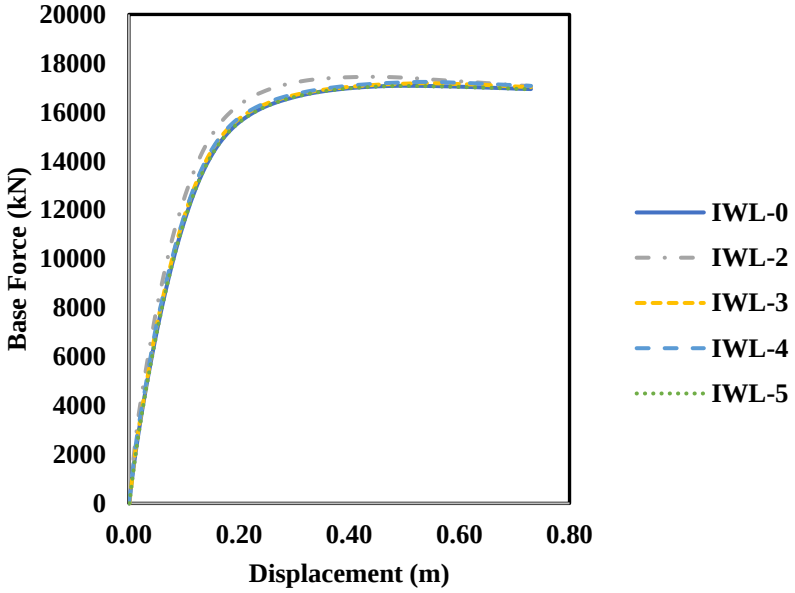

Figure 44: Capacity curves for plan symmetry-3 and IM-2.

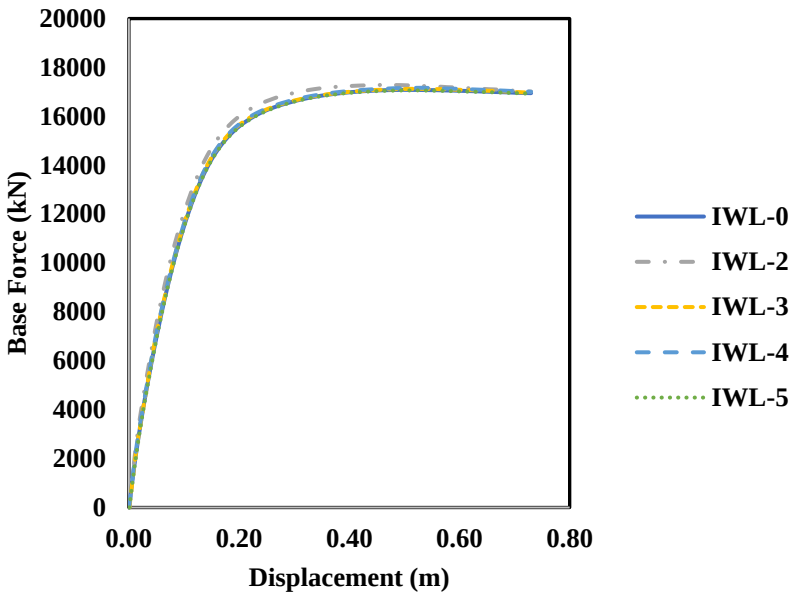

Figure 45: Capacity curves for plan symmetry-3 and IM-3.

The following can be seen in high-rise building capacity curves. Weaker infills were found to have slightly lower building capacities compared to stronger infills across all infill layouts. Regarding infill layouts, IWL-1 and IWL-2 demonstrated a notable increase in capacity. Moreover, IWL-3 and IWL-4 had a slight increase in capacity. Lastly, IWL-5 revealed a slight decrease in capacity. As a result, infill has had a less positive and negative impact on the capacity of high-rise buildings, which might be due to the presence of shear walls in the buildings.

Although IWL-2, IWL-3 and IWL-4 layouts showed relatively greater stiffness and capacity either in mid-rise or high-rise structures, the torsional effect (due to infill distribution as in IWL-3, IWL-4, and IWL-5), soft-storey effect (such as IWL-2) and P-Δ effect caused the structure to have a certain collapse mechanism, hence structural performance was affected. For instance, performance changed from CD (IWL-0) to CP or CC (other layouts) where negative and unfavorable effect of infills were observed as presented in the performance levels results in the coming section.

5.3 Performance Levels

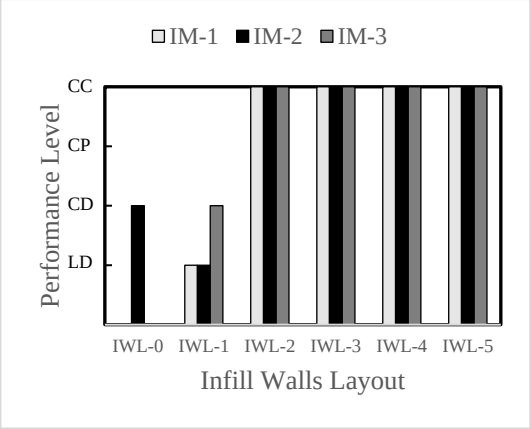

(a) Soil Type ZC & PGA 0.75g.

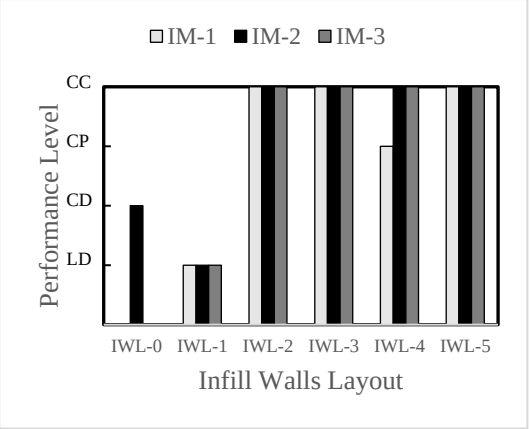

(b) Soil Type ZC & PGA 0.45g.

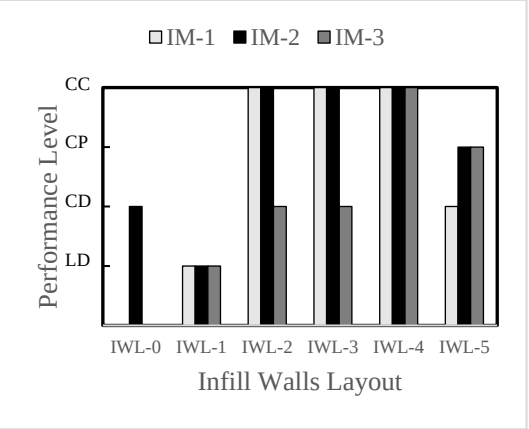

(c) Soil Type ZB & PGA 0.75g.

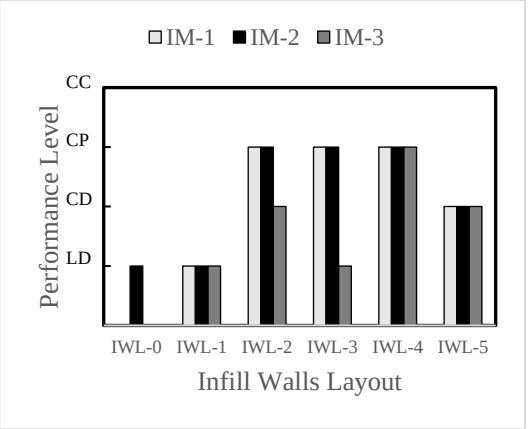

(d) Soil Type ZB & PGA 0.45g.

Figure 46: Performance levels of plan symmetry-1 mid-rise buildings according to infill walls layouts.

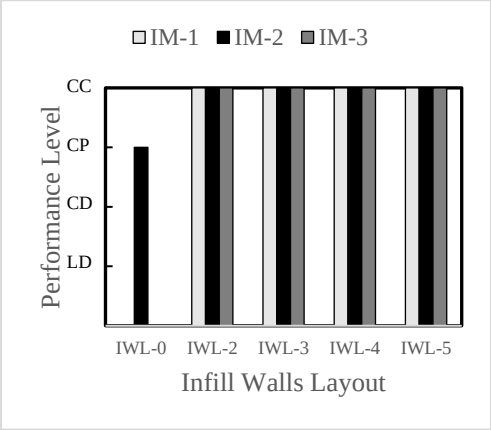

(a) Soil Type ZC & PGA 0.75g.

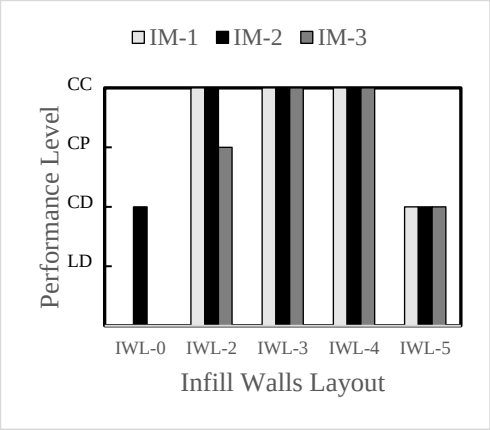

(b) Soil Type ZC & PGA 0.45g.

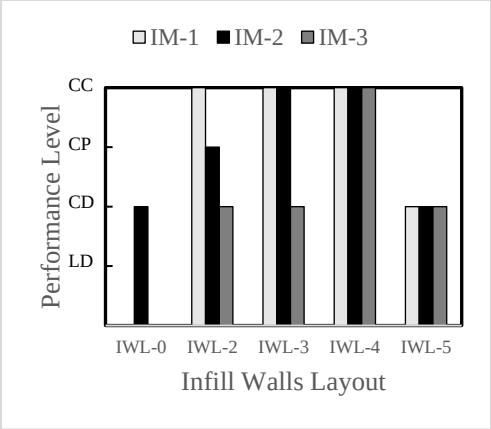

(c) Soil Type ZB & PGA 0.75g.

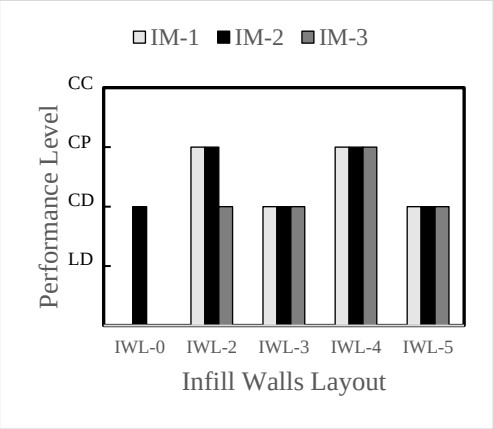

(d) Soil Type ZB & PGA 0.45g.

Figure 47: Performance levels of plan symmetry-2 mid-rise buildings according to infill walls layouts.

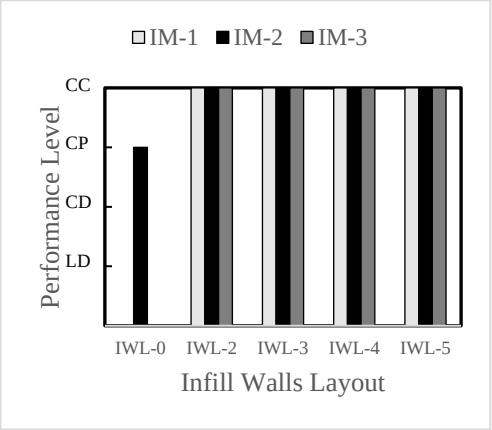

(a) Soil Type ZC & PGA 0.75g.

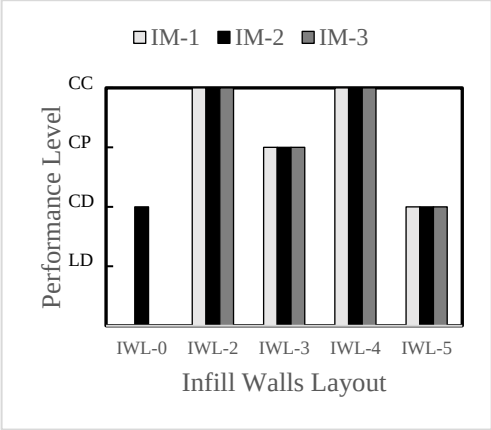

(b) Soil Type ZC & PGA 0.45g.

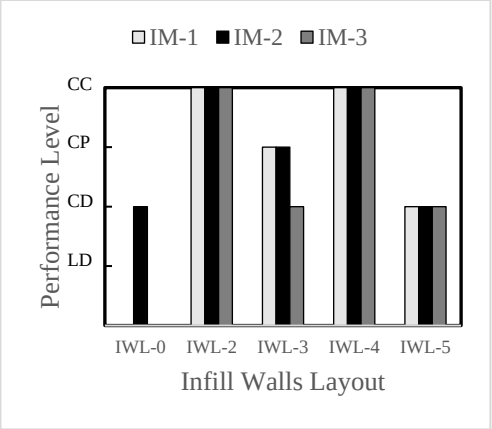

(c) Soil Type ZB & PGA 0.75g.

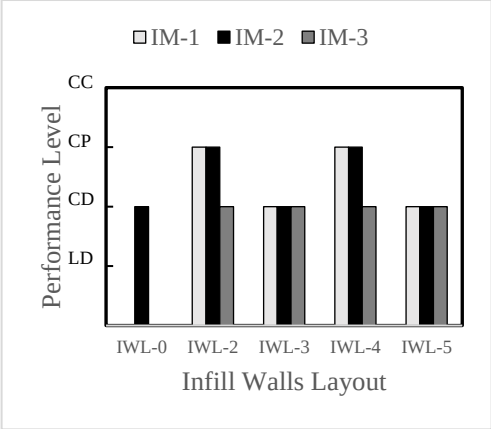

(d) Soil Type ZB & PGA 0.45g.

Figure 48: Performance levels of plan symmetry-3 mid-rise buildings according to infill walls layouts.

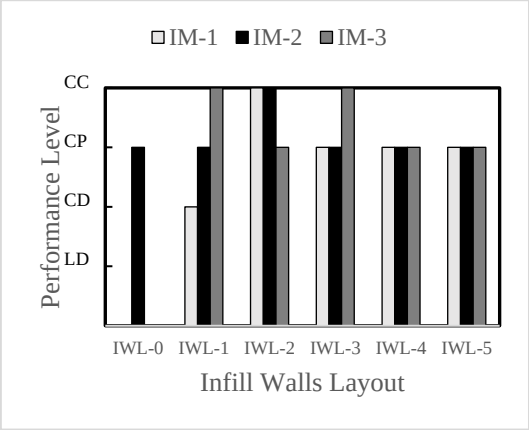

(a) Soil Type ZC & PGA 0.75g.

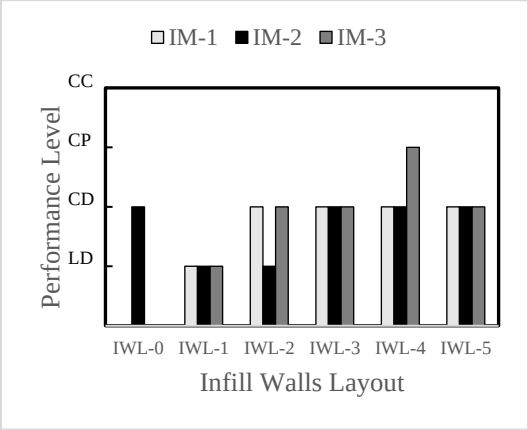

(b) Soil Type ZC & PGA 0.45g.

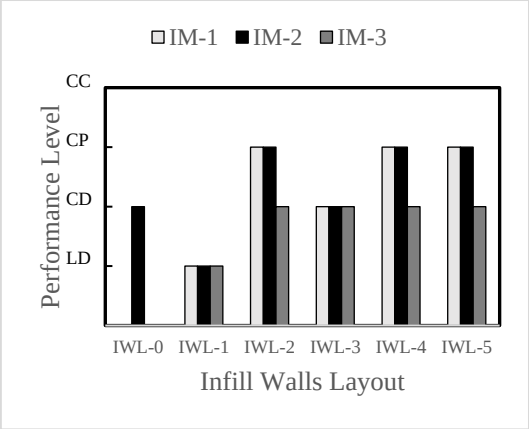

(c) Soil Type ZB & PGA 0.75g.

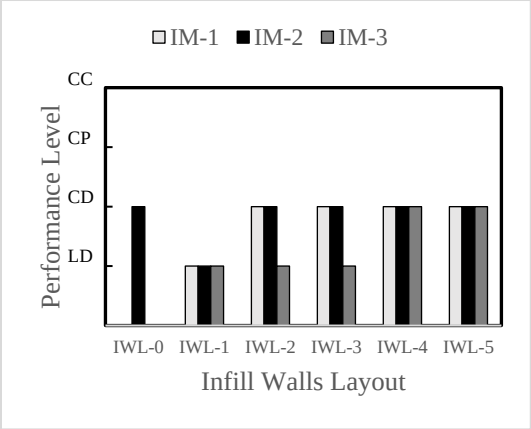

(d) Soil Type ZB & PGA 0.45g.

Figure 49: Performance levels of plan symmetry-1 high-rise buildings according to infill walls layouts.

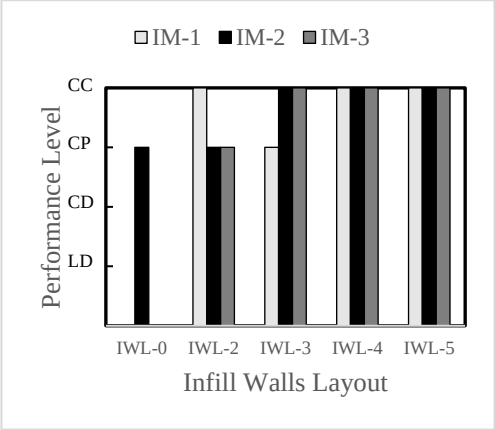

(a) Soil Type ZC & PGA 0.75g.

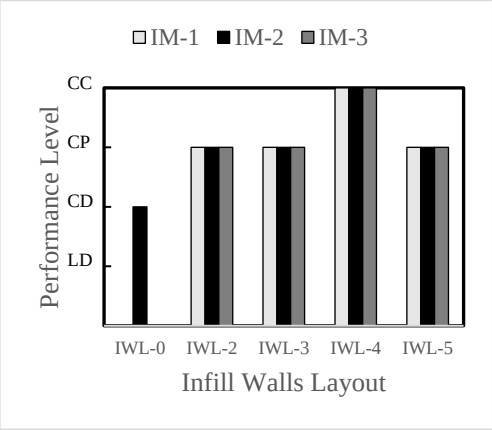

(b) Soil Type ZC & PGA 0.45g.

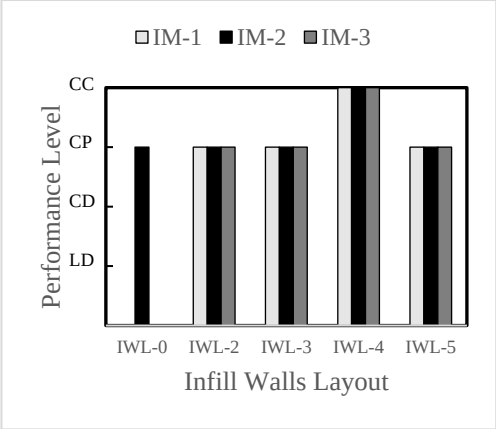

(c) Soil Type ZB & PGA 0.75g.

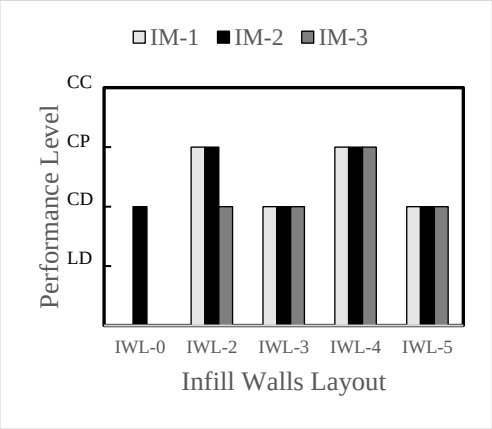

(d) Soil Type ZB & PGA 0.45g.

Figure 50: Performance levels of plan symmetry-2 high-rise buildings according to infill walls layouts.

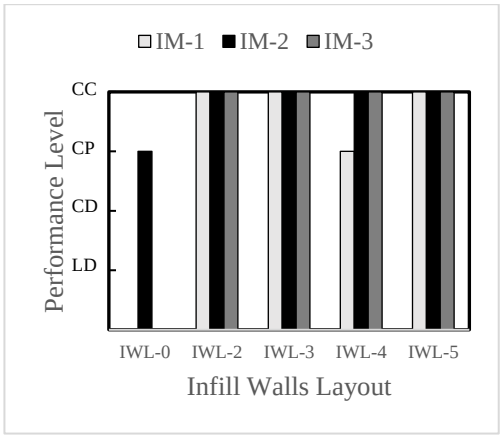

(a) Soil Type ZC & PGA 0.75g.

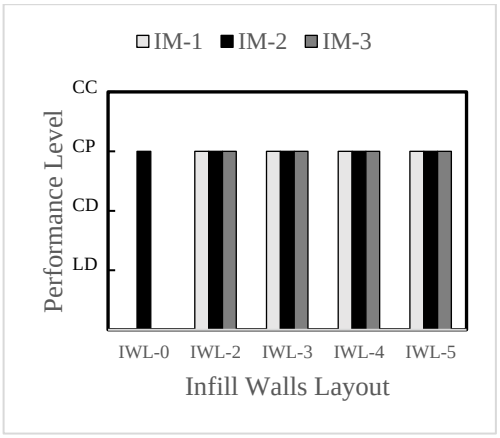

(b) Soil Type ZC & PGA 0.45g.

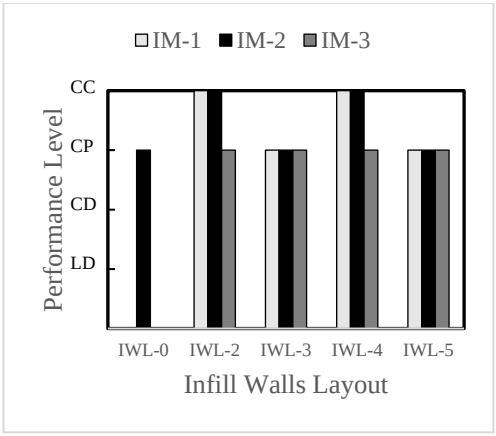

(c) Soil Type ZB & PGA 0.75g.

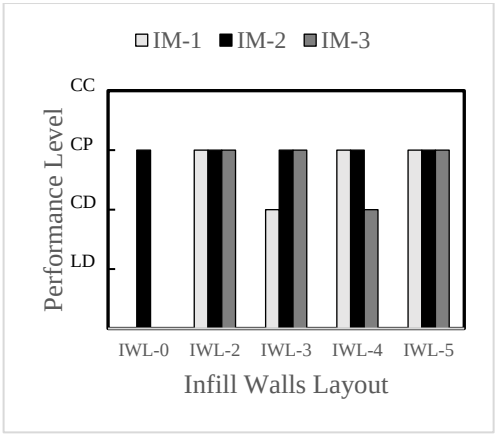

(d) Soil Type ZB & PGA 0.45g.

Figure 51: Performance levels of plan symmetry-3 high-rise buildings according to infill walls layouts.

Previous figures show that in most of the models, the reduction of peak ground acceleration resulted in better performance, so the performance was changed one level up, for instance, from collapse case to collapse prevention. In addition, the soil type effect on performance was also presented by comparing soil type ZC cases and soil type ZB, where the performance is higher for those models with soil type ZB. In terms of infill material, IM-1 shows better performance in the infill wall layout 1, where infills are symmetrically placed and expected to contribute positively to the frame rigidity. In comparison, the other layouts where infills are not symmetrical would

negatively affect the performance level, resulting in the initiation of a soft story as per layouts 2, 3, 4, and 5, in addition to the torsional effect in cases 3, 4, and 5.

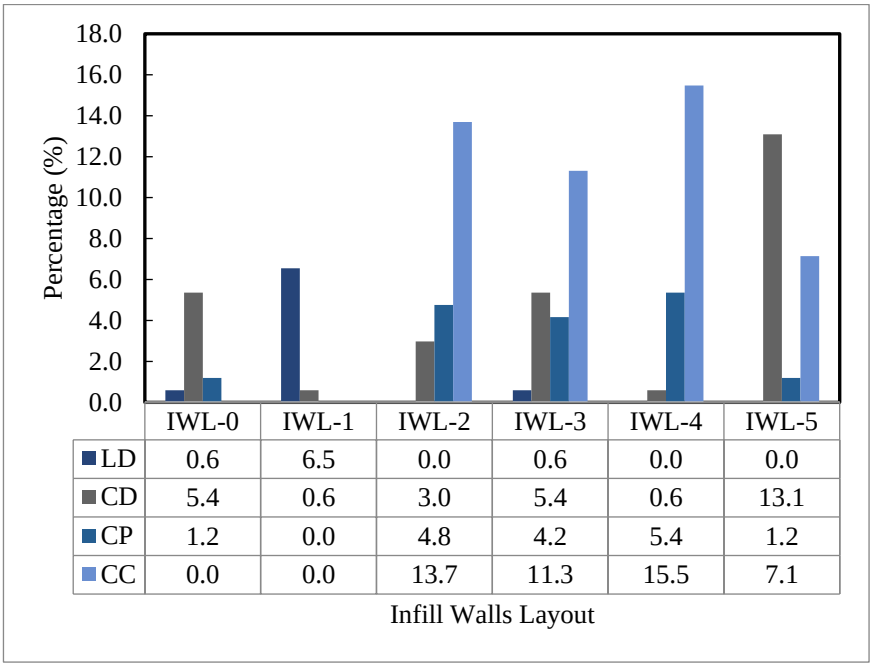

	IWL-0	IWL-1	IWL-2	IWL-3	IWL-4	IWL-5
LD	0.6	6.5	0.0	0.6	0.0	0.0
CD	5.4	0.6	3.0	5.4	0.6	13.1
CP	1.2	0.0	4.8	4.2	5.4	1.2
CC	0.0	0.0	13.7	11.3	15.5	7.1

Figure 52: Mid-rise models performance percentages.

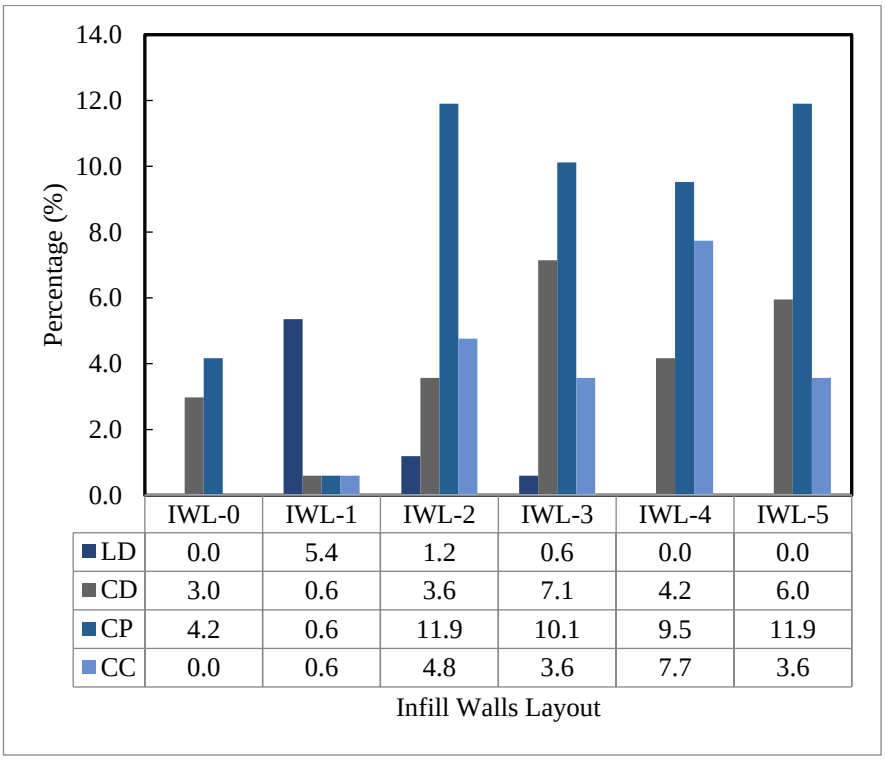

	IWL-0	IWL-1	IWL-2	IWL-3	IWL-4	IWL-5
LD	0.0	5.4	1.2	0.6	0.0	0.0
CD	3.0	0.6	3.6	7.1	4.2	6.0
CP	4.2	0.6	11.9	10.1	9.5	11.9
CC	0.0	0.6	4.8	3.6	7.7	3.6

Figure 53: High-rise models performance percentages.

As can be seen in previous figures, the performance of bare frames was primarily as CD (controlled damage) for mid-rise buildings and CP (collapse prevention) for high-rise buildings. While taking the effects of infill walls, an improvement in the performance can be observed in symmetrical infill wall layout IWL-1 for both mid-rise and high-rise models. Nevertheless, in IWL-2 and IWL-4, the infill effect caused the structure's performance in most cases to be a CC (collapse case) in mid-rise structures and CP in high-rise structures.

5.4 Fundamental Structure Period Plots

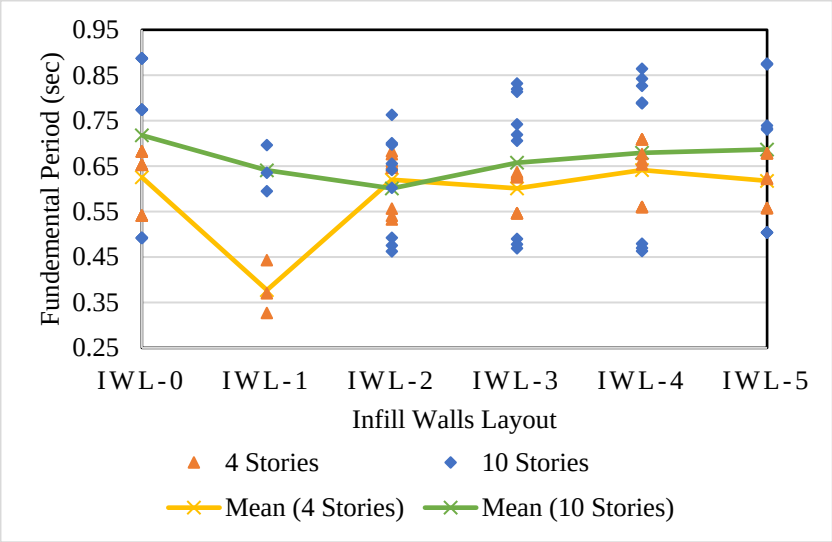

Figure 54: Models fundamental period versus infill walls layouts.

Above figure shows scatter of the fundamental period of the mid-rise four stories structures and high-rise ten stories structures according to the change of infill layouts. Mean of the values was plotted. Therefore, one could observe that the mid-rise structures showed great change as layouts changes, especially in IWL-1 compared to IWL-0 (bare frame). On the contrary, the high-rise structures mean showed less change, according to the change of infill layouts, compared to mid-rise structures

where presence of shear walls in the high-rise structures reduced infill walls effect on the fundamental period.

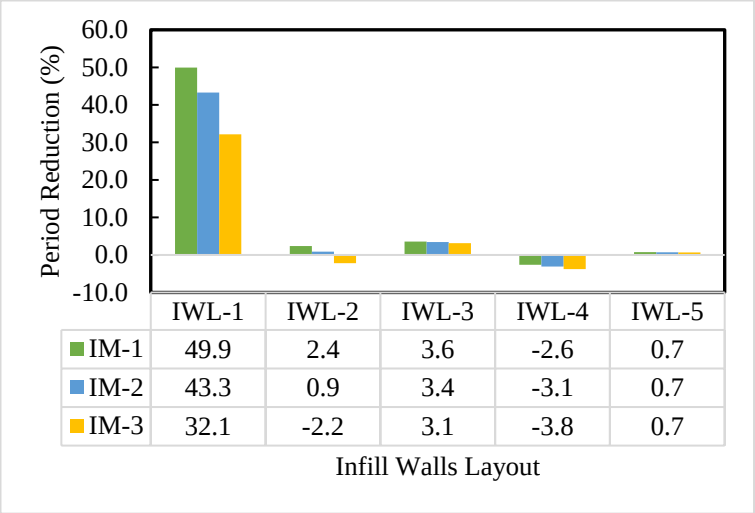

	IWL-1	IWL-2	IWL-3	IWL-4	IWL-5
IM-1	49.9	2.4	3.6	-2.6	0.7
IM-2	43.3	0.9	3.4	-3.1	0.7
IM-3	32.1	-2.2	3.1	-3.8	0.7

Figure 55 Fundamental period reduction percentage for the mid-rise models based on infill wall material and different layouts.

The above figure shows a significant reduction in the period in IWL-1, approximately 50% for IM-1, and reduces to 30% with material type change since infill strength is weak. Moreover, the percent reduction in IWL-1 is more significant than in other layouts since frames are fully infilled in all the building stories. Adverse effects can be observed in IWL-4, where the negative values represent an increase in the fundamental period therefore ductility demand increases resulting in greater seismic forces since period is involved in the calculation of lateral seismic loads.

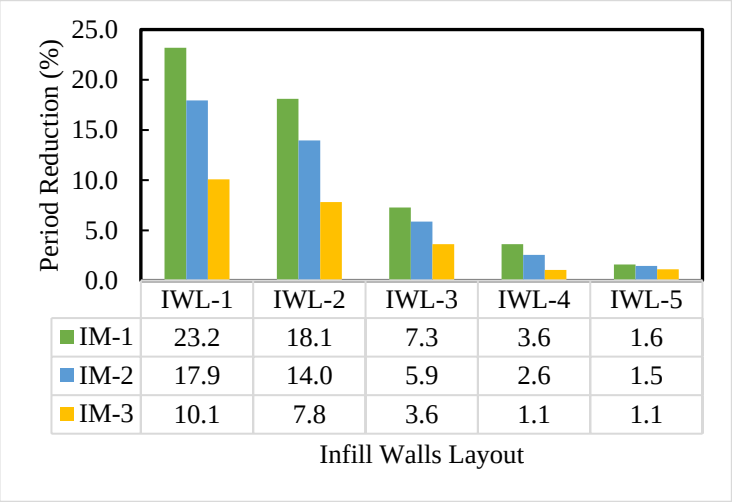

	IWL-1	IWL-2	IWL-3	IWL-4	IWL-5
IM-1	23.2	18.1	7.3	3.6	1.6
IM-2	17.9	14.0	5.9	2.6	1.5
IM-3	10.1	7.8	3.6	1.1	1.1

Figure 56: Fundamental period reduction percentage for the high-rise models based on infill wall material and different layouts.

As can be seen in the previous figure, for high-rise buildings, there was always a reduction in the period of structures but with differences in infill material type, where the IM-1 type resulted in a more significant reduction percentage in all the cases. In terms of infill walls layouts, the more significant reduction was in IWL-1, and the minor reduction was observed in IWL-5.

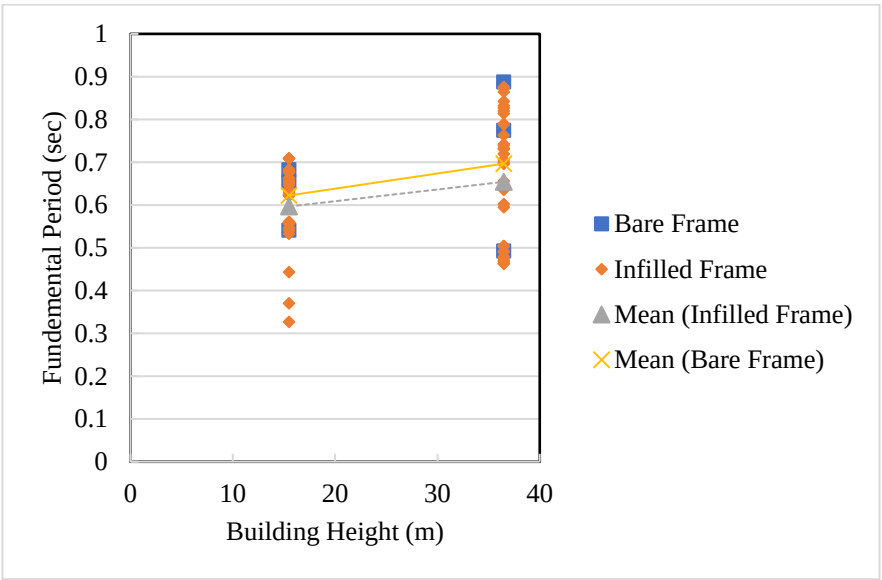

Figure 57: Models fundamental period versus structure height.

The above figure shows an increase in the fundamental period of the structure as building height increases, where an increase of 11.94% in the case of a bare frame is observed and an increase of 11.03% in the case of infilled frames. The percent of increase for infilled frames were less since the presence of infills reduced the fundamental period in most of the layouts.

5.5 Target Displacement Reduction Percentage by Infill Walls Layouts

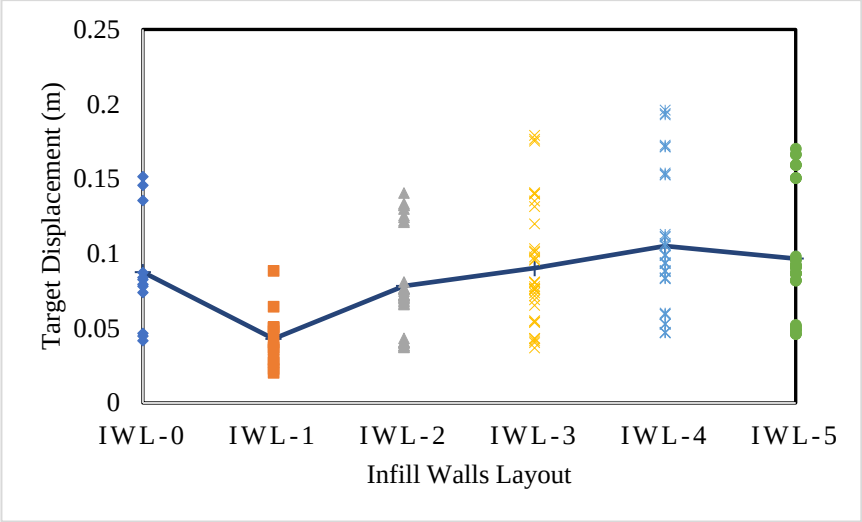

Figure 58: Mid-rise models target displacement versus infill walls layouts.

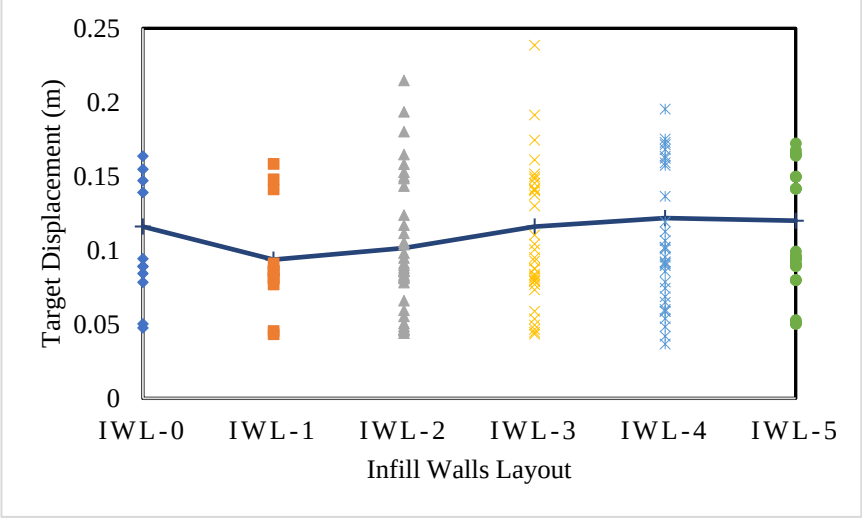

Figure 59: High-rise models target displacement versus infill walls layouts.

As can be seen from the figures 58 and 59, which shows a plot of target displacements obtained according to the change of infill layouts in addition to their mean, from the mean plot in both figures, one can observe that target displacement of the mid-rise structures was greatly affected by the infill walls presence and changed considerably especially in IWL-1 compared to IWL-0 (bare frame), while high-rise structures showed less change compared to the mid-rise structures. This change can be seen clearly in the following figures where it shows change percentage compared to bare frame case IWL-0.

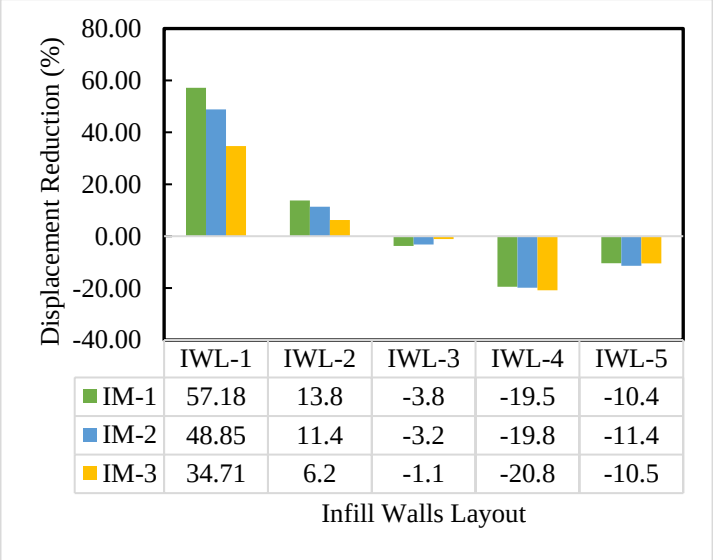

	IWL-1	IWL-2	IWL-3	IWL-4	IWL-5
IM-1	57.18	13.8	-3.8	-19.5	-10.4
IM-2	48.85	11.4	-3.2	-19.8	-11.4
IM-3	34.71	6.2	-1.1	-20.8	-10.5

Figure 60: Target displacement reduction percentage for the mid-rise models based on infill wall material and different layouts.

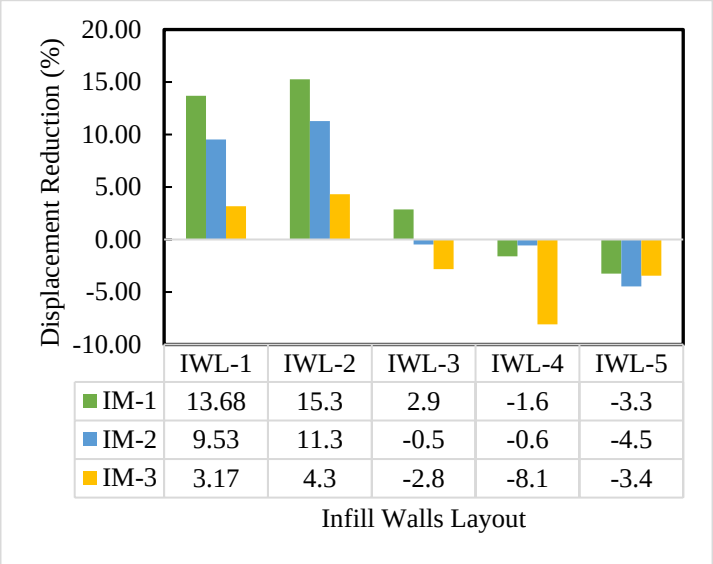

Figure 61: Target displacement reduction percentage for the high-rise models based on infill wall material and different layouts.

An increase in the target displacement was observed in infill layouts 3, 4, and 5 since the negative reduction percentage reflects an increase instead of a reduction. In comparison, a reduction in target displacement was observed in layouts 1 and 2. Moreover, either the increment (shown as negative) or reduction percentage of target displacement for mid-rise and high-rise structures, mid-rise structures showed greater percentage values where infill walls effects clearly observed. Additionally, differences between the infill materials results can be observed, where stronger infills such as IM-1 had a greater effect, while less effects were obtained by weaker infills such as IM-2 and IM-3.

5.6 ANN Models Results

This section shows ANN models results, showing their performance charts, training progress charts, result plots, and error plots. For training, validation, and testing, defaults were used so that 70% of the data was used as the training set, 15% was for validation, and 15% was for testing. The training process is being tracked using Mean

Square Error (MSE). One of the following conditions must be met for the training process to end:

- Number of epochs has reached the maximum.
- When the objective is reached by the average training error.
- Performance has been adjusted to the required level.
- When the number of errors in the validation set begins to rise.

Plotting the training, validation, and test Mean Square Error (MSE) vs. the actual number of iterations conducted allowed for the examination of the training's progress.

5.6.1 Performance Level Model

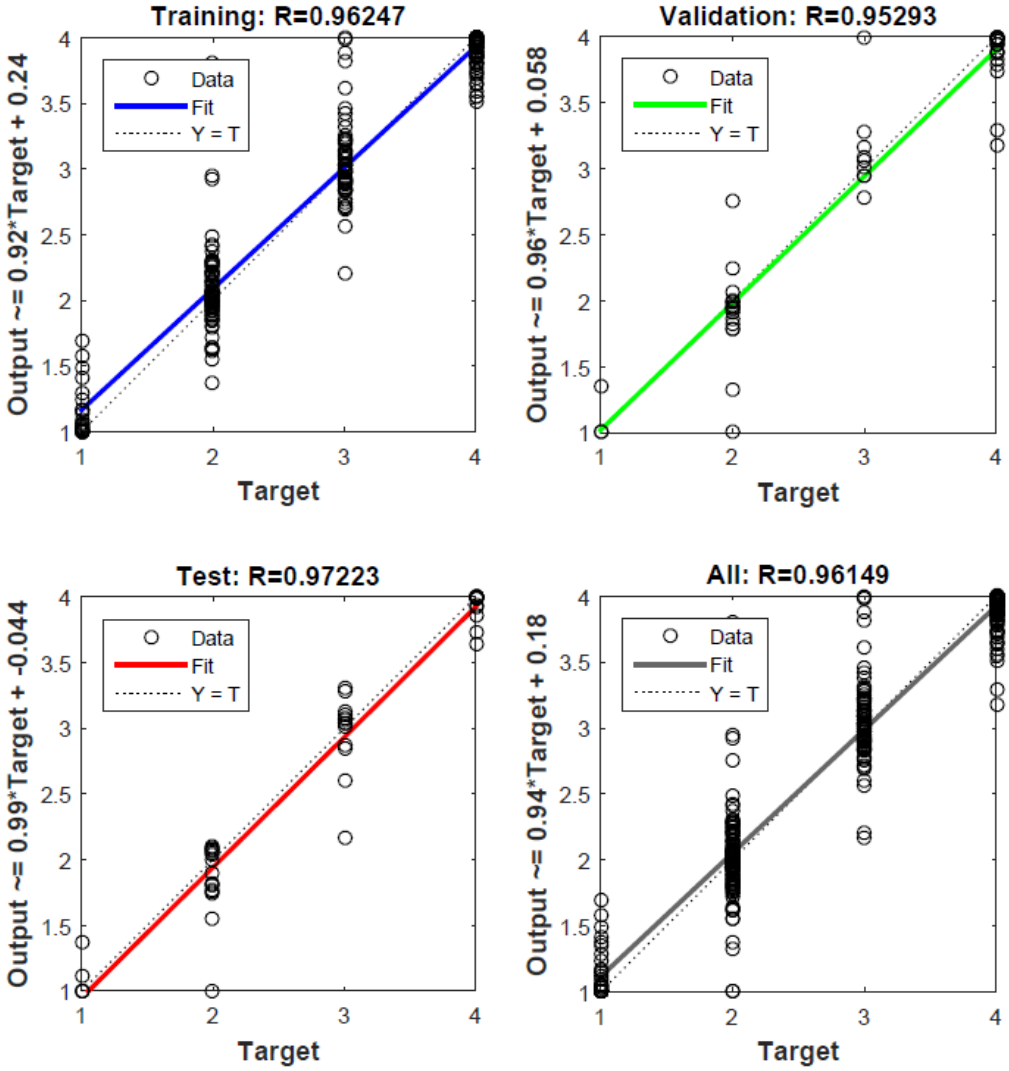

Figure 62: Performance of performance level ANN model.

The figure above shows the coefficient of correlation for training, validation, and testing in addition to the overall value. The overall performance is 96.15% which shows remarkable accuracy.

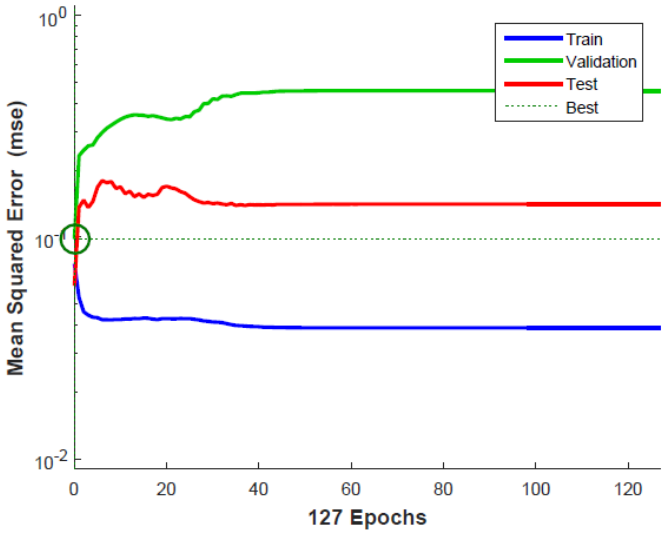

Figure 63: Training progress of the ANN model.

Figure 63 shows the training progress of the ANN, where the plot is the mean squared error versus epochs (one complete iteration of the algorithm using the training dataset). The best validation performance was 0.09809.

5.6.2 Fundamental Period Model

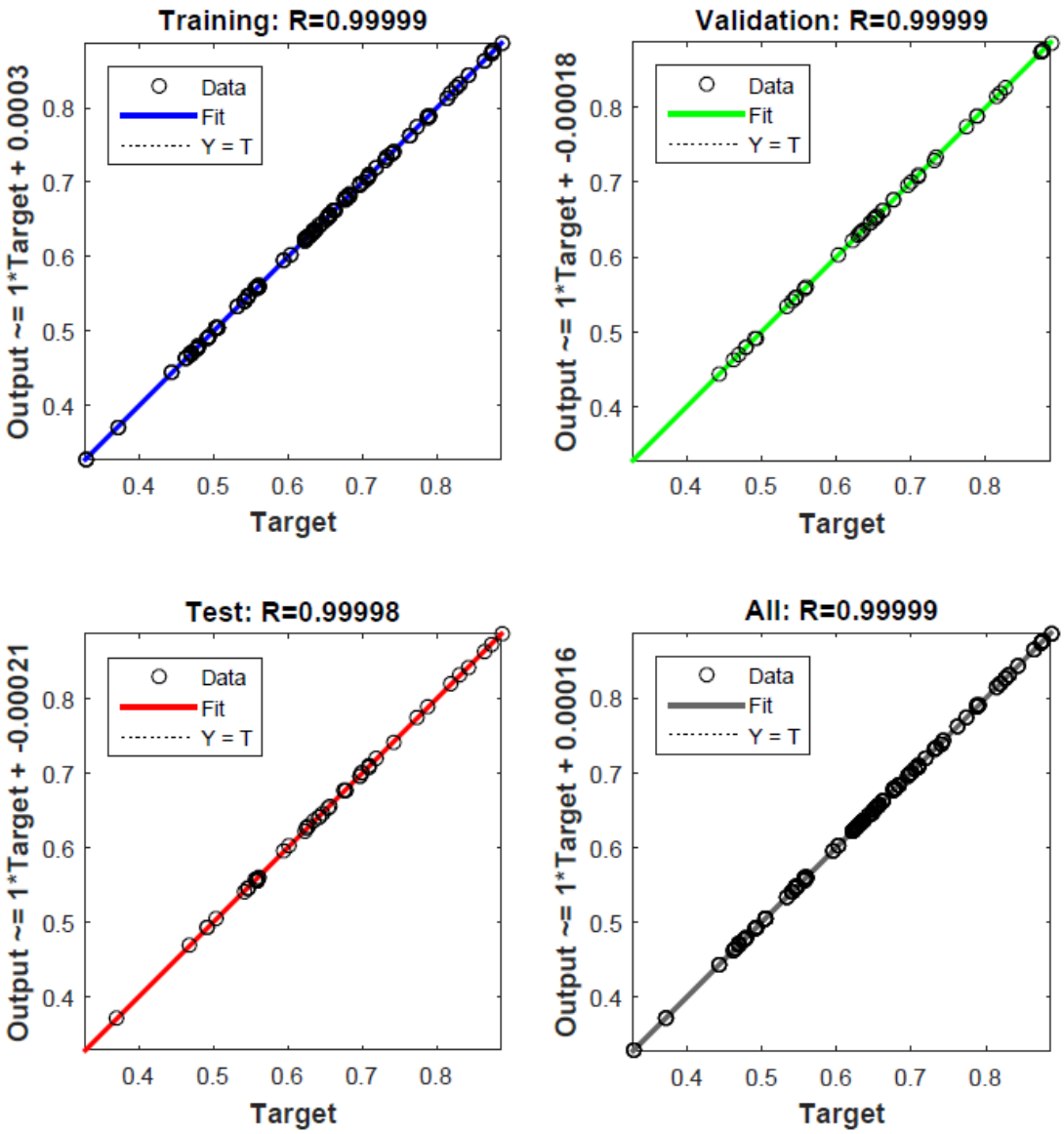

Figure 64: Performance of period ANN model.

Figure 64 shows the training, validation, and testing of the ANN model, which resulted in an excellent accuracy with a coefficient of correlation of 99.999% which is approximately 100%.

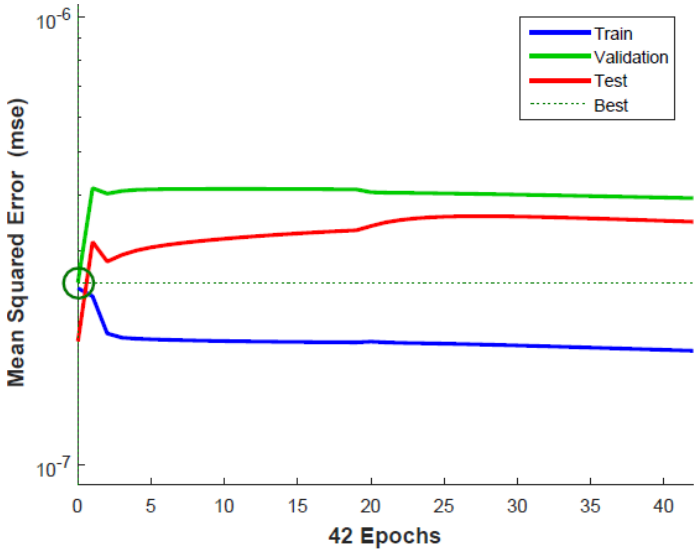

Figure 65: Training progress of the ANN model.

As shown in figure 65, in the progress of ANN training, the best validation performance was 2.5535E-7.

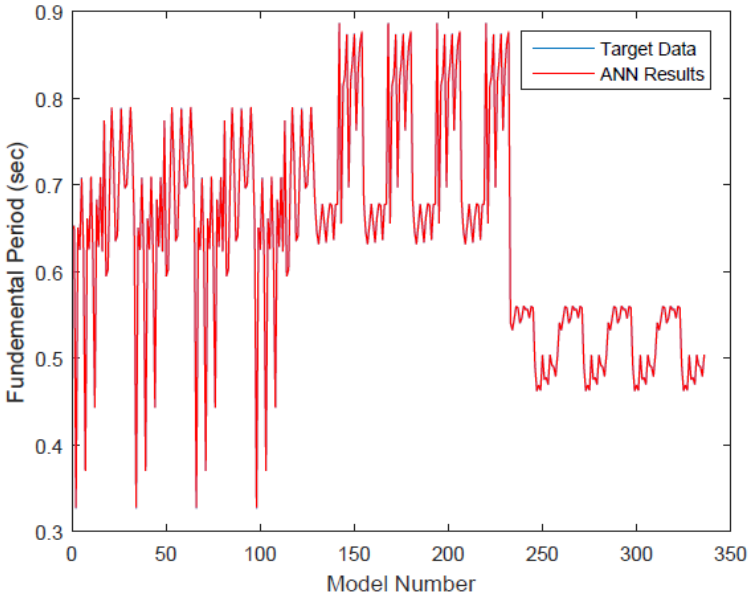

Figure 66: Results plot of the ANN model and target data versus model number.

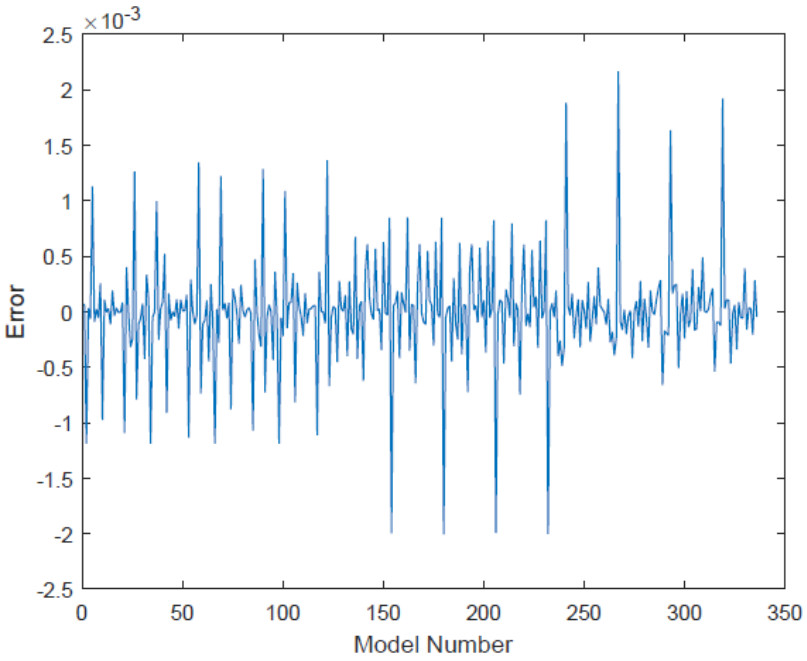

Figure 67: Error plot of the ANN model.

Figure 66 shows the ANN model estimated fundamental period results and target fundamental period results (user-defined) plotted versus model numbers (336 models). One cannot differentiate between the ANN plot and the target data plot since the error is minimized. Moreover, the error plot in figure 67 shows the difference between fundamental period obtained by the analysis and the ANN model results, where the maximum difference is 0.002.

5.6.3 Target Displacement Model

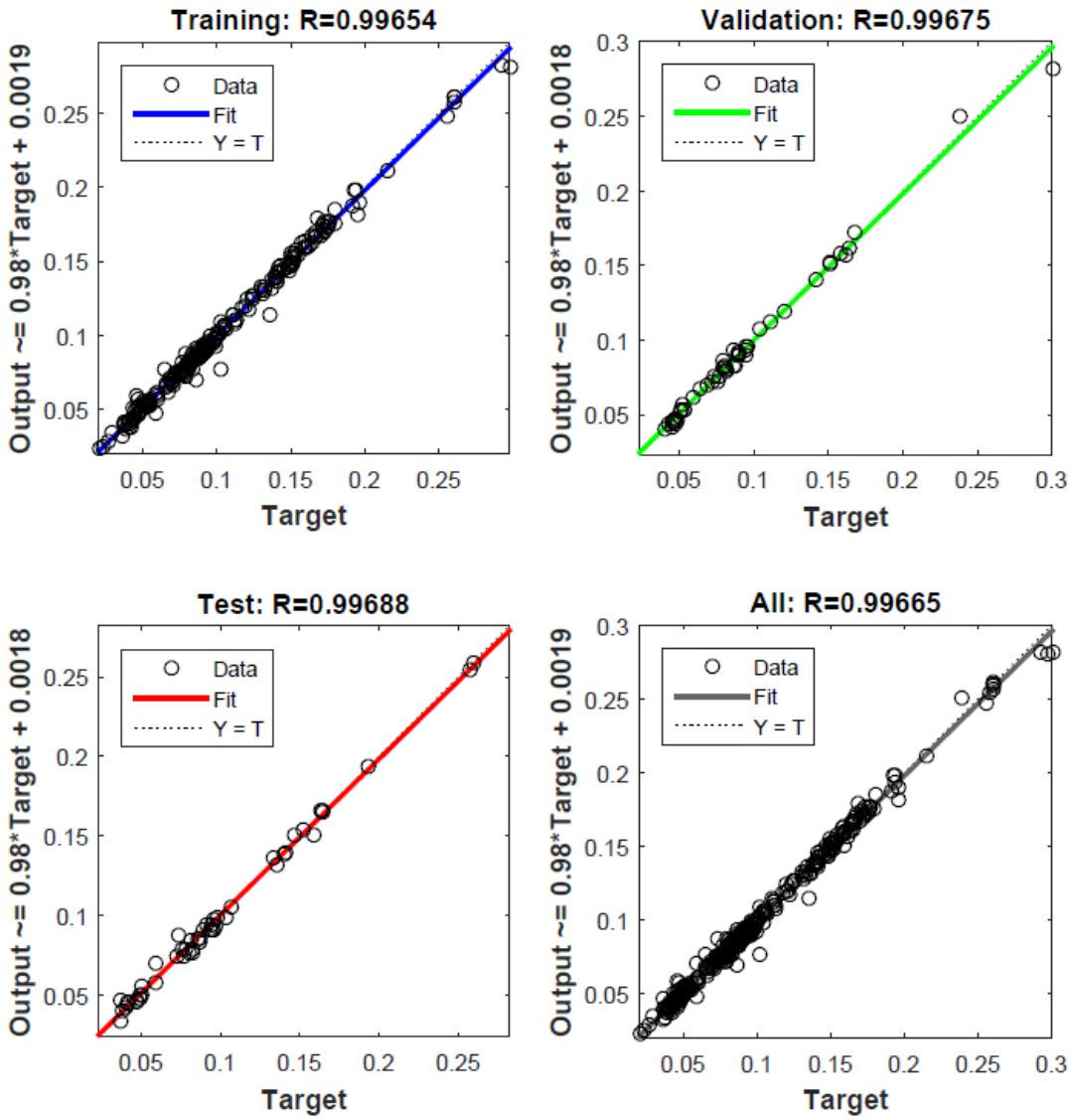

Figure 68: Performance of target displacement ANN model.

The target displacement ANN model's training, validation, and testing are shown in Figure 68, where it produced excellent accuracy with a coefficient of correlation of 99.67%.

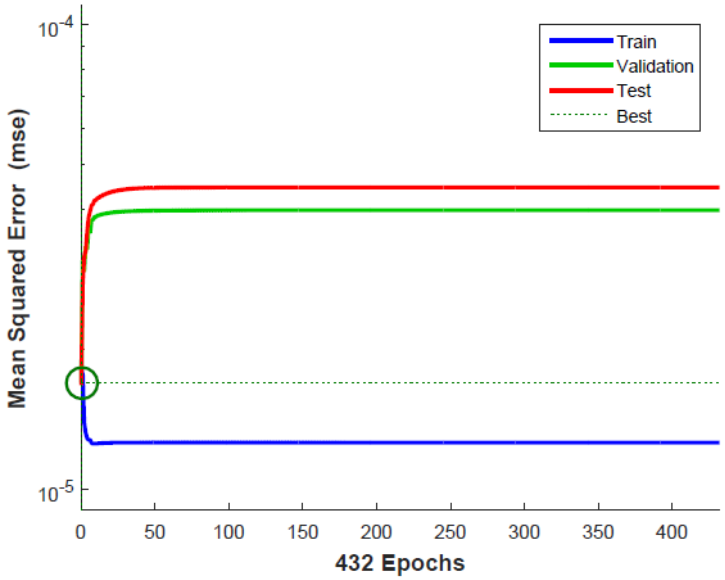

Figure 69: Training progress of the ANN model.

The best validation performance during ANN training, as shown in figure 69, was 1.6952E-5.

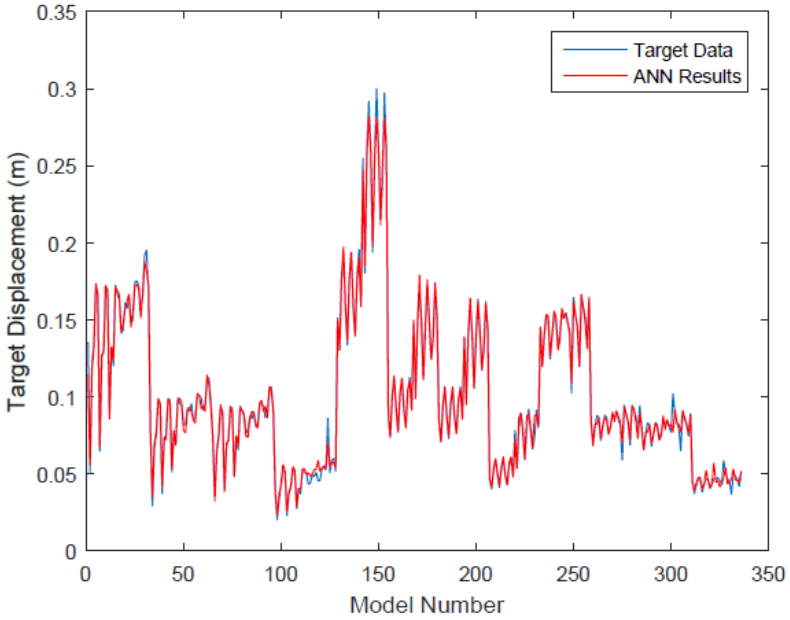

Figure 70: Results plot of the ANN model and target data versus model number.

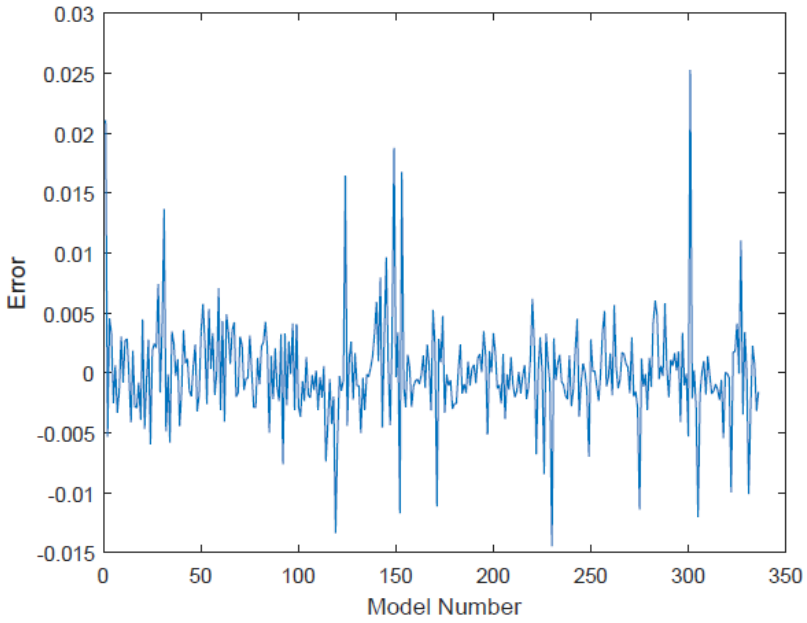

Figure 71: Error plot of the ANN model.

Figure 70 displays the approximated target displacement results from the ANN model and the user-defined target displacement results plotted against model numbers (336 models). From the figure, the plot of the ANN results is not perfectly identical to the target data, where the error is slightly more than the fundamental period model's error. Furthermore, the analysis's target displacement and the ANN model's displacement results differ by a maximum of 0.025, as shown by the error plot in figure 71.

Chapter 6

CONCLUSION

6.1 Introduction

In this study the use of machine learning such as artificial neural network models were adressed in order to estimate the structure fundamental period, target displacement and performance level considering the effect of infill walls as well. Several cases were considered in terms of plan symmetry, building height, infill material, peak ground acceleration and soil type. In terms of the results the following can be highlighted.

6.2 Buildings Capacity and Performance Level

Fully infilled frames (IWL-1) with IM-1 showed greater capacity compared to bare frame and other infill walls layouts despite the brittle failure of bricks that takes place afterwards. While this increase in capacity reduces with the reduction of brick's strength as the case in IM-2 and IM-3.

For mid rise buildings case, by checking capacity curves an increase in building capacity was observed in infill walls layouts 1 and 3, while the cases 2, 4 and 5 showed lower capacity compared to the bare frame that is mostly because of soft storey (in IWL-2) and torsional effects (in IWL 4 and 5).

For high rise buildings case, capacity curves showed an increase in building capacity in most infill walls layouts, except case 5 where the capacity was nearly equivalent to the bare frame.

Effect of brick's material strength on building capacity was observed, where higher IM strength gives higher capacity and vice versa. While, in terms of performance, higher IM strength improved building performance as in IWL 1 and 3. Where lower IM strength such as IM-3 resulted in a better performance in IWL 2, 3, 4 and 5, and that is because of it's lower contribution to the frame rigdity where it lowers the possibility of soft storey effect (in IWL-2) and torsional effects (in IWL 3, 4 and 5).

6.3 Fundamental Period

Distribution of infill walls in-elevation greatly affect the period for instance in mid-rise buildings, in IWL-1, the results showed reduction in period of roughly 50% for IM-1 and reduces to 30% with material type change due to weaker infill strength. While an increase in period was observed in IWL-4, where unfavorable results were observed.

For high-rise buildings, the period of structures was always reduced, however IM-1 type resulted in a greater reduction percentage. IWL-1 had the greater reduction and IWL-5 the least.

6.4 ANN Models

Three ANN models were created and backpropagation using Bayesian regularization was utilized for all of the ANN models. The ANN models, particularly the period and target displacement models, showed a high degree of accuracy. The following are the results that were obtained regarding the accuracy of the models: the accuracy of the performance level model was found to be 96.15%, the accuracy of the fundamental period of structure was found to be 99.99%, and finally, the accuracy of the target displacement was found to be 99.66%.

6.5 Recommendations for Future Studies

The results of this study showed a great result especially in predicting the period and performance level of structures effortlessly, however some points would be recommended for the extension of this study into future research which are:

1- Nonlinear static analysis were adopted in this study, while nonlinear dynamic analysis would be more promising technique where a seismic record is applied to the building's base, and structural behavior is assessed. However, incremental dynamic analysis is also preferable where it applies a multiple dynamic analysis under set of ground motion records then the structure is assessed.

2- Implementing more input options such as soil types, base storey height, normal storey height to obtain more training data to feed the ANN training.

3- Implementing span length and more building plans in order to widen the application of the ANN models to accurately predict performance and period of different buildings.

4- Addition of the infill opening ratio as an input would be greatly practical where the results would be more related to the buildings cases in practice.

REFERENCES

Ahmad, M. E., Ahmad, N., Pervez, S., Iqbal, A., Khan, A. Z., Rahim, M. E., Hassan, W., Umer, K., & Khan, K. (2019). Seismic performance evaluation of modern bare and masonry-infilled RC SMRF structures. *Advances in Civil Engineering, 2019. https://doi.org/10.1155/2019/6572465.*

Alshaer, I. M. (2016). Collapse vulnerability of reinforced concrete buildings using neural networks.

Altin, S., U. Ersoy & T. Tankut, (1992). Hysteretic response of reinforced concrete infilled frames. *J. Structural Eng., 118: 2133-2150. DOI: 10.1061/(ASCE)0733-9445(1992)118:8(2133).*

Antoniou S., Pinho R. (2004a). Advantages and limitations of force-based adaptive and non-adaptive pushover procedures, *Journal of Earthquake Engineering, Vol. 8, No. 4, pp. 497-522.*

Antoniou S., Pinho R. (2004b). Development and Verification of a Displacement-based Adaptive Pushover Procedure, *Journal of Earthquake Engineering, Vol. 8, No. 5, pp. 643-661.*

Asteris, P. G., Tsaris, A. K., Cavaleri, L., Repapis, C. C., Papalou, A., di Trapani, F., & Karypidis, D. F. (2016). Prediction of the fundamental period of infilled RC frame structures using artificial neural networks. *Computational Intelligence and Neuroscience, 2016. https://doi.org/10.1155/2016/5104907.*

Charalampakis, A. E., Tsiatas, G. C., & Kotsiantis, S. B. (2020). Machine learning and nonlinear models for the estimation of fundamental period of vibration of masonry infilled RC frame structures. *Engineering Structures, 216. https://doi.org/10.1016/j.engstruct.2020.110765*.

Chopra A.K. (1995). Dynamics of structures: *Theory and Applications to Earthquake Engineering, Prentice-Hall.*

Chrislb (2005). Neural Network Diagrams. Available at: https://commons.wikimedia.org/wiki/User:Chrislb#My_diagrams (Accessed 6 May 2022).

Clough R.W., Penzien J. (1994). *Dynamics of Structures, 2nd Edition, McGraw Hill.*

Cömert, Z., & Kocamaz, A. F. (2017). Artificial neural network training algorithms for classification of cardiotocography signals. *Journal of Science and Technology, 7(2), 93–103. www.dergipark.ulakbim.gov.tr/beuscitech/*

Coşan, H. (2014). *Earthquake performance of reinforced concrete frames with different infill walls*. Msc Thesis, Eastern Mediterranean Universe, Turkish Republic of Northern Cyprus.

Crisafulli, F. J. (1997). *Seismic behaviour of reinforced concrete structures with masonry infills*. PhD Thesis, University of Canterbury, New Zealand.

Crisafulli, F. J., & Carr, A. J. (2007). Proposed macro-model for the analysis of infilled frame structures.

Decanini, L.D., & Fantin, G.E. (1986). Simplified models of masonry included in frames. Characteristics of stiffness and lateral resistance in limit state. *Argentine Conference on Structural Engineering, Buenos Aires, Argentina, Vol.2, 817-836.*

Dennis, J. J.E., and Schnabel, R. B., (1996). Numerical methods for unconstrained optimization and nonlinear equations. *SIAM.*

Dilmac, H., Ulutas, H., Tekeli, H., & Demir, F. (2018). The investigation of seismic performance of existing RC buildings with and without infill walls. *Computers and Concrete, 22(5), 439–447. https://doi.org/10.12989/cac.2018.22.5.439.*

Dowrick, D. J., & Rhoades, D. A. (1993). Damage costs for commercial and industrial property as a function of intensity in the 1987 Edgecumbe earthquake. *Earthquake engineering & structural dynamics, 22(10), 869-884.*

Filippou F.C., Popov E.P., Bertero V.V. (1983). Effects of bond deterioration on hysteretic behavior of reinforced concrete joints, *Report EERC 83-19, Earthquake Engineering Research Center, University of California, Berkeley.*

Foresee and Hagan, *Proceedings of the International Joint Conference on Neural Networks, June, 1997.*

Fragiadakis M., Pinho R., Antoniou S. (2008). Modelling inelastic buckling of reinforcing bars under earthquake loading, *in Progress in Computational Dynamics and Earthquake Engineering, Eds. M. Papadrakakis, D.C. Charmpis, N.D. Lagaros and Y. Tsompanakis, A.A. Balkema Publishers – Taylor & Francis, The Netherlands.*

Furtado, A., Rodrigues, H., Arêde, A., & Varum, H. (2021). A review of the performance of infilled rc structures in recent earthquakes. *In Applied Sciences (Switzerland) (Vol. 11, Issue 13). MDPI. https://doi.org/10.3390/app11135889.*

Jadhao, V. P., & Pajgade, P. S. (2013). Influence of masonry infill walls on seismic performance of RC framed structures: a comparison of AAC and conventional brick infill. *International Journal of Engineering and Advanced Technology, 2(4), 148-153.*

Kalman Šipoš, T., & Strukar, K. (2019). Prediction of the seismic response of multi-storey multi-bay masonry infilled frames using artificial neural networks and a bilinear approximation. *Buildings, 9(5), 121.*

Kameli, I., Miri, M. and Raji, A. (2011), Prediction of target displacement of reinforced concrete frames using artificial neural networks, *Adv. Mater. Res., 255, 2345-2349.*

Kareem, K. M., & Güneyisi, E. M. (2019). Effect of masonry infill wall configuration and modelling approach on the behaviour of RC frame structures. *Arabian*

Journal for Science and Engineering, 44(5), 4309–4324. https://doi.org/10.1007/s13369-018-3389-6.

Karim, R. bin. (2016). Seismic behavior of reinforced concrete frame structures with and without masonry infill walls.

Khan, N. A., Monti, G., Nuti, C., & Vailati, M. (2021). Effects of infills in the seismic performance of an RC factory building in Pakistan. Buildings, 11(7). *https://doi.org/10.3390/buildings11070276.*

Koçak, A. (2020). The effects of infill walls and basement shear walls on the seismic performance of existing damaged building. *Engineering Failure Analysis, 118. https://doi.org/10.1016/j.engfailanal.2020.104797.*

Kose, M. M. (2009). Parameters affecting the fundamental period of RC buildings with infill walls. *Engineering Structures, 31(1), 93–102. https://doi.org/10.1016/j.engstruct.2008.07.017.*

Kumar, S. M., & Satyanarayanan, K. S. (2018). Study the effect of elastic materials as interface medium used in infilled frames. *Materials Today: Proceedings, 5(2), 8986-8995.*

Liauw, T.C. and K.H. Kwan. 1983. Plastic theory of non integral infilled frames. *Proc. Instit. Civil Eng., 75: 379-396. DOI: 10.1680/iicep.1983.1437.*

MacKay, *Neural Computation, Vol. 4, No. 3, 1992, pp. 415–447.*

Madas P. (1993). *Advanced Modelling of Composite Frames Subjected to Earthquake Loading*, PhD Thesis, Imperial College, University of London, London, UK.

Mallick, D. V. & Severn, R. T. (1967). The behaviour of infilled frames under static loading. *Proceedings of the Institution of Civil Engineering, 38, 639-56.*

Mander J.B., Priestley M.J.N., Park R. (1988). Theoretical stress-strain model for confined concrete, *Journal of Structural Engineering, Vol. 114, No. 8, pp. 1804-1826.*

Martinez-Rueda J.E., Elnashai A.S. (1997) Confined concrete model under cyclic load, *Materials and Structures, Vol. 30, No. 197, pp. 139-147.*

Matlab. Choose a multilayer neural network training function; MathWorks. (2018). Available online: *https://www.mathworks.com/help/deeplearning/ug/choose-a-multilayer-neural-network-training-function.html.*

Menegotto M., Pinto P.E. (1973). Method of analysis for cyclically loaded r.c. Plane frames including changes in geometry and non-elastic behaviour of elements under combined normal force and bending, *International Association for Bridge and Structural Engineering, Zurich, Switzerland, pp. 15-22.*

Monti, G., Nuti, C., Santini, S. (1996). CYRUS, Cyclic response of upgraded sections, *Report No. 96-2, University of Chieti, Italy.*

Naoum, R. S., Abid, N. A., & Al-Sultani, Z. N. (2012). An enhanced resilient backpropagation artificial neural network for intrusion detection system. *International Journal of Computer Science and Network Security (IJCSNS), 12(3), 11.*

Parsaeimaram, M., Jiao, S., Rama, D. K., Rao, M., & Poursalehi, A. (2013). An artificial neural network for prediction of seismic behavior in RC buildings with and without infill walls. *International Journal of Modern Engineering Research (IJMER), 3(5), 3071–3078. www.ijmer.com.*

Paulay T., Priestley M.J.N. (1992). Seismic design of reinforced concrete and masonry buildings, *John Wiley & Sons Inc., New York.*

Perrone, D., Leone, M., & Aiello, M. A. (2017). Non-linear behaviour of masonry infilled RC frames: Influence of masonry mechanical properties. *Engineering Structures, 150, 875–891. https://doi.org/10.1016/j.engstruct.2017.08.001.*

Polyakov, S. V. (1966). Some investigations of the problem the strength of elements of buildings subjected to horizontal loads. *Symposium on Tall Buildings, University of Sourthampton, 465-86.*

Prota A., Cicco F., Cosenza E. (2009). Cyclic behavior of smooth steel reinforcing bars: experimental analysis and modeling issues, *Journal of Earthquake Engineering, Vol. 13, No. 4, pp. 500–519.*

Samarasinghe, Sandhya. (2016). Neural networks for applied sciences and engineering: *from fundamentals to complex pattern recognition.*

Sapna, S., Tamilarasi, A., & Kumar, M. P. (2012). Backpropagation learning algorithm based on levenberg marquardt algorithm. *Comp Sci Inform Technol (CS and IT), 2, 393-398.*

Sharma, S., Sharma, S., & Athaiya, A. (2020). Activation functions in neural networks. *International Journal of Engineering Applied Sciences and Technology (Vol. 4). http://www.ijeast.com.*

Sivanandam, S. N., & Deepa, S. N. (2006). Introduction to neural networks using Matlab 6.0. *Tata McGraw-Hill Education.*

Smyrou E, Blandon CA, Antoniou S, Pinho R, Crowley H (2006). Implementation and verification of a masonry panel model for nonlinear pseudo-dynamic analysis of infilled RC frames. *In: Proceedings of the first European conference on earthquake engineering and seismology. Paper no. 355, Geneva, Switzerland.*

Soyluk, A. & Harmankaya, Z., (2012). The history of development in Turkish seismic design codes. *International Journal of Civil & Environmental Engineering, 12(1), pp. 25-29.*

Stafford Smith, B. & C. Carter, 1969. A method of analysis for infilled frames. Proc. *Instit. Civil Eng, 44: 31-48. DOI: 10.1680/iicep.1969.7290.*

Stafford Smith, B., 1966. Behavior of square infilled frames. *J. Struct. Division, 92: 381-404.*

TS-500.(2000). Turkish Requirements for Design and Construction of Reinforced Concrete Structures.

TSC.(2007). Turkish Seismic Code.

TSCB.(2018). Turkish Seismic Code for Buildings.

Vafaei, M., Alih, S. C., Shad, H., Falah, A., & Halim, N. H. F. A. (2018). Prediction of strain values in reinforcements and concrete of a RC frame using neural networks. *International Journal of Advanced Structural Engineering, 10(1), 29–35. https://doi.org/10.1007/s40091-018-0178-0.*

Varum, H. S. (2003). *Seismic Assessment, Strengthening and Repair of Existing Buildings*. PhD Thesis, University of Aveiro, Portugal.

Yassin M.H.M. (1994). *Nonlinear analysis of prestressed concrete structures under monotonic and cyclic loads*, PhD Thesis, University of California, Berkeley, USA.

Zhang, B. (2006). *Parametric study on the influence of infills on the displacement capacity of RC frames for earthquake loss estimation*. Master Thesis, European School for Advanced Studies in Reduction of Seismic Risk, Rose School.

APPENDICES

Appendix A: Input Parameters

Model	Plan Symmetry	Width in x	Width in y	Stories Number	Infill Material	Infill Layout	Columns Ratio	Shear wall ratio	Soil Type [C (1), B (2)]	PGA
1	1	21.5	14.3	4	1	0	0.0166	0	1	0.749
2	1	21.5	14.3	4	1	1	0.0166	0	1	0.749
3	1	21.5	14.3	4	1	2	0.0166	0	1	0.749
4	1	21.5	14.3	4	1	3	0.0166	0	1	0.749
5	1	21.5	14.3	4	1	4	0.0166	0	1	0.749
6	1	21.5	14.3	4	1	5	0.0166	0	1	0.749
7	1	21.5	14.3	4	2	1	0.0166	0	1	0.749
8	1	21.5	14.3	4	2	2	0.0166	0	1	0.749
9	1	21.5	14.3	4	2	3	0.0166	0	1	0.749
10	1	21.5	14.3	4	2	4	0.0166	0	1	0.749
11	1	21.5	14.3	4	2	5	0.0166	0	1	0.749
12	1	21.5	14.3	4	3	1	0.0166	0	1	0.749
13	1	21.5	14.3	4	3	2	0.0166	0	1	0.749
14	1	21.5	14.3	4	3	3	0.0166	0	1	0.749
15	1	21.5	14.3	4	3	4	0.0166	0	1	0.749
16	1	21.5	14.3	4	3	5	0.0166	0	1	0.749
17	1	21.5	14.3	4	1	0	0.0166	0	1	0.448
18	1	21.5	14.3	4	1	1	0.0166	0	1	0.448
19	1	21.5	14.3	4	1	2	0.0166	0	1	0.448

20	1	21.5	14.3	4	1	3	0.0166	0	1	0.448
21	1	21.5	14.3	4	1	4	0.0166	0	1	0.448
22	1	21.5	14.3	4	1	5	0.0166	0	1	0.448
23	1	21.5	14.3	4	2	1	0.0166	0	1	0.448
24	1	21.5	14.3	4	2	2	0.0166	0	1	0.448
25	1	21.5	14.3	4	2	3	0.0166	0	1	0.448
26	1	21.5	14.3	4	2	4	0.0166	0	1	0.448
27	1	21.5	14.3	4	2	5	0.0166	0	1	0.448
28	1	21.5	14.3	4	3	1	0.0166	0	1	0.448
29	1	21.5	14.3	4	3	2	0.0166	0	1	0.448
30	1	21.5	14.3	4	3	3	0.0166	0	1	0.448
31	1	21.5	14.3	4	3	4	0.0166	0	1	0.448
32	1	21.5	14.3	4	3	5	0.0166	0	1	0.448
33	1	21.5	14.3	4	1	0	0.0166	0	2	0.749
34	1	21.5	14.3	4	1	1	0.0166	0	2	0.749
35	1	21.5	14.3	4	1	2	0.0166	0	2	0.749
36	1	21.5	14.3	4	1	3	0.0166	0	2	0.749
37	1	21.5	14.3	4	1	4	0.0166	0	2	0.749
38	1	21.5	14.3	4	1	5	0.0166	0	2	0.749
39	1	21.5	14.3	4	2	1	0.0166	0	2	0.749
40	1	21.5	14.3	4	2	2	0.0166	0	2	0.749
41	1	21.5	14.3	4	2	3	0.0166	0	2	0.749
42	1	21.5	14.3	4	2	4	0.0166	0	2	0.749
43	1	21.5	14.3	4	2	5	0.0166	0	2	0.749
44	1	21.5	14.3	4	3	1	0.0166	0	2	0.749

45	1	21.5	14.3	4	3	2	0.0166	0	2	0.749
46	1	21.5	14.3	4	3	3	0.0166	0	2	0.749
47	1	21.5	14.3	4	3	4	0.0166	0	2	0.749
48	1	21.5	14.3	4	3	5	0.0166	0	2	0.749
49	1	21.5	14.3	4	1	0	0.0166	0	2	0.448
50	1	21.5	14.3	4	1	1	0.0166	0	2	0.448
51	1	21.5	14.3	4	1	2	0.0166	0	2	0.448
52	1	21.5	14.3	4	1	3	0.0166	0	2	0.448
53	1	21.5	14.3	4	1	4	0.0166	0	2	0.448
54	1	21.5	14.3	4	1	5	0.0166	0	2	0.448
55	1	21.5	14.3	4	2	1	0.0166	0	2	0.448
56	1	21.5	14.3	4	2	2	0.0166	0	2	0.448
57	1	21.5	14.3	4	2	3	0.0166	0	2	0.448
58	1	21.5	14.3	4	2	4	0.0166	0	2	0.448
59	1	21.5	14.3	4	2	5	0.0166	0	2	0.448
60	1	21.5	14.3	4	3	1	0.0166	0	2	0.448
61	1	21.5	14.3	4	3	2	0.0166	0	2	0.448
62	1	21.5	14.3	4	3	3	0.0166	0	2	0.448
63	1	21.5	14.3	4	3	4	0.0166	0	2	0.448
64	1	21.5	14.3	4	3	5	0.0166	0	2	0.448
65	2	25.9	13.7	4	1	0	0.0158	0	1	0.749
66	2	25.9	13.7	4	1	2	0.0158	0	1	0.749
67	2	25.9	13.7	4	1	3	0.0158	0	1	0.749
68	2	25.9	13.7	4	1	4	0.0158	0	1	0.749
69	2	25.9	13.7	4	1	5	0.0158	0	1	0.749

70	2	25.9	13.7	4	2	2	0.0158	0	1	0.749
71	2	25.9	13.7	4	2	3	0.0158	0	1	0.749
72	2	25.9	13.7	4	2	4	0.0158	0	1	0.749
73	2	25.9	13.7	4	2	5	0.0158	0	1	0.749
74	2	25.9	13.7	4	3	2	0.0158	0	1	0.749
75	2	25.9	13.7	4	3	3	0.0158	0	1	0.749
76	2	25.9	13.7	4	3	4	0.0158	0	1	0.749
77	2	25.9	13.7	4	3	5	0.0158	0	1	0.749
78	2	25.9	13.7	4	1	0	0.0158	0	1	0.448
79	2	25.9	13.7	4	1	2	0.0158	0	1	0.448
80	2	25.9	13.7	4	1	3	0.0158	0	1	0.448
81	2	25.9	13.7	4	1	4	0.0158	0	1	0.448
82	2	25.9	13.7	4	1	5	0.0158	0	1	0.448
83	2	25.9	13.7	4	2	2	0.0158	0	1	0.448
84	2	25.9	13.7	4	2	3	0.0158	0	1	0.448
85	2	25.9	13.7	4	2	4	0.0158	0	1	0.448
86	2	25.9	13.7	4	2	5	0.0158	0	1	0.448
87	2	25.9	13.7	4	3	2	0.0158	0	1	0.448
88	2	25.9	13.7	4	3	3	0.0158	0	1	0.448
89	2	25.9	13.7	4	3	4	0.0158	0	1	0.448
90	2	25.9	13.7	4	3	5	0.0158	0	1	0.448
91	2	25.9	13.7	4	1	0	0.0158	0	2	0.749
92	2	25.9	13.7	4	1	2	0.0158	0	2	0.749
93	2	25.9	13.7	4	1	3	0.0158	0	2	0.749
94	2	25.9	13.7	4	1	4	0.0158	0	2	0.749

95	2	25.9	13.7	4	1	5	0.0158	0	2	0.749
96	2	25.9	13.7	4	2	2	0.0158	0	2	0.749
97	2	25.9	13.7	4	2	3	0.0158	0	2	0.749
98	2	25.9	13.7	4	2	4	0.0158	0	2	0.749
99	2	25.9	13.7	4	2	5	0.0158	0	2	0.749
100	2	25.9	13.7	4	3	2	0.0158	0	2	0.749
101	2	25.9	13.7	4	3	3	0.0158	0	2	0.749
102	2	25.9	13.7	4	3	4	0.0158	0	2	0.749
103	2	25.9	13.7	4	3	5	0.0158	0	2	0.749
104	2	25.9	13.7	4	1	0	0.0158	0	2	0.448
105	2	25.9	13.7	4	1	2	0.0158	0	2	0.448
106	2	25.9	13.7	4	1	3	0.0158	0	2	0.448
107	2	25.9	13.7	4	1	4	0.0158	0	2	0.448
108	2	25.9	13.7	4	1	5	0.0158	0	2	0.448
109	2	25.9	13.7	4	2	2	0.0158	0	2	0.448
110	2	25.9	13.7	4	2	3	0.0158	0	2	0.448
111	2	25.9	13.7	4	2	4	0.0158	0	2	0.448
112	2	25.9	13.7	4	2	5	0.0158	0	2	0.448
113	2	25.9	13.7	4	3	2	0.0158	0	2	0.448
114	2	25.9	13.7	4	3	3	0.0158	0	2	0.448
115	2	25.9	13.7	4	3	4	0.0158	0	2	0.448
116	2	25.9	13.7	4	3	5	0.0158	0	2	0.448
117	3	16.5	9.3	4	1	0	0.0352	0	1	0.749
118	3	16.5	9.3	4	1	2	0.0352	0	1	0.749
119	3	16.5	9.3	4	1	3	0.0352	0	1	0.749

120	3	16.5	9.3	4	1	4	0.0352	0	1	0.749
121	3	16.5	9.3	4	1	5	0.0352	0	1	0.749
122	3	16.5	9.3	4	2	2	0.0352	0	1	0.749
123	3	16.5	9.3	4	2	3	0.0352	0	1	0.749
124	3	16.5	9.3	4	2	4	0.0352	0	1	0.749
125	3	16.5	9.3	4	2	5	0.0352	0	1	0.749
126	3	16.5	9.3	4	3	2	0.0352	0	1	0.749
127	3	16.5	9.3	4	3	3	0.0352	0	1	0.749
128	3	16.5	9.3	4	3	4	0.0352	0	1	0.749
129	3	16.5	9.3	4	3	5	0.0352	0	1	0.749
130	3	16.5	9.3	4	1	0	0.0352	0	1	0.448
131	3	16.5	9.3	4	1	2	0.0352	0	1	0.448
132	3	16.5	9.3	4	1	3	0.0352	0	1	0.448
133	3	16.5	9.3	4	1	4	0.0352	0	1	0.448
134	3	16.5	9.3	4	1	5	0.0352	0	1	0.448
135	3	16.5	9.3	4	2	2	0.0352	0	1	0.448
136	3	16.5	9.3	4	2	3	0.0352	0	1	0.448
137	3	16.5	9.3	4	2	4	0.0352	0	1	0.448
138	3	16.5	9.3	4	2	5	0.0352	0	1	0.448
139	3	16.5	9.3	4	3	2	0.0352	0	1	0.448
140	3	16.5	9.3	4	3	3	0.0352	0	1	0.448
141	3	16.5	9.3	4	3	4	0.0352	0	1	0.448
142	3	16.5	9.3	4	3	5	0.0352	0	1	0.448
143	3	16.5	9.3	4	1	0	0.0352	0	2	0.749
144	3	16.5	9.3	4	1	2	0.0352	0	2	0.749

145	3	16.5	9.3	4	1	3	0.0352	0	2	0.749
146	3	16.5	9.3	4	1	4	0.0352	0	2	0.749
147	3	16.5	9.3	4	1	5	0.0352	0	2	0.749
148	3	16.5	9.3	4	2	2	0.0352	0	2	0.749
149	3	16.5	9.3	4	2	3	0.0352	0	2	0.749
150	3	16.5	9.3	4	2	4	0.0352	0	2	0.749
151	3	16.5	9.3	4	2	5	0.0352	0	2	0.749
152	3	16.5	9.3	4	3	2	0.0352	0	2	0.749
153	3	16.5	9.3	4	3	3	0.0352	0	2	0.749
154	3	16.5	9.3	4	3	4	0.0352	0	2	0.749
155	3	16.5	9.3	4	3	5	0.0352	0	2	0.749
156	3	16.5	9.3	4	1	0	0.0352	0	2	0.448
157	3	16.5	9.3	4	1	2	0.0352	0	2	0.448
158	3	16.5	9.3	4	1	3	0.0352	0	2	0.448
159	3	16.5	9.3	4	1	4	0.0352	0	2	0.448
160	3	16.5	9.3	4	1	5	0.0352	0	2	0.448
161	3	16.5	9.3	4	2	2	0.0352	0	2	0.448
162	3	16.5	9.3	4	2	3	0.0352	0	2	0.448
163	3	16.5	9.3	4	2	4	0.0352	0	2	0.448
164	3	16.5	9.3	4	2	5	0.0352	0	2	0.448
165	3	16.5	9.3	4	3	2	0.0352	0	2	0.448
166	3	16.5	9.3	4	3	3	0.0352	0	2	0.448
167	3	16.5	9.3	4	3	4	0.0352	0	2	0.448
168	3	16.5	9.3	4	3	5	0.0352	0	2	0.448
169	1	21.5	14.3	10	1	0	0.0088	0.0264	1	0.749

170	1	21.5	14.3	10	1	1	0.0088	0.0264	1	0.749
171	1	21.5	14.3	10	1	2	0.0088	0.0264	1	0.749
172	1	21.5	14.3	10	1	3	0.0088	0.0264	1	0.749
173	1	21.5	14.3	10	1	4	0.0088	0.0264	1	0.749
174	1	21.5	14.3	10	1	5	0.0088	0.0264	1	0.749
175	1	21.5	14.3	10	2	1	0.0088	0.0264	1	0.749
176	1	21.5	14.3	10	2	2	0.0088	0.0264	1	0.749
177	1	21.5	14.3	10	2	3	0.0088	0.0264	1	0.749
178	1	21.5	14.3	10	2	4	0.0088	0.0264	1	0.749
179	1	21.5	14.3	10	2	5	0.0088	0.0264	1	0.749
180	1	21.5	14.3	10	3	1	0.0088	0.0264	1	0.749
181	1	21.5	14.3	10	3	2	0.0088	0.0264	1	0.749
182	1	21.5	14.3	10	3	3	0.0088	0.0264	1	0.749
183	1	21.5	14.3	10	3	4	0.0088	0.0264	1	0.749
184	1	21.5	14.3	10	3	5	0.0088	0.0264	1	0.749
185	1	21.5	14.3	10	1	0	0.0088	0.0264	1	0.448
186	1	21.5	14.3	10	1	1	0.0088	0.0264	1	0.448
187	1	21.5	14.3	10	1	2	0.0088	0.0264	1	0.448
188	1	21.5	14.3	10	1	3	0.0088	0.0264	1	0.448
189	1	21.5	14.3	10	1	4	0.0088	0.0264	1	0.448
190	1	21.5	14.3	10	1	5	0.0088	0.0264	1	0.448
191	1	21.5	14.3	10	2	1	0.0088	0.0264	1	0.448
192	1	21.5	14.3	10	2	2	0.0088	0.0264	1	0.448
193	1	21.5	14.3	10	2	3	0.0088	0.0264	1	0.448
194	1	21.5	14.3	10	2	4	0.0088	0.0264	1	0.448

195	1	21.5	14.3	10	2	5	0.0088	0.0264	1	0.448
196	1	21.5	14.3	10	3	1	0.0088	0.0264	1	0.448
197	1	21.5	14.3	10	3	2	0.0088	0.0264	1	0.448
198	1	21.5	14.3	10	3	3	0.0088	0.0264	1	0.448
199	1	21.5	14.3	10	3	4	0.0088	0.0264	1	0.448
200	1	21.5	14.3	10	3	5	0.0088	0.0264	1	0.448
201	1	21.5	14.3	10	1	0	0.0088	0.0264	2	0.749
202	1	21.5	14.3	10	1	1	0.0088	0.0264	2	0.749
203	1	21.5	14.3	10	1	2	0.0088	0.0264	2	0.749
204	1	21.5	14.3	10	1	3	0.0088	0.0264	2	0.749
205	1	21.5	14.3	10	1	4	0.0088	0.0264	2	0.749
206	1	21.5	14.3	10	1	5	0.0088	0.0264	2	0.749
207	1	21.5	14.3	10	2	1	0.0088	0.0264	2	0.749
208	1	21.5	14.3	10	2	2	0.0088	0.0264	2	0.749
209	1	21.5	14.3	10	2	3	0.0088	0.0264	2	0.749
210	1	21.5	14.3	10	2	4	0.0088	0.0264	2	0.749
211	1	21.5	14.3	10	2	5	0.0088	0.0264	2	0.749
212	1	21.5	14.3	10	3	1	0.0088	0.0264	2	0.749
213	1	21.5	14.3	10	3	2	0.0088	0.0264	2	0.749
214	1	21.5	14.3	10	3	3	0.0088	0.0264	2	0.749
215	1	21.5	14.3	10	3	4	0.0088	0.0264	2	0.749
216	1	21.5	14.3	10	3	5	0.0088	0.0264	2	0.749
217	1	21.5	14.3	10	1	0	0.0088	0.0264	2	0.448
218	1	21.5	14.3	10	1	1	0.0088	0.0264	2	0.448
219	1	21.5	14.3	10	1	2	0.0088	0.0264	2	0.448

220	1	21.5	14.3	10	1	3	0.0088	0.0264	2	0.448
221	1	21.5	14.3	10	1	4	0.0088	0.0264	2	0.448
222	1	21.5	14.3	10	1	5	0.0088	0.0264	2	0.448
223	1	21.5	14.3	10	2	1	0.0088	0.0264	2	0.448
224	1	21.5	14.3	10	2	2	0.0088	0.0264	2	0.448
225	1	21.5	14.3	10	2	3	0.0088	0.0264	2	0.448
226	1	21.5	14.3	10	2	4	0.0088	0.0264	2	0.448
227	1	21.5	14.3	10	2	5	0.0088	0.0264	2	0.448
228	1	21.5	14.3	10	3	1	0.0088	0.0264	2	0.448
229	1	21.5	14.3	10	3	2	0.0088	0.0264	2	0.448
230	1	21.5	14.3	10	3	3	0.0088	0.0264	2	0.448
231	1	21.5	14.3	10	3	4	0.0088	0.0264	2	0.448
232	1	21.5	14.3	10	3	5	0.0088	0.0264	2	0.448
233	2	25.9	13.7	10	1	0	0.0101	0.0245	1	0.749
234	2	25.9	13.7	10	1	2	0.0101	0.0245	1	0.749
235	2	25.9	13.7	10	1	3	0.0101	0.0245	1	0.749
236	2	25.9	13.7	10	1	4	0.0101	0.0245	1	0.749
237	2	25.9	13.7	10	1	5	0.0101	0.0245	1	0.749
238	2	25.9	13.7	10	2	2	0.0101	0.0245	1	0.749
239	2	25.9	13.7	10	2	3	0.0101	0.0245	1	0.749
240	2	25.9	13.7	10	2	4	0.0101	0.0245	1	0.749
241	2	25.9	13.7	10	2	5	0.0101	0.0245	1	0.749
242	2	25.9	13.7	10	3	2	0.0101	0.0245	1	0.749
243	2	25.9	13.7	10	3	3	0.0101	0.0245	1	0.749
244	2	25.9	13.7	10	3	4	0.0101	0.0245	1	0.749

245	2	25.9	13.7	10	3	5	0.0101	0.0245	1	0.749
246	2	25.9	13.7	10	1	0	0.0101	0.0245	1	0.448
247	2	25.9	13.7	10	1	2	0.0101	0.0245	1	0.448
248	2	25.9	13.7	10	1	3	0.0101	0.0245	1	0.448
249	2	25.9	13.7	10	1	4	0.0101	0.0245	1	0.448
250	2	25.9	13.7	10	1	5	0.0101	0.0245	1	0.448
251	2	25.9	13.7	10	2	2	0.0101	0.0245	1	0.448
252	2	25.9	13.7	10	2	3	0.0101	0.0245	1	0.448
253	2	25.9	13.7	10	2	4	0.0101	0.0245	1	0.448
254	2	25.9	13.7	10	2	5	0.0101	0.0245	1	0.448
255	2	25.9	13.7	10	3	2	0.0101	0.0245	1	0.448
256	2	25.9	13.7	10	3	3	0.0101	0.0245	1	0.448
257	2	25.9	13.7	10	3	4	0.0101	0.0245	1	0.448
258	2	25.9	13.7	10	3	5	0.0101	0.0245	1	0.448
259	2	25.9	13.7	10	1	0	0.0101	0.0245	2	0.749
260	2	25.9	13.7	10	1	2	0.0101	0.0245	2	0.749
261	2	25.9	13.7	10	1	3	0.0101	0.0245	2	0.749
262	2	25.9	13.7	10	1	4	0.0101	0.0245	2	0.749
263	2	25.9	13.7	10	1	5	0.0101	0.0245	2	0.749
264	2	25.9	13.7	10	2	2	0.0101	0.0245	2	0.749
265	2	25.9	13.7	10	2	3	0.0101	0.0245	2	0.749
266	2	25.9	13.7	10	2	4	0.0101	0.0245	2	0.749
267	2	25.9	13.7	10	2	5	0.0101	0.0245	2	0.749
268	2	25.9	13.7	10	3	2	0.0101	0.0245	2	0.749
269	2	25.9	13.7	10	3	3	0.0101	0.0245	2	0.749

270	2	25.9	13.7	10	3	4	0.0101	0.0245	2	0.749
271	2	25.9	13.7	10	3	5	0.0101	0.0245	2	0.749
272	2	25.9	13.7	10	1	0	0.0101	0.0245	2	0.448
273	2	25.9	13.7	10	1	2	0.0101	0.0245	2	0.448
274	2	25.9	13.7	10	1	3	0.0101	0.0245	2	0.448
275	2	25.9	13.7	10	1	4	0.0101	0.0245	2	0.448
276	2	25.9	13.7	10	1	5	0.0101	0.0245	2	0.448
277	2	25.9	13.7	10	2	2	0.0101	0.0245	2	0.448
278	2	25.9	13.7	10	2	3	0.0101	0.0245	2	0.448
279	2	25.9	13.7	10	2	4	0.0101	0.0245	2	0.448
280	2	25.9	13.7	10	2	5	0.0101	0.0245	2	0.448
281	2	25.9	13.7	10	3	2	0.0101	0.0245	2	0.448
282	2	25.9	13.7	10	3	3	0.0101	0.0245	2	0.448
283	2	25.9	13.7	10	3	4	0.0101	0.0245	2	0.448
284	2	25.9	13.7	10	3	5	0.0101	0.0245	2	0.448
285	3	16.5	9.3	10	1	0	0.0103	0.0572	1	0.749
286	3	16.5	9.3	10	1	2	0.0103	0.0572	1	0.749
287	3	16.5	9.3	10	1	3	0.0103	0.0572	1	0.749
288	3	16.5	9.3	10	1	4	0.0103	0.0572	1	0.749
289	3	16.5	9.3	10	1	5	0.0103	0.0572	1	0.749
290	3	16.5	9.3	10	2	2	0.0103	0.0572	1	0.749
291	3	16.5	9.3	10	2	3	0.0103	0.0572	1	0.749
292	3	16.5	9.3	10	2	4	0.0103	0.0572	1	0.749
293	3	16.5	9.3	10	2	5	0.0103	0.0572	1	0.749
294	3	16.5	9.3	10	3	2	0.0103	0.0572	1	0.749

295	3	16.5	9.3	10	3	3	0.0103	0.0572	1	0.749
296	3	16.5	9.3	10	3	4	0.0103	0.0572	1	0.749
297	3	16.5	9.3	10	3	5	0.0103	0.0572	1	0.749
298	3	16.5	9.3	10	1	0	0.0103	0.0572	1	0.448
299	3	16.5	9.3	10	1	2	0.0103	0.0572	1	0.448
300	3	16.5	9.3	10	1	3	0.0103	0.0572	1	0.448
301	3	16.5	9.3	10	1	4	0.0103	0.0572	1	0.448
302	3	16.5	9.3	10	1	5	0.0103	0.0572	1	0.448
303	3	16.5	9.3	10	2	2	0.0103	0.0572	1	0.448
304	3	16.5	9.3	10	2	3	0.0103	0.0572	1	0.448
305	3	16.5	9.3	10	2	4	0.0103	0.0572	1	0.448
306	3	16.5	9.3	10	2	5	0.0103	0.0572	1	0.448
307	3	16.5	9.3	10	3	2	0.0103	0.0572	1	0.448
308	3	16.5	9.3	10	3	3	0.0103	0.0572	1	0.448
309	3	16.5	9.3	10	3	4	0.0103	0.0572	1	0.448
310	3	16.5	9.3	10	3	5	0.0103	0.0572	1	0.448
311	3	16.5	9.3	10	1	0	0.0103	0.0572	2	0.749
312	3	16.5	9.3	10	1	2	0.0103	0.0572	2	0.749
313	3	16.5	9.3	10	1	3	0.0103	0.0572	2	0.749
314	3	16.5	9.3	10	1	4	0.0103	0.0572	2	0.749
315	3	16.5	9.3	10	1	5	0.0103	0.0572	2	0.749
316	3	16.5	9.3	10	2	2	0.0103	0.0572	2	0.749
317	3	16.5	9.3	10	2	3	0.0103	0.0572	2	0.749
318	3	16.5	9.3	10	2	4	0.0103	0.0572	2	0.749
319	3	16.5	9.3	10	2	5	0.0103	0.0572	2	0.749

320	3	16.5	9.3	10	3	2	0.0103	0.0572	2	0.749
321	3	16.5	9.3	10	3	3	0.0103	0.0572	2	0.749
322	3	16.5	9.3	10	3	4	0.0103	0.0572	2	0.749
323	3	16.5	9.3	10	3	5	0.0103	0.0572	2	0.749
324	3	16.5	9.3	10	1	0	0.0103	0.0572	2	0.448
325	3	16.5	9.3	10	1	2	0.0103	0.0572	2	0.448
326	3	16.5	9.3	10	1	3	0.0103	0.0572	2	0.448
327	3	16.5	9.3	10	1	4	0.0103	0.0572	2	0.448
328	3	16.5	9.3	10	1	5	0.0103	0.0572	2	0.448
329	3	16.5	9.3	10	2	2	0.0103	0.0572	2	0.448
330	3	16.5	9.3	10	2	3	0.0103	0.0572	2	0.448
331	3	16.5	9.3	10	2	4	0.0103	0.0572	2	0.448
332	3	16.5	9.3	10	2	5	0.0103	0.0572	2	0.448
333	3	16.5	9.3	10	3	2	0.0103	0.0572	2	0.448
334	3	16.5	9.3	10	3	3	0.0103	0.0572	2	0.448
335	3	16.5	9.3	10	3	4	0.0103	0.0572	2	0.448
336	3	16.5	9.3	10	3	5	0.0103	0.0572	2	0.448

Appendix B: Neural Network Training

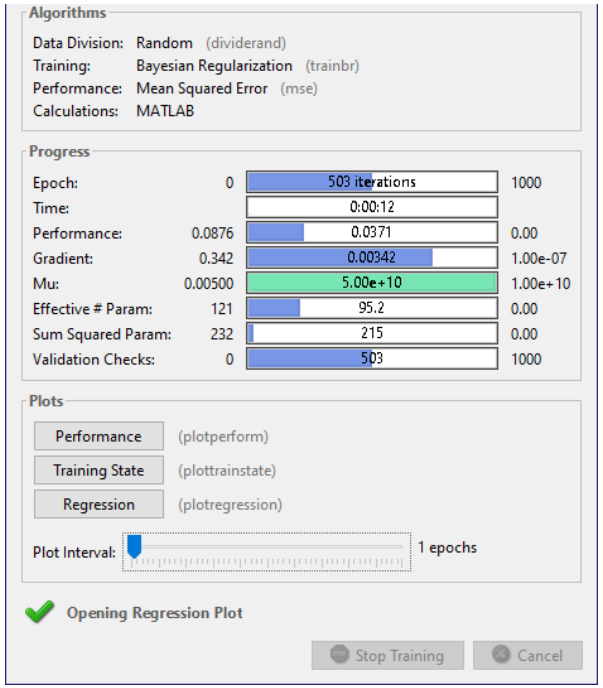

Performance Level Model

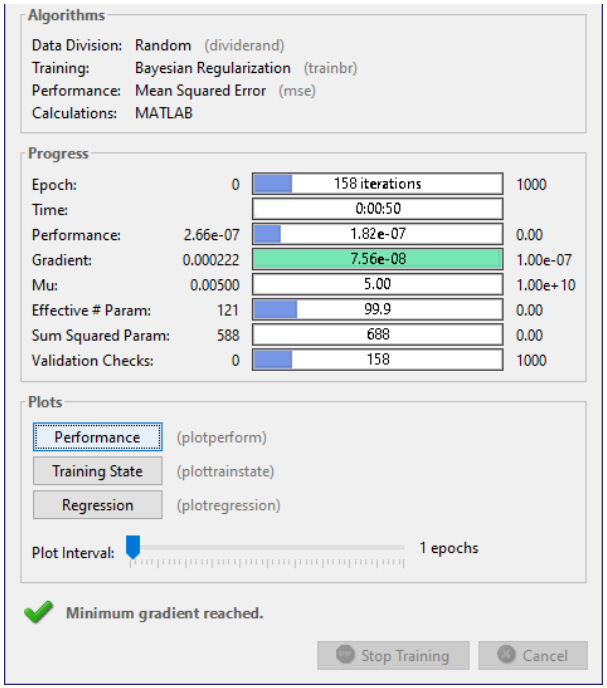

Fundamental Period Model

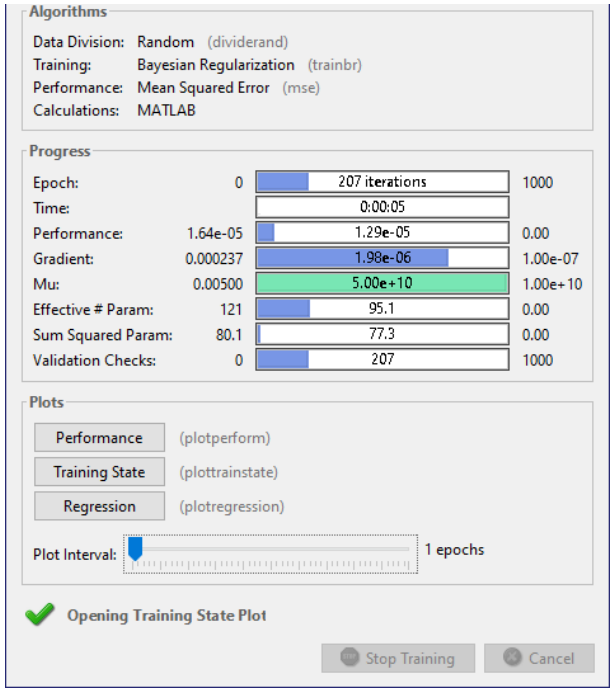

Target Displacement Model